GAIT OPTIMIZATION WITH A REAL-TIME CLOSED-LOOP ARTIFICIAL SENSORY FEEDBACK

A Dissertation
Presented to
The Academic Faculty

by

Hangue Park

In Partial Fulfillment
of the Requirements for the Degree
Doctor of Philosophy in the
School of Electrical and Computer Engineering

Georgia Institute of Technology
August 2017

GAIT OPTIMIZATION WITH A REAL-TIME CLOSED-LOOP ARTIFICIAL SENSORY FEEDBACK

Approved by:

Dr. Stephen P. DeWeerth, Advisor
School of Electrical and Computer Engineering &
Department of Biomedical Engineering
Georgia Institute of Technology

Dr. Boris I. Prilutsky, Co-advisor
School of Biological Sciences
Georgia Institute of Technology

Dr. Robert J. Butera
School of Electrical and Computer Engineering &
Department of Biomedical Engineering
Georgia Institute of Technology

Dr. Young-Hui Chang
School of Biological Sciences
Georgia Institute of Technology

Dr. Martha A. Grover
School of Chemical and Biomolecular Engineering
Georgia Institute of Technology

Dr. Michel A. Lemay
Bioengineering Department
Temple University

Date Approved: July 03, 2017

ACKNOWLEDGEMENTS

I would like to thank my advisors, Dr. DeWeerth and Dr. Prilutsky. I deeply respect their personality as well as their insight to the research. I am proud and happy to have them as my advisors. Also, I would like to thank my family. I love my son William, my wife Jeonghee, my sister, my mother, and my father without whose support I would not be here.

TABLE OF CONTENTS

LIST OF TABLES

LIST OF FIGURES

LIST OF SYMBOLS AND ABBREVIATIONS

Anesth	Anesthesia
CPG	Central pattern generator
EMG	Electromyogram
GRF	Ground reaction forces
IP	Iliopsoas muscle
LS walking	Lateral sequence walking
L-belt	Belt on the left side
MCP	Metacarpophalangeal joint
MCU	Microprocessor control unit
MG	Medial Gastrocnemius muscle
MTP	Metatarsophalangeal joint
Quad	Quadriceps
R-belt	Belt on the right side
Sart	Sartorius muscle
SO	Soleus muscle
Stim	Stimulation
TA	Tibialis Anterior muscle

SUMMARY

Individuals with unilateral lower limb musculoskeletal and neurological conditions, including lower limb prosthetic users, experience asymmetric walking. Asymmetric walking may result in asymmetric loading of intact musculoskeletal structures and undesirable compensations by the body to maintain balance and stability. This might lead to secondary conditions (osteoarthritis, low back pain, etc.). Asymmetry of prosthetic walking might be caused in part by the lack of both motion-dependent feedback from the prosthesis and active control of the prosthetic limb. Recently, means for bi-directional neural communications between the limb prosthesis and user's nervous system has been developed, e.g. bone-anchored pylons with peripheral nerve interfaces. In addition, technology has been advanced to elicit natural sensory perceptions from the prosthesis by electrical stimulation of sensory nerves.

The goal of this research was to develop a real-time closed-loop control system for a sensing, bone-anchored transtibial prosthesis interfaced with residual peripheral nerves and muscles. The prosthesis and control system would allow to sense touch during walking and control the prosthetic ankle using natural motor commands to automatically correct asymmetries and instability of walking. To inform the design of the prosthesis and control system, I investigated in walking cats the effects of manipulating tactile perception from paw pads (by anesthesia and electrical stimulation of a sensory nerve) and stretch-dependent feedback from thigh muscles (by varying treadmill speed and by muscle self-reinnervation) on symmetry and stability of walking.

I found that removal of the tactile and muscle length-dependent feedback resulted in profound changes in symmetry and stability of walking. In addition, electrical

stimulation of the distal tibial nerve, innervating paw pads, during the stance phase of walking substantially reduced and sometimes reversed the effects of sensory feedback removal on several characteristics of walking symmetry and stability. I then designed a real-time closed-loop gait control system and tested it in the intact walking cat. I demonstrated that step length symmetry could be controlled in real time by stimulation of the distal tibial nerve.

This system could be used, for example, for correcting asymmetries during walking in people with sensorimotor deficits. I also developed a prototype of an active sensing transtibial prosthesis with an ankle joint controlled by the muscle activity. During testing, the prototype could reproduce the magnitude and pattern of the ground reaction force recorded during walking in the cat. The results of this study provide new insights into the role of sensory feedback in control of locomotion and offer new engineering solutions for a sensing bone-anchored limb prosthesis, interfaced with the peripheral nervous system, and for improving kinematic characteristics of pathological gait.

CHAPTER 1

INTRODUCTION

Individuals with unilateral lower limb musculoskeletal and neurological conditions, including lower limb prosthetic users, experience asymmetric walking (Lloyd et al. 2010; Schaarschmidt et al. 2012; Kaufman et al. 2012). The asymmetric walking may result in asymmetric loading of intact musculoskeletal structures and undesirable compensation by the body to maintain balance and stability. This might lead to secondary conditions (osteoarthritis, low back pain, etc.) (Lloyd et al. 2010; Hendershot et al. 2013). The asymmetry in prosthetic gait might be caused in part by the lack of both motion-dependent feedback from the prosthesis and active control of the prosthetic limb. Recently, a means for bi-directional neural communications between the prosthesis and user has been developed to deliver both ascending sensory feedback and descending motor control signals (e.g. bone-anchored pylon with a peripheral nerve interface (Ortiz-Catalan et al. 2014; Pitkin et al. 2012)). In addition, technology has been advanced to elicit sensory perception from the prosthesis by electrical stimulation of sensory nerves (Graczyk et al. 2016; Tan et al. 2014).

My research goal is to solve the problem of prosthetic gait (e.g. asymmetry) by a closed-loop optimization of ascending and descending signals, via a bone-anchored neural interface. This goal will be achieved with both (1) a scientific study of the effects of somatosensory feedback modulations on walking kinematics and stability and (2) an engineering approach to develop a neuroprosthesis controlled by closed-loop optimization with feedback and feedforward controller. In this dissertation, I will show how quality of asymmetric walking can be improved with a closed-loop optimization of ascending/descending neural signals via a bone-anchored neural interface. After describing the specific aims and background of the research, I will show the effects of somatosensory feedback modulations on full-body cat kinematics (chapter 2) and stability

(chapter 3) during walking on a split-belt treadmill. In chapter 4, I will show how I implemented the design of a transtibial neuroprosthesis for the cat and the closed-loop control.

1.1. Specific aims

Aim 1: Determine the effects of manipulating cutaneous feedback from paw pad afferents and muscle stretch-dependent feedback from quadriceps and sartorius muscles on kinematics of walking in the cat.

Hypotheses: (i) During the split-belt treadmill walking, tactile modulation will show greater effect when two belts move at different speeds, than at the same speed. It is because tactile feedback plays an important role in challenging gait conditions (Bouyer et al. 2003; Bolton et al. 2009; Corriveau et al. 2000).

(ii) During the split-belt treadmill walking, modulation of belt speed ratio will cause cats to shift their body weight to the slower belt. This shift is assumed to reduce the distance travelled by the center of mass (COM) in each walking cycle and thus to decrease energy expenditure.

(iii) Removal or reduction of cutaneous afferent feedback from ipsilateral paw pads will cause body weight shift to the affected side, possibly to increase tactile input. This will lead to an increase in the duty cycle of the affected limbs (Monzee and Smith, 2002; Nowak et al., 2001).

(iv) Electrical stimulation of the distal-tibial nerve innervating skin on hindpaw pads will reverse or reduce the locomotor changes caused by the paw-pad anesthesia. Justification for this hypothesis is based on studies, in which individuals with hand loss were able to perceive natural touch sensations of the phantom hand when the residual cutaneous nerves were electrically stimulated (Graczyk et al. 2016; Tan et al. 2014).

(v) Removal of stretch reflex from muscles crossing the hip joints (quadriceps and sartorius, Quad-Sart) would delay the stance-swing transition in the affected hindlimb.

This expectation is based on the current understanding of the role of length-dependent sensory feedback from hip flexors in locomotor phase resetting and the stance-swing phase transition (Kriellaars et al. 1994; Markin et al. 2016; Pearson 2008) – the stance-swing transition is triggered by the stretch of hip flexor muscles whose length approach peak values in late stance (Gregor et al. 2006).

(vi) Stimulation of the distal-tibial nerve during the stance phase of walking in cats with the self-reinnervated Quad-Sart would further increase the delay of the stance-swing transition and thus make kinematics of walking more asymmetric. This proposition follows from the currently accepted conditions for the cessation of the stance and initiation of swing phase – the sufficient stretch of hip flexors and unloading the hindlimb (Pearson 2008). If stimulation of the distal-tibial nerve, innervating hindlimb cutaneous paw pad afferents, reduced the effects of paw pad anesthesia (see hypothesis 2), this stimulation might provide some perception of contact with the ground and limb loading and thus delay the stance to swing transition.

Aim 2: Determine the effects of manipulating cutaneous feedback from paw pad afferents and muscle stretch-dependent feedback from quadriceps and sartorius muscles on static and dynamic stability during walking in the cat.

Hypotheses: (i) With removal or reduction of cutaneous afferent feedback from ipsilateral paw pads, cats will decrease diagonal 2-limb support phase, the most unstable phase of the walking cycle.

(ii) Removal or reduction of cutaneous afferent feedback from ipsilateral paw pads will increase the step width, mean area of support in the walking cycle, static stability and lateral dynamic stability on the affected side.

(iii) Distal-tibial nerve stimulation will reverse or reduce the effects of paw-pad anesthesia on walking stability if the stimulation recovers spatial and temporal kinematic parameters of walking.

(iv) With removal of length dependent feedback from right Quad-Sart, cats will decrease diagonal 2-limb support phase. This will increase the the mean area of support in the walking cycle and static stability.

(v) Removal of length dependent feedback from Quad-Sart will increase the step width and lateral dynamic stability on the affected side.

(vi) Distal-tibial nerve stimulation will reduce the changes caused by Quad-Sart self-reinnervation.

Aim 3: Develop a closed-loop control system for a bone-anchored prosthesis with a peripheral nerve interface for correcting asymmetry of prosthetic walking.

Hypothesis: (i) Closed-loop control of the stimulation parameters of the sensory distal-tibial nerve will control spatial step symmetry of intact cat walking on split-belt treadmill.

(ii) Cat transtibial prosthesis with an active ankle joint and artificial sensory feedback will reproduce the intact ground reaction force pattern.

1.2. Background of the research

1.2.1. Functional anatomy of cutaneous nerves in cat paws

Bernard and colleagues well described the functional anatomy of cutaneous nerves in cat paws in their paper (Bernard et al. 2007). Five cutaneous nerves innervate paws in all directions: saphenous nerve, caudal cutaneous sural nerve, superficial peroneal nerve, distal tibial nerve, and deep peroneal nerve. Saphenous nerve and caudal cutaneous sural nerve innervate medial and lateral area of foot, respectively. They are strict sensory nerves and do not innervate any muscle. Superficial peroneal nerve innervates skin on the dorsum of foot, and it also innervate muscles that evert the foot. Distal tibial nerve innervates most of the plantar surface including paw pads, and it also

innervates to muscles for plantarflexion of ankle joint and flexion of five digits. Deep peroneal nerve innervates to distal and medial surface of paw pads, and it also innervates muscular branches to the anterior compartment of extensor muscles in the leg.

1.2.2. Role of tactile sensory feedback from the foot

Since Sherrington (Sherrington 1910) and Brown (Brown 1911) introduced the notions of the spinal reflexes and central pattern generator (CPG), the effects of sensory feedback from the moving limbs on the locomotor control have been actively explored (Lundberg 1979; McCrea 2001; Grillner 2011). Currently, it is generally accepted that motion-dependent somatosensory feedback plays an important role in control of locomotion from invertebrates to vertebrates, although the extent might differ among species (Pearson 1993). However, the understanding of the role of somatosensory feedback in locomotion is limited. For example, how sensory feedback reorganizes the function of the central networks in cats cannot be fully explained yet (Pearson 2004). The tactile feedback from the foot, especially from the sole of the foot (i.e. plantar cutaneous feedback) might play an important role in locomotion, considering it is well synchronized with the stance phase. However, the role of the plantar cutaneous feedback in locomotion is still unclear (Pearson 2008). In the following, I will show examples of several studies exploring the role of tactile feedback in locomotion, mostly in humans and cats.

In humans, Zehr and colleagues have found, through the electrical stimulation of the nerves innervating either the dorsum or the sole of the foot, that the tactile feedback from the foot makes walking more stable (Zehr et al. 1997). The superficial peroneal nerve stimulation causes dorsiflexion to correct the stumbling response and the tibial nerve stimulation causes plantarflexion to prevent tripping of the swing leg and to assist foot placing and weight acceptance at the beginning of stance. They also found that the effect of stimulation depends upon both the phase and the intensity of stimulation (Zehr et al. 1998). Höhne and colleagues have tested the reduced tactile sensation from the sole

of the foot using the intradermal injections of an anesthetic solution, and found that the reduced tactile sensation from the sole of the foot modifies gait dynamics, lower-limb kinematics, and muscle activity during locomotion (Höhne et al. 2012). The tactile feedback from the sole of the foot also plays an important role in regulating the balance of the body during the locomotion. It helped people properly react to sudden changes in rigidity of surface (Höhne et al. 2011).

In cats, Bouyer and Rossignol have showed that loss of tactile feedback from the hindpaw, caused by denervation of five paw cutaneous nerves innervating all area of paw (i.e. saphenous nerve, caudal cutaneous sural nerve, superficial peroneal nerve, distal tibial nerve, and deep peroneal nerve), led to rather small motor deficits in level treadmill walking, and the deficits were rapidly compensated (Bouyer and Rossignol 2003). However, in the slope walking or the ladder walking, cats showed considerable motor deficits. In addition, cats could not recover the original kinematics of walking, even though they showed compensatory adaptation during slope and ladder walking several weeks after denervation. The authors concluded that the locomotor system of the adult cat cannot regain fine control of the movement in the absence of tactile feedback from the hindpaw. They also concluded that cutaneous input from the paw becomes more important in demanding situations such as walking on a ladder or on inclines than in level walking (Bouyer and Rossignol 2003). Bolton and Misiaszek have showed that loss of tactile sensation from the hindpaws leads to instability during walking in the cat. After denervation of five cutaneous nerves, as used in Bouyer and Rossignol 2003, for both hindlimbs, all the cats increased their step width. Cats also lowered their pelvis and spent more time with the hindlegs in double-support phase when walking across the walkway. Furthermore, after the denervation, cats lost the corrective responses to medial-lateral perturbations. The paw placements were markedly shifted from the original walking path by medial-lateral perturbation (Bolton and Misiaszek 2009).

1.2.3. Generation of artificial sensory feedback

The generation of artificial sensory feedback by stimulation of sensory nerves has been studied for some time. Several research groups have been actively focusing on generating realistic tactile perceptions from the phantom hand in people with upper limb loss. Tan and colleagues have demonstrated that electrical stimulation of the residual median, ulnar, and radial nerves via flat cuff electrodes generates long-term stable tactile sensations (Tan et al. 2014). They have also found that the pulse width modulation produced sensations that were more natural and without tingling or paresthesia. Davis and colleagues have demonstrated that electrical stimulation of the median and ulnar nerves using intrafascicular microelectrodes generates more than 80 types of tactile sensation on the hand (Davis et al. 2016).

Artificial sensory feedback could also help with the problems caused by the missing sensory feedback from the plantar surface of the foot. For example, asymmetric walking in people with a unilateral lower limb prosthesis or people post stroke might be partly caused by loss of sensory feedback from the foot (Schaarschmidt et al. 2012; Wutzke et al. 2013). Abnormal plantar pressure distribution in diabetic patients, which often results in skin ulcers, might be likewise caused by loss of tactile feedback from the foot (Birke et al. 1991). Since electrical stimulation of the median, ulnar and radial nerves can evoke tactile sensations from the phantom hand, it is reasonable to suggest that electrical stimulation of the distal-tibial nerve can evoke tactile sensations from the foot sole. The cat experiments provide evidence that a phase-dependent electrical stimulation of either tibial or sural nerve changes locomotor kinematics and muscle activity patterns (Duysens and Pearson 1976; Ollivier-Lanvin et al. 2011).

1.2.4. Closed-loop sensorimotor integration

It has been suggested that in the closed-loop sensorimotor system, motor commands are updated during the execution of task as sensory feedback reports the

performance error in real time, whereas motor commands depend on the prediction in the open-loop sensorimotor system (Todorov 2004). As the fine control of prosthetic limbs and decoding of body signals into commands to the prosthesis are developed, the restoration of sensory feedback becomes the primary challenge for human-machine interfaces to facilitate a closed-loop sensorimotor integration (Weber et al. 2012; Ortiz-Catalan et al. 2014).

Because of the complexities of generating a target sensation, the sensory feedback is sometimes applied in alternative forms, such as visual feedback and haptic feedback (Fan et al. 2008; Lewek et al. 2012). However, this type of feedback is not as intuitive as the natural sensory feedback, because additional processing is necessary in the brain. Recently, electrical stimulation to sensory nerves has replicated natural touch sensation from a phantom hand. Two subjects with upper limb loss could perform an accurate finger-grip task using the prosthetic hand much better when the artificial tactile feedback from the prosthetic fingertip was on (Tan et al. 2014). Although the map between the electrical stimulation and the sensory feedback has not been fully revealed, the optimization of both ascending and descending maps in the closed-loop sensorimotor system makes it possible to compensate for the incompleteness of the artificial sensory feedback (Todorov 2004).

1.2.5. Split-belt treadmill locomotion

Split-belt treadmill is a useful experimental environment for the analysis of locomotor behaviors because it allows for regulation of speed for each side of the body independently and permits recordings of 3D full-body kinematics of multiple locomotor cycles. Split-belt treadmill locomotion has been actively explored for the post-stroke rehabilitative training, because the asymmetric walking patterns could be remediated by the split-belt walking (Reisman et al. 2007). It has also been used to study the organization of interlimb coordination in humans and cats (Dietz et al. 1994; Frigon et al.

2013). Changes in metabolic cost and mediolateral center of mass position, during split-belt walking, have been also investigated to see the neural adaptation (Selgrade et al. 2017). These studies have revealed some neural constraints on left-right interlimb coordination and brain structures contributing to locomotor adaptation (Morton and Bastian 2006).

To interpret data obtained from split-belt treadmill locomotion, left-right step symmetry has been analyzed to understand how the neural circuitry manages the speed difference between left and right belt. To evaluate the left-right step symmetry, I will adopt both spatial and temporal step symmetry parameters from the prior work (Malone et al. 2012; Malone and Bastian 2014). The spatial step symmetry has been defined as the normalized difference between left step length and right step length (Malone and Bastian 2014), and temporal step symmetry has been defined as the difference in either stance onset or stance offset time between left and right legs normalized by the stride time (Malone et al. 2012). To evaluate the individual movement of the limb relative to the body, the limb angle has been defined as the angle between a vertical line and the line from the hip joint to the ankle joint on a sagittal plane (Malone et al. 2012). Because cats walk on the toes, I will define the limb angle differently – as the angle between a vertical line and the line from the hip joint to the metatarsophalangeal (MTP) joint in a sagittal plane (Pantall et al. 2012). In addition, walking kinematic parameters between the ipsilateral forelimb and hindlimb will be necessary to consider to fully understand quadrupedal locomotion. The phase difference between the ipsilateral forelimb and hindlimb at the stance onset has been evaluated for cats or quadrupedal mammals (Blaszczyk and Loeb 1993; Cartmill et al. 2002).

CHAPTER 2

EFFECTS OF MODULATING SELECTED PERIPHERAL SENSORY FEEDBACK ON SPATIAL AND TEMPORAL GAIT PARAMETERS

2.1. Introduction

Somatosensory motion-dependent feedback has been suggested to regulate the level of muscle activity and to reset movement phases during locomotion (Duysens et al. 2000; Pearson 2008; Rossignol et al. 2006). For example, the cutaneous sensory feedback from plantar surface of the foot is involved in regulation of balance and locomotor phase durations. Several studies in humans and cats have demonstrated that this type of sensory feedback is critical for maintaining balance during postural tasks (Meyer et al. 2004; Honeycutt and Nichols, 2010), for recovery of balance after postural perturbations during locomotion (Bolton and Misiaszek, 2009; Hohne et al. 2011) and for the successful performance of demanding locomotor motor behaviors, e.g. walking on a horizontal ladder or slopped surface (Bouyer and Rossignol, 2003). Cutaneous paw pad afferents are also involved in regulation of the stance phase duration during locomotion. A low-intensity electrical stimulation of the hindlimb paw skin or cutaneous afferents in the sural or distal-tibial nerve during the stance (or extensor) phase of walking enhances activity of extensor muscles and changes the duration of the stance and swing phase (Duysens and Pearson 1976; Guertin et al. 1995; Loeb 1993), whereas the same stimulations of the cutaneous nerves during flexor activity triggers the transition from the flexor to extensor activity (Guertin et al. 1995).

Muscle length-dependent sensory feedback from hip muscles has been suggested to reset locomotor rhythm and regulate phase transitions. For instance, imposed

movements of the hip joint cause entrainment of fictive locomotor rhythm in the decerebrate cat preparation (Andersson and Grillner 1983; Kriellaars et al. 1994). Electrical stimulation of group II afferents from the sartorius and iliopsoas nerves during the flexor phase of fictive locomotion resets the ongoing flexor activity to extensor throughout the hindlimb muscle nerves, whereas stimulation of sartorius and iliopsoas group I afferents enhances the ongoing flexor activity (Stecina et al. 2005). The hip flexion angle and length of hip extensor muscles in the terminal swing phase during level and slope walking in the cat correlates strongly with the termination of the flexor activity and onset of extensor activity (Gregor et al. 2006; McVea et al. 2005).

The described effects of somatosensory feedback from cutaneous afferents on the plantar surface of the foot and muscle stretch-dependent afferents from hip muscles appear to be profound and can potentially severely disrupt symmetry and stability of walking in people with neuropathy or lower limb loss. These effects may be greater during more complex tasks demanding an additional level of inter-joint and inter-limb coordination, e.g. in slope walking or split-belt treadmill locomotion. On the other hand, removal of muscle stretch-dependent feedback by muscle self-reinnervation (Cope et al. 1994; Cope and Clark 1993) from the ankle extensor muscles demonstrates only modest movement deficiency during downslope walking (exaggerated ankle yield in the stance phase) but not during level or upslope walking (Abelew et al. 2000; Maas et al. 2007) or in paw shake responses in the cat (Mehta and Prilutsky 2014). Thus, it appears that the effects of somatosensory feedback on rhythmic movements, including locomotion, depend on the source and modality of sensory information.

Computational modeling of the locomotor central pattern generator (CPG) and its control by sensory feedback (McCrea and Rybak 2007; Rybak et al. 2006) might suggest that somatosensory pathways that have access to the CPG circuitry, as opposed to sensory feedback that controls local reflexes, have more profound effects on locomotion. Neuromechanical computer simulations have provided some preliminary evidence for

such a conclusion. For example, stable walking of a cat neuromechanical model could not be achieved without force dependent excitatory input from ankle extensors (Ekeberg and Pearson 2005; Markin et al. 2016). This input (presumably mostly from group Ib Golgi tendon afferents; (Conway et al. 1987; Gossard et al. 1994; McCrea et al. 1995)) enhances activity of all hindlimb extensor muscles in the hindlimb and thus apparently has access to the CPG extensor half-center (Gossard et al. 1994; Pearson and Collins 1993; Rybak et al. 2006). Stable walking of a neuromechanical model is disrupted by removal of length-dependent sensory feedback from spindle group Ia and II afferents from hip muscles that in the model triggers the transitions between the flexor and extensor phases of the locomotor rhythm by excitatory input to a half-center (Markin et al. 2010; 2016).

The potentially profound effect of the foot cutaneous afferent pathways on activity of multiple muscles (Guertin et al. 1995; Hoogkamer et al. 2012) and locomotor kinematics (Ollivier-Lanvin et al. 2011; Zehr et al. 1998) and the accessibility of these afferents for external manipulation of their activity, raise the possibility to use these pathways for correcting locomotor deficiencies due to various neuromuscular conditions (limb loss, neuropathies, stroke, etc.).

Therefore, the general goal of this study was to determine the effects of manipulation of cutaneous feedback from paw pad afferents and muscle stretch-dependent feedback from quadriceps and sartorius muscles, crossing the hip and knee joints, on kinematics of walking in the cats. The cutaneous feedback was manipulated by injecting lidocaine into each paw pad of ipsilateral hindpaw and forepaw and by electrical stimulation of the distal-tibial nerve during stance. The muscle length and velocity-dependent feedback was manipulated by changing speed of a split-belt treadmill and by self-reinnervation of the quadriceps (Quad) and sartorius (Sart) muscles that removes muscle stretch-reflex (Lyle et al. 2016).

The following hypotheses were tested**:** (1) During the split-belt treadmill walking, tactile modulation will show greater effect when two belts move at different speeds, than at the same speed. It is because tactile feedback plays an important role in challenging gait conditions (Bouyer et al. 2003; Bolton et al. 2009; Corriveau et al. 2000).

(2) During the split-belt treadmill walking, modulation of belt speed ratio will cause cats to shift their body weight to the slower belt. This shift is assumed to reduce the distance travelled by the center of mass (COM) in each walking cycle and thus to decrease energy expenditure.

(3) Anesthesia of ipsilateral paw pads would cause changes in walking kinematics, and the changes would increase with increasing the speed of the ipsilateral treadmill belt with respect to the contralateral belt. This hypothesis is based on the fact that cats with denervated paws are able to recover kinematics of normal level walking, but have kinematic deficits during challenging tasks such as slope and ladder walking (Bouyer and Rossignol 2003) or maintenance of stable walking after postural perturbations (Bolton and Misiaszek 2009).

(4) Changes in walking kinematics caused by paws' anesthesia would be reduced by electrical stimulation of the distal-tibial nerve during the stance phase of the affected hindlimb. Justification for this hypothesis is based on studies, in which individuals with hand loss were able to perceive natural touch sensations of the phantom hand when the residual cutaneous nerves were electrically stimulated (Graczyk et al. 2016; Tan et al. 2014).

(5) Removal of stretch reflex from muscles crossing the hip joints (Quad-Sart) would delay the stance-swing transition in the affected hindlimb. This expectation is based on the current understanding of the role of length-dependent sensory feedback from hip flexors in locomotor rhythm resetting and the stance-swing phase transition (Kriellaars et al. 1994; Markin et al. 2016; Pearson 2008) – the stance-swing transition is

triggered by the stretch of hip flexor muscles whose length approaches peak values in late stance (Gregor et al. 2006).

(6) Stimulation of the distal-tibial nerve during the stance phase of walking in cats with the self-reinnervated Quad-Sart would further increase the delay of the stance-swing transition and thus make kinematics of walking more asymmetric. This proposition follows from the currently accepted conditions for the cessation of the stance and initiation of swing phase – the sufficient stretch of hip flexors and unloading the hindlimb (Pearson 2008). If stimulation of the distal-tibial nerve, innervating hindlimb cutaneous paw pad afferents, reduced the effects of paw pad anesthesia (see hypothesis iii), this stimulation might provide some perception of contact with the ground and limb loading and thus delay the stance to swing transition.

2.2. Materials and Methods

All surgical and experimental procedures were conducted in agreement with the Principles of Laboratory Animal Care (NIH publication No.86-23, revised 1985) as approved by the Georgia Tech Institutional Animal Care and Use Committee.

Experimental Procedures. Four female adult cats (mass 3.3±0.5 kg, Table 2.1) were trained to walk on an instrumented split-belt treadmill (Bertec Corporation, Columbus, OH, USA) using food reward prior to any surgical procedures. Four speed combinations of the left and right treadmill belts were used for training and during experiments (Fig. 2.1) and speed ratio is defined by the right belt speed divided by the left belt speed: 0.8 and 0.4 m/s (speed ratio 0.5), 0.4 and 0.4 m/s (speed ratio 1.0), 0.4 and 0.6 m/s (speed ratio 1.5) and 0.4 and 0.8 m/s (speed ratio 2.0). For every speed combinations, both left and right belt initially moved at 0.4 m/s for 15 seconds. Then speed of one belt was increased within approximately 2-5 s and stayed at each speed for 60 s. After that, speed of that belt returned to 0.4 m/s and the cat walked for another 15

seconds with both belts moving at 0.4 m/s. Within each experimental session, speed conditions were randomized. Cats walked on the split-belt treadmill with 6 different afferent modulation conditions: (1) intact condition; (2) right fore- and hind paw-pads anesthetized; (3) right fore- and hind paw-pads anesthetized and the right distal-tibial nerve stimulated during the stance period; (4) the right Quad-Sart self-reinnervated; and finally; (5) condition 4 was repeated with the right distal-tibial nerve stimulated during the stance period. Set of experiments for each experimental condition took about 30 min and was conducted at separate day.

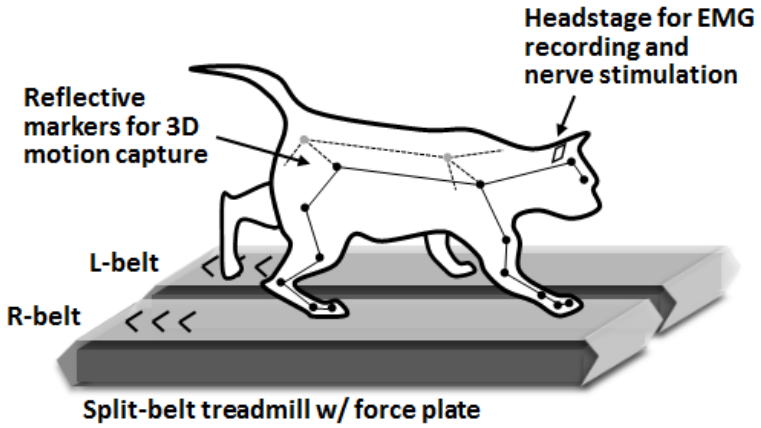

	Baseline (same speed)	Adaptation (four different speed ratios)	Post (same speed)
L-belt	0.4 m/s	L|R: 0.8|0.4, 0.4|0.4, 0.4|0.6, or 0.4|0.8	0.4 m/s
R-belt	0.4 m/s		0.4 m/s
	15 sec	60 sec	15 sec

Figure 2.1. Experimental setting on the split-belt treadmill. See text for details.

Table 2.1. Cat characteristics and the number of analyzed walking cycles

Cat	Mass, kg	Analyzed cycles in each experimental condition (speed ratio 0.5/1.0/1.5/2.0)				
		Intact	Anesth	Anesth + Stim	Self-reinner	Self-reinner + Stim
TA	3.00	-/56/80/25	-/54/60/14	-/61/58/10	-	-
MO	4.10	67/52/65/72	68/46/69/76	71/38/47/76	-	-
WE	2.55	75/33/71/76	47/52/75/34	76/58/69/45	-	-
NO	2.65	75/20/53/43	37/12/18/9	-/37/38/7	-	-
JU	3.45	-	-	-	-/72/73/70	-/58/78/80
VE	3.35	-	-	-	74/42/59/67	65/47/63/65
ES	3.83	-	-	-	-/56/34/61	-
AM	3.20	-	-	-	-/29/-/-	-
Mean±SD	**3.3±0.5**	**57±19**	**45±23**	**49±22**	**58±16**	**65±11**

Notes: Stim, electrical stimulation of the distal-tibial nerve during the stance phase of walking; Anesth, anesthesia of paw pads of the right hind- and forelimb; Reinner, self-reinnervation.

After locomotor training and recovery from surgical implantation of EMG and nerve cuff-electrodes (see below), 3D positions of 28 small reflective markers on the cat (Fig. 2.2) were recorded by Vicon high-speed motion capture system (Oxford, UK) with sampling rate of 120 Hz. In addition, electromyographic (EMG) activity of selected muscles in the right hindlimb was recorded with sampling rate of 3000 Hz. In selected cats, the vertical component of the ground reaction force from each treadmill belt were recorded with sampling rate of 120 Hz.

Surgical procedures. Two surgeries were performed – one for implantation of EMG and nerve cuff-electrodes and another one for transection and repair of Quad and Sart nerves. All surgeries were performed in sterile conditions under isoflurane anesthesia as described in details elsewhere (Lyle et al. 2016; Pantall et al. 2016; Prilutsky et al. 2011). Selected muscles of the right hindlimb were implanted with bipolar EMG electrodes made of Teflon-insulated multi-stranded stainless steel wires (Conner Wire, Chatsworth, CA, USA). Leads of the electrodes were passed under skin to a multi-pin connector fixed on the skull with titanium screws and dental cement. Location of the implanted wires was verified during the surgery by mild electrical stimulation through the

connector on the skull. Two custom-made nerve-cuff electrodes were implanted on the distal-tibial nerve at the level of the Achilles tendon and on the sciatic nerve in the mid-thigh. The procedures for fabrication and implantation of these electrodes were described in details in (Ollivier-Lanvin et al. 2011). The bipolar cuff electrode on the distal-tibial nerve was implanted for stimulating cutaneous afferents on hindpaw pads and plantar skin of the foot. The tripolar sciatic cuff electrode was implanted to establish the activation threshold of afferents activated by stimulation of the distal-tibial nerve. The cuff electrodes were made of platinum foil (thickness 0.025 mm, width 3 mm, lengths depended on nerve diameter; Sigma-Aldrich, St. Louis, MO, USA) embedded in silicon and Teflon-insulated multi-stranded stainless steel wires (Fig. 2.3).

After surgery, each cat received pain medication for 3 days and antibiotics for 10 days, and recovered for at least 14 days. Once the recording and stimulation electrodes were implanted and the animal recovered, locomotor experiments were conducted that did not involve conditions with self-reinnervated Quad and Sart (Table 1). These conditions included intact walking, paw anesthesia and stimulations of the distal-tibial nerve.

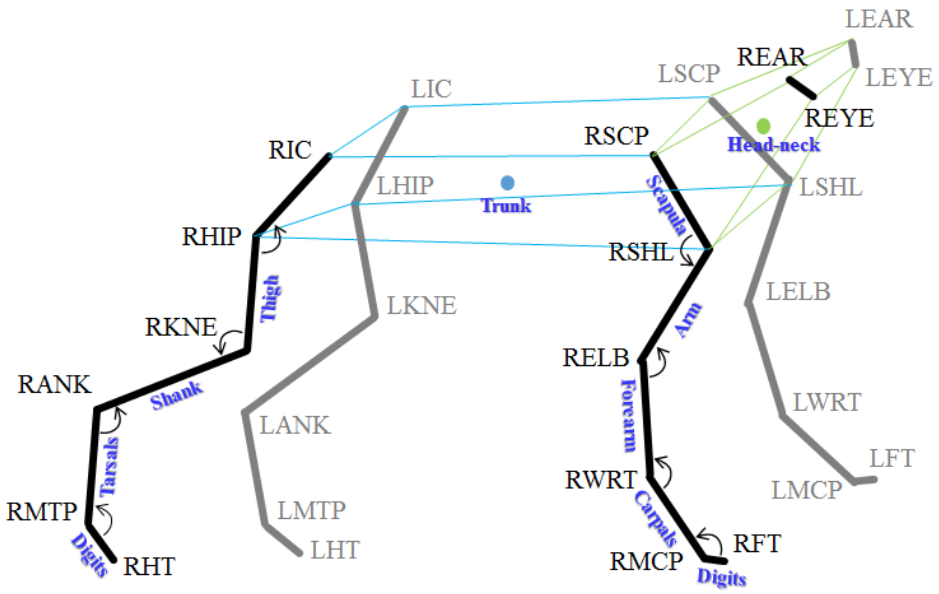

Figure 2.2. A schematic of a mechanical model of the cat. The cat was represented as a system of 20 rigid segments with frictionless joints (Prilutsky et al. 2005). Reflective markers placed on the cat defined joint locations and the body segments. The mass, position of the center of mass and moment of inertia of each segment were calculated using the regression equations (Hoy and Zernicke 1985) and measured cat mass and length of each segment. The general center of mass (CoM, blue circle) is computed based on the positions of center of mass of each segment (Farrell et al. 2014). Abbreviations: RIC and LIC, right and left iliac crest; RHIP and LHIP, right and left hip, RKNE and LKNE, right and left knee; RANK and LANK, right and left ankle; RMTP and LMTP, right and left metatarsophalangeal joint; RHT and LHT, right and left toe; RSCP and LSCP, right and left scapular; RSHL and LSHL, right and left shoulder; RELB and LELB, right and left elbow; RWRT and LWRT, right and left wrist; RMCP and LMCP, right and left metacarpophalangeal joint; RFT and LFT, right and left fore toe; REAR and LEAR, right and left ear; and REYE and LEYE, right and left eye.

At a conclusion of these experiments, a second survival surgery was conducted, during which nerves to Quad and Sart were transected, aligned in original position and secured in place by a fibrin glue (equal parts of thrombin and a 1:1 mixture of fibrin and fibronectin; Sigma-Aldrich, St. Louis, MO, USA; (English 2005; Lyle et al. 2016; Prilutsky et al. 2011)). Three to four months later, the EMG magnitude of the muscles with the repaired nerves reached or exceeded the pre-surgery level (Mehta et al. 2014; Mehta and Prilutsky 2014; Pantall et al. 2016) indicating that the self-reinnervation process was largely completed. Self-reinnervated muscles, e.g. heads of cat triceps surae or quadriceps, lack stretch reflex (Cope et al. 1994; Lyle et al. 2016; Maas et al. 2007), i.e. their length-dependent feedback is substantially degraded.

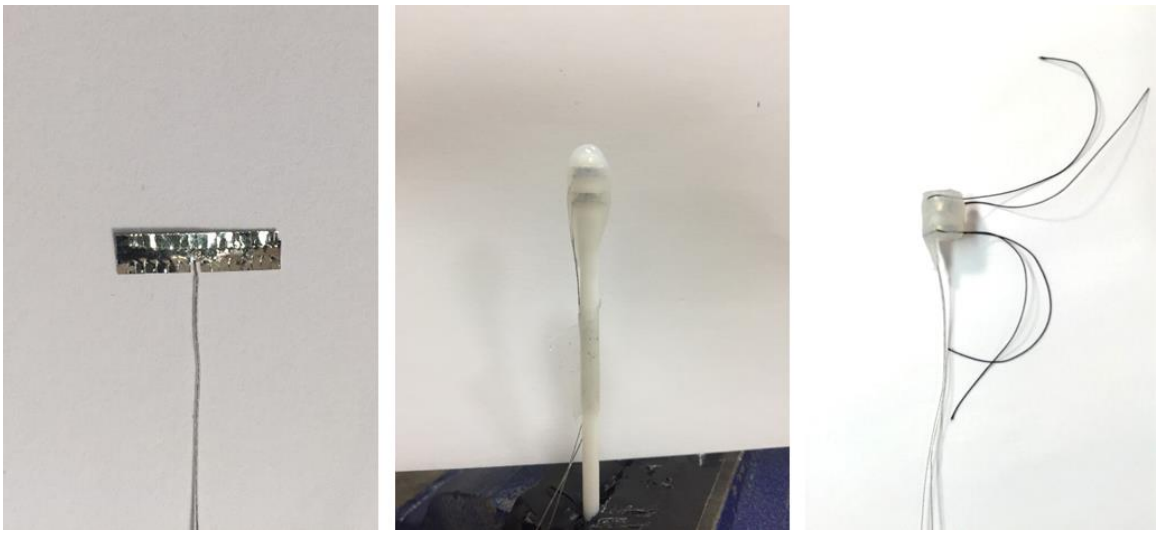

(a) (b) (c)

Figure 2.3. Nerve cuff electrode used for electrical nerve stimulation and recording. (a) platinum foil with a welded conducting wire, (b) two electrodes with platinum foils covered by silicon, and (c) finished nerve cuff electrode with two conducting wires and two sutures to close the gap in the silicon after implantation on the nerve.

Design of the stimulator. Stimulator was designed with two P-channel MOS transistors and two N-channel MOS transistors, along with a current steering circuit on the bottom (Shulyzki et al. 2010). It is designed to generate a biphasic constant current stimulus under a single supply voltage. This stimulator can generate arbitrary form of stimulus with user-defined frequency and pulse width, because the MOS transistors are controlled by the digital signals of MCU programmed by the user via JTAG interface. In addition, the MCU controls the current steering circuit on the bottom of the stimulator, to set amplitude of the stimulus as programmed by the user via JTAG interface.

Determining activation threshold of hindpaw cutaneous afferents. After animals fully recovered from the surgery, the stimulation threshold (T) for activating cutaneous afferents in the distal-tibial nerve was established in each cat by recording the compound action potential in the sciatic cuff electrode in response to distal-tibial nerve stimulations of different intensities (Ollivier-Lanvin et al., 2011). The parameters of the nerve

stimulation were selected based on the reports of natural touch sensation in the phantom hand of human subjects with upper limb loss whose residual cutaneous nerves were stimulated with these parameters (Tan et al. 2014). The distal-tibial nerve was stimulated by trains of 200-μs biphasic rectangular pulses at 100 Hz for 500 ms duration. The duration of stimulation was selected based on the approximate mean duration of the stance phase during walking across all experimental conditions. To establish the activation threshold of cutaneous afferents in the distal-tibial nerve to this stimulation, the cat was sedated by intramuscular injection of dexmedetomidine (40-60 μg/kg). Stimulation trains of a given strength were delivered to the tibial nerve for 500 ms and the responses recorded in the sciatic nerve. Each stimulation train was separated by a period of 2-3 min. The stimulation strength varied from 5 μA to 1.5 mA with a logarithmic scale of steps from 2.5μA to 250 μA. An example of sciatic nerve activity in response to distal-tibial nerve stimulation is shown in Fig. 2.4. The smallest magnitude of stimulation that evoked a detectable response in the sciatic nerve was considered an activation threshold of cutaneous afferents. Although the distal-tibial nerve also innervates intrinsic toe flexors and their low threshold muscle spindle and Golgi tendon afferents, no detectable toe flexion occurred at the threshold stimulation of the nerve. This indicated that there was no substantial activation of low threshold group I afferents of toe flexors; otherwise, a substantial number of muscle motor units would have been activated (H-reflex) and cause a visible muscle twitch. Muscle twitches typically occurred at stimulation strength of 20~25T in all cats. Limb withdrawal, indicating activation of high threshold nociceptive group III-IV afferents, typically occurred at 50~100T.

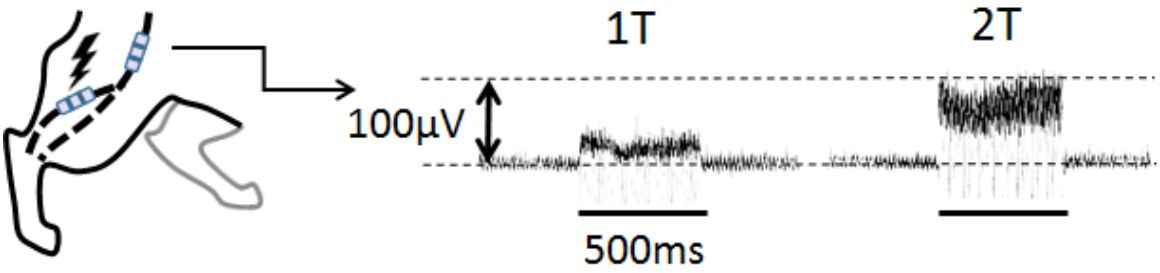

Figure 2.4. Compound action potential evoked in the sciatic nerve by electrical stimulation of the distal-tibial nerve. Two horizontal lines indicate the periods of nerve stimulation. 1T indicates the smallest detectable sciatic nerve activity in response to stimulation of the distal-tibial nerve. 2T indicates sciatic nerve activity in response to tibial nerve stimulation with strength of 2 x threshold.

Reversible removal of tactile sensation from paw pads. To remove tactile sensation from right forepaw and hindpaw, the cat was sedated by intramuscular injection of dexmedetomidine (40-60 μg/kg). Each paw pad of the right hindpaw and forepaw was injected with 1 ml of the 1% diluted lidocaine solution. Then the animal was awaken by receiving intramuscularly antipamezole (same volume as dexmedetomidine). Effectiveness of paw anesthesia was tested continuously by attaching a piece of adhesive tape to the paw to evoke paw shaking or by pin pricks to evoke limb withdrawal. Paw anesthesia was effective for at least 30 min. Locomotor experiments with paw anesthesia were conducted during this period. The experiments were stopped as soon as paw shaking or limb withdrawal was first observed.

Stimulation of distal-tibial nerve during locomotion. Stimulation of the right distal-tibial nerve was triggered by the right hindpaw contact with the ground. To detect a hindpaw ground contact, a force sensor has been installed below the right treadmill belt. The force sensor triggered the stimulation if the applied force was larger than 5 N, and it prepared itself to generate next trigger signal if the applied force is smaller than 1 N (i.e. both right hindpaw and forepaw were in the air). The stimulation parameters were as follows: trains of 200-μs biphasic rectangular pulses at 100 Hz for 500 ms duration, stimulation strength 1.2T.

Degrading length-dependent sensory feedback from right Quad and Sart. Nerve transection and repair of Quad and Sart and their subsequent self-reinnervation, indicated by recovering EMG activity in vasti and rectus femoris muscles (heads of Quad) during walking (Mehta et al. 2014), removed stretch-reflex from these muscles. The lack of stretch reflex in heads of Quad (vasti and rectus femoris) from cats received this procedure (Table 2.1) was confirmed in terminal experiments conducted at completion of the locomotion studies in the lab of Dr. T. Richard Nichols (Lyle et al. 2016). EMG activity or stretch reflex of Sart were not recorded; although given previous studies cited above, it is likely that Sart was also self-reinnervated and lacked stretch reflex.

Data Analysis. To exclude possible effects of motor adaptation to split-belt treadmill locomotion (see results below), I excluded the first 10 cycles after each speed change for gait analysis. Kinematic analysis was performed for each walking cycle (see Table 2.1 for the number of analyzed cycles for each cat and experimental condition). Recorded marker coordinates were first low-pass filtered by a 4^{th} order, zero-lag Butterworth filter with a cut-off frequency of 6 Hz. Filtered coordinates were used to determine kinematic parameters of walking, including limb excursion (or stride length during split-belt treadmill walking (Hoogkamer et al. 2014)), step length, stride and step durations, duty factor, pacing, spatial and temporal symmetry (Torres-Oviedo et al. 2011), etc.).

EMG analysis. EMG activity recorded at 3000 Hz during selected walking conditions from soleus (SO), medial gastrocnemius (MG) and iliopsoas (IL) was bandpass filtered from 30 Hz to 1000 Hz and full-wave rectified. The rectified raw EMG was used to identify EMG burst onset and offset using a 2SD threshold above the baseline (Gregor et al. 2006; Hodson-Tole et al. 2012). The identified burst was time integrated to determine the mean burst activity. The mean EMG activity was normalized to the maximum mean activity found for a given muscle across all walking trials of a given cat.

Walking cycle. Onset and offset of a walking cycle for each limb was identified using the limb angle with respect to the vertical (Pantall et al. 2012). According to this method, the stance phase and limb cycle onset corresponded to the maximum positive (counterclockwise) limb angle, whereas the stance and limb cycle offset corresponded to the minimum negative limb angle (Fig. 2.5). The maximum and minimum limb angles were also called the forward and backward limb angle, respectively.

Phase duration and duty factor. The duration of the stance and swing phases was defined based on the stance onset and offset timing (see Fig. 2.5). The duty factor for each limb was defined as the ratio of the stance duration to the sum of stance and swing phase durations.

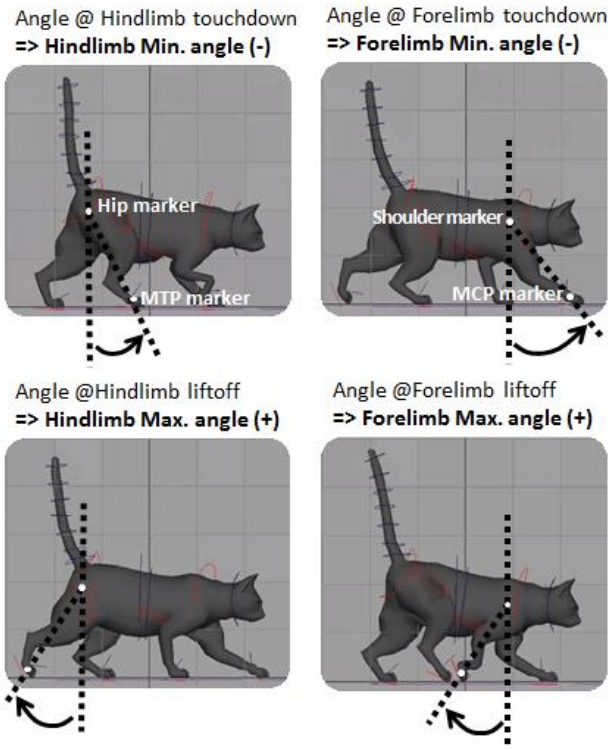

Figure 2.5. Definitions of the stance or cycle onset and offset for fore- and hindlimbs. Forelimb and hindlimb angle was defined as the angle between the vertical and the limb line. Forelimb line was defined as the line connecting the shoulder and MCP markers; hindlimb line, as the line between the hip and MTP markers.

Step length and spatial step symmetry were defined as shown in Fig. 2.6. Specifically, the step length of the right hindlimb was defined as the distance in the sagittal plane between the right MTP and left MTP markers at the moment of the right paw contact. The step length for other limbs was defined similarly (Fig. 2.6). Spatial step symmetry for hindlimbs was defined as the ratio of the right hindlimb step length to the sum of the left and right step lengths (Malone and Bastian 2014), see Fig. 2.6.

$$Spatial\ step\ symmetry\ (forelimb) = \frac{Step.L_{RF}}{Step.L_{LF} + Step.L_{RF}}$$

$$Spatial\ step\ symmetry\ (hindlimb) = \frac{Step.L_{RH}}{Step.L_{LH} + Step.L_{RH}}$$

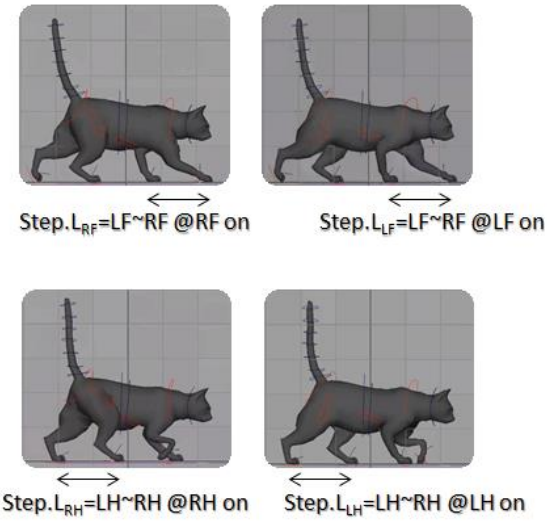

Figure 2.6. Definitions of spatial step symmetry for fore- and hindlimbs. L_{RF}, L_{LF}, L_{RH}, L_{LH} are step length for the right forelimb, left forelimb, right hindlimb and left hindlimb, respectively.

Temporal step symmetry was defined using step durations. The right-forelimb step duration was defined as the elapsed time from the left-forelimb stance onset to the right-forelimb stance onset. Then the right-forelimb temporal step symmetry was determined as the ratio of the right-forelimb step duration to the left-forelimb stride duration (elapsed time between the current stance onset and the next stance onset of the left forelimb). Hindlimb temporal step symmetry was defined in the same way. The graphical

representation of the hindlimb temporal step symmetry is shown in Fig. 2.7. Additionally, the temporal step symmetry at stance offset was determined. In this case, the step duration was defined as the elapsed time from the stance offset of a left limb to the stance offset of the corresponding contralateral limb.

$$Temporal\ step\ symmetry\ (onset, forelimb) = \frac{t_{RF.on} - t_{LF.on}}{t_{LF.on}{}' - t_{LF.on}}$$

$$Temporal\ step\ symmetry\ (onset, forelimb) = \frac{t_{RF.on} - t_{LF.on}}{t_{LF.on}{}' - t_{LF.on}}$$

$$Temporal\ step\ symmetry\ (offset, hindlimb) = \frac{t_{RH.off} - t_{LH.off}}{t_{LH.off}{}' - t_{LH.off}}$$

$$Temporal\ step\ symmetry\ (offset, hindlimb) = \frac{t_{RH.off} - t_{LH.off}}{t_{LH.off}{}' - t_{LH.off}}$$

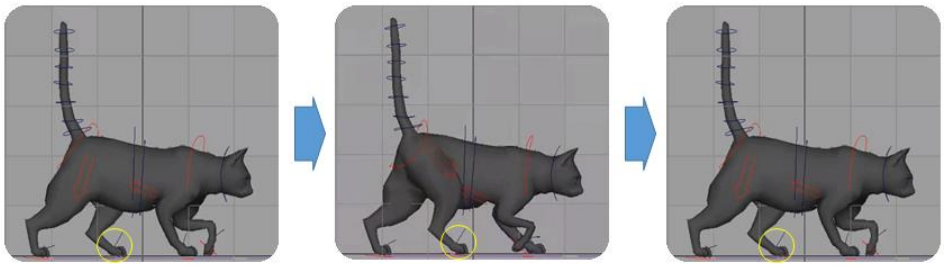

Figure 2.7. Definitions of temporal step symmetry for hindlimbs. $t_{LH.on}$, $t_{RH.on}$, $t_{LF.on}$, $t_{RF.on}$ are time of stance onset by left hindlimb, right hindlimb, left forelimb and right forelimb, respectively. $t_{LH.off}$, $t_{RH.off}$, $t_{LF.off}$, $t_{RF.off}$ are time of stance onset by left hindlimb, right hindlimb, left forelimb and right forelimb, respectively.

Step width. The hindlimb step width was defined as the mean value of left hindlimb step width and right hindlimb step width. Each hindlimb step width, as shown in Fig. 2.8, was defined as the lateral distance between the centers of the ipsilateral and contralateral hindpaws determined at the stance onset of ipsilateral hindlimb. Forelimb step width was defined in the same way. To determine the paw center of each limb, the coordinates of the toe marker was shifted by the distance comprising the marker radius (4.5 mm) and a half of paw width (15 mm). The graphical representation of the definition of the hindlimb step width is shown in Fig. 2.8.

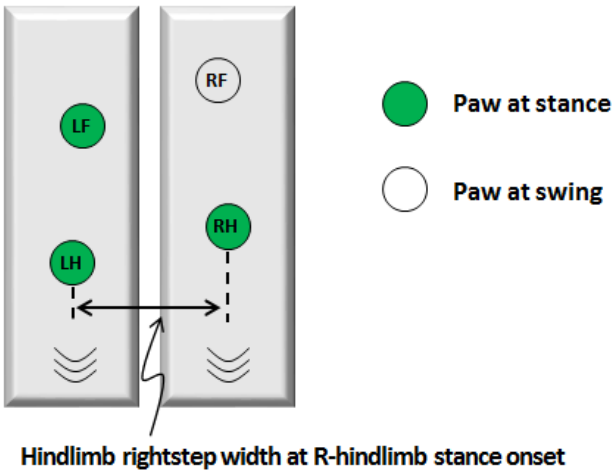

Figure 2.8. A schematic demonstrating the step width definition for hind- and forelimbs. LF, RF, LH and RH are the left forelimb, right forelimb, left hindlimb and right hindlimb, respectively.

Center of mass (COM) lateral bias was defined as the ratio of the lateral distance between the CoM and the center of right hindpaw (CoM – RH) averaged over the hindlimb stride to the lateral distance between the centers of left and right hindpaws (LH – RH) averaged over the hindlimb stride (Fig. 2.9).

$$\textit{CoM lateral bias} = \textit{mean}\left(\frac{CoM \sim RH}{LH \sim RH}\right) \textit{per cycle}$$

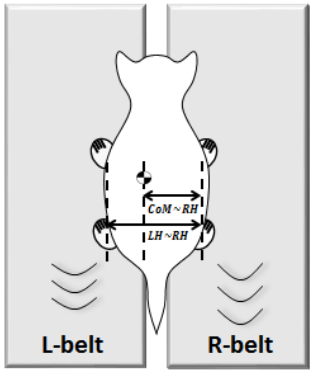

Figure 2.9. A schematic demonstrating the definition of the lateral bias of the center of mass (COM). LH and RH are the left hindlimb and right hindlimb position, respectively.

Pacing or Diagonality was defined for left limbs and right limbs as the phase difference between the forelimb stance onset and the ipsilateral hindlimb stance onset (Hildebrand 1965); see Fig. 2.10.

$$Diagonality.L = \frac{t_{LF.on} - t_{LH.on}}{t_{LH.on}{}' - t_{LH.on}}$$

$$Diagonality.R = \frac{t_{RF.on} - t_{RH.on}}{t_{RH.on}{}' - t_{RH.on}}$$

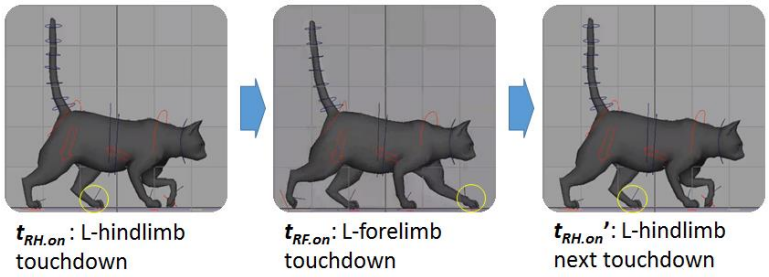

Figure 2.10. A schematic demonstrating the definition of the pacing or diagonality. LH and RH are the left hindlimb and right hindlimb position, respectively. $t_{LH.on}$, $t_{RH.on}$, $t_{LF.on}$, $t_{RF.on}$ are the normalized times of stance onset by left hindlimb, right hindlimb, left forelimb and right forelimb, respectively.

Statistics. A linear mixed model analysis (SPSS 19, IBM SPSS, Chicago, IL, USA) was used to determine effects of independent factors (anesthesia, nerve stimulation, treadmill speed ratio, Quad-Sart self-reinnervation) on the dependent kinematic and EMG variables. For each dependent variable, the main effect of independent factors and their interactions were determined. If effects were found significant, a post-hoc paired comparison with Bonferroni adjustment was performed. Significance level was set at 0.05.

2.3. Results

2.3.1. Effects of Belt Speed Ratio on Kinematics of Split-Belt Treadmill Walking

To establish whether there was no substantial changes in walking kinematics during split-belt walking due to motor adaptation, as reported in (Kuczynski et al. 2015), the spatial and

temporal step symmetry, as well as the duty factor were determined for each walking cycle for one split-belt speed ratio of 1.5 (0.4 m/s and 0.6 m/s for the left and right belt, respectively). There was a significant difference ($p<0.05$) in the spatial step symmetry of the fore- and hindlimb between the mean of the first 5 cycles of walking with the new speed ratio and the mean of next 5 cycles (paired t-test; Fig. 2.11). No significant difference was found between the mean of the spatial step symmetry in the second 5 cycles and in the mean of any subsequent sets of 5 cycles (Fig. 2.11). No significant change in the temporal step symmetry of the fore- and hindlimb was found throughout the recording session, including during walking with speed ratio of 1.5 (Fig. 2.11). Finally, the duty factor did not show signs of motor adaptation during switching to a new speed ratio (Fig. 2.11). Since the analyzed kinematic variables did not change beyond cycle 10 after the transition to a new speed ratio, all kinematic variables were averaged at a given speed ratio except the first 10 cycles that were excluded from the analysis.

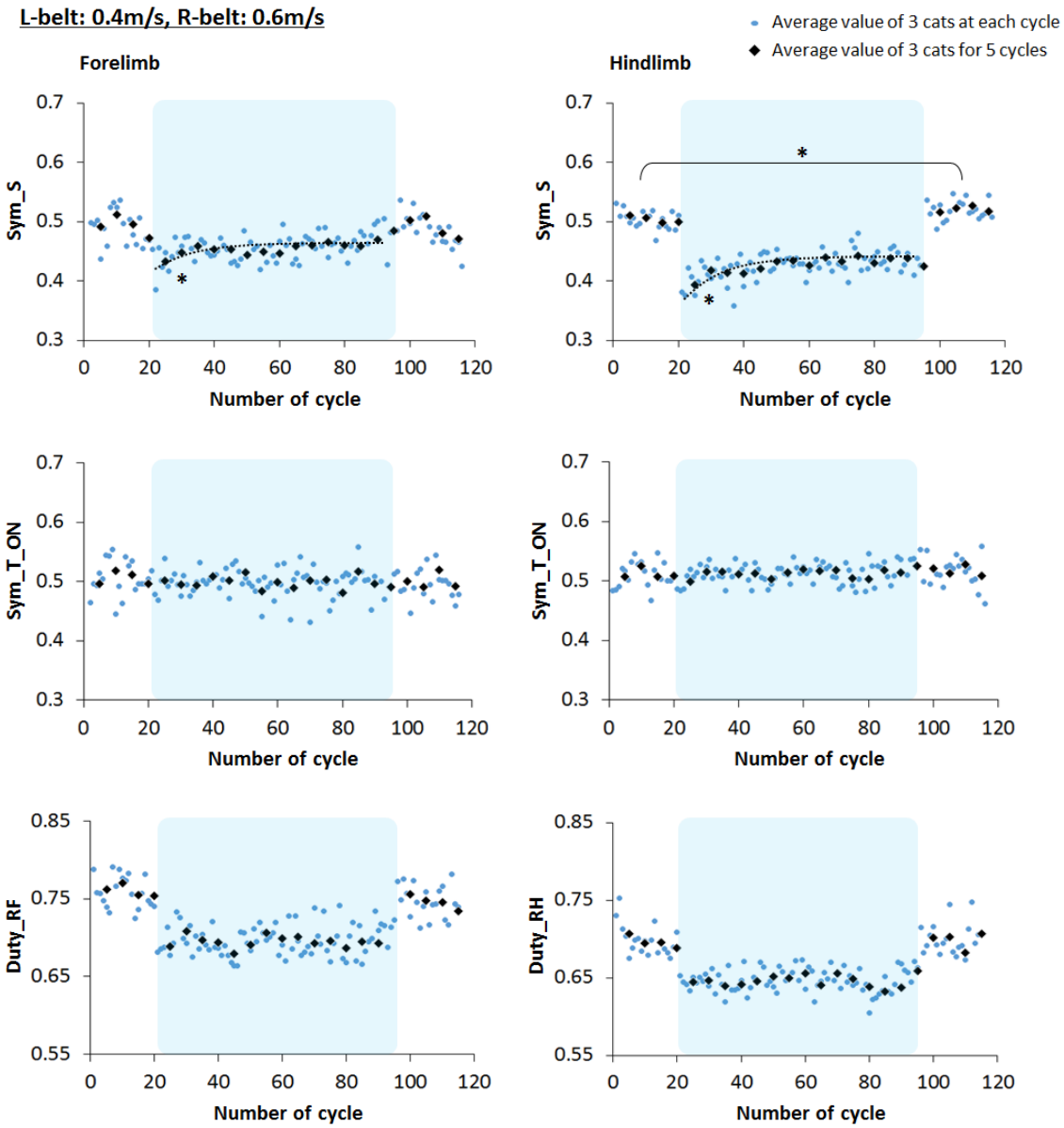

Figure 2.11. Averaged transient response to a change in the speed ratio between 1.0 and 1.5 for the spatial step symmetry (Sym_S), temporal step symmetry at stance onset (Sym_T_ON) and duty factor of right fore- and hindlimb for three cats.

COM lateral bias increased from 0.476±0.012 (a slight bias to the right, which might be caused by the surgery on right hindlimb) at the smallest speed ratios of 0.5 to 0.650±0.013 (a strong left bias) at the maximum speed ratio of 2.0 (Fig. 2.12). Note a slight left COM bias at the speed ratio of 1.0 (0.521±0.013).

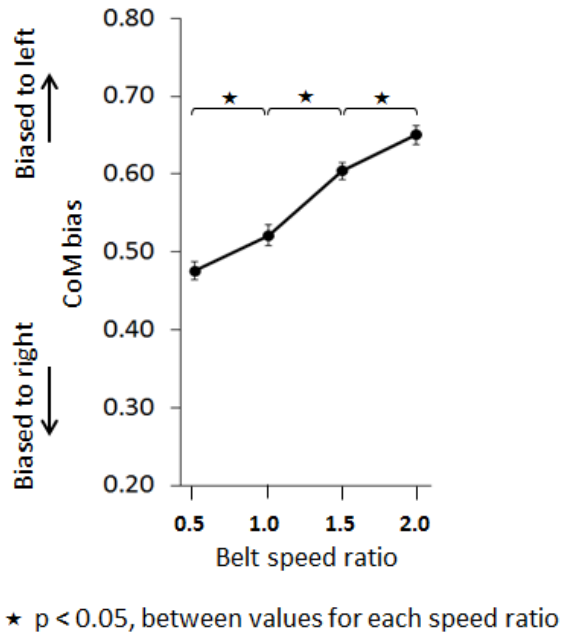

Figure 2.12. Mean (±95% confidence interval) of COM lateral bias as a function of belt speed ratio.

Duty factor of the left fore- and hindlimbs increased with the belt speed ratio from 0.626±0.006 and 0.583±0.006 at ratio 0.5 to 0.767±0.004 and 0.758±0.004 at ratio 2.0 ($p<0.05$). For the right limbs the duty factor decreased from 0.768±0.005 and 0.746±0.004 at ratio 0.5 to 0.637±0.005 and 0.602±0.005 at ratio 2.0 ($p<0.05$). The duty factor was also significantly lower for the hindlimbs than forelimbs ($p<0.05$) (Fig. 2.13).

Phase duration. Durations of the cycle, stance phase and swing phase of the left and right hindlimbs were significantly affected by the speed ratio (Fig. 2.14) even for the left fore- and hindlimbs that were walking on the belt that did not change speed at speed ratios 1.0, 1.5 and 2.0. Specifically, the cycle duration was longest (near 0.9 s) for all limbs at speed ratio 1.0 (both belts moved at speed of 0.4 m/s), and decreased when one of the belts moved at a faster speed (speed ratio different from 1.0). There was not significant difference in cycle duration between forelimbs and hindlimbs on either side of the body.

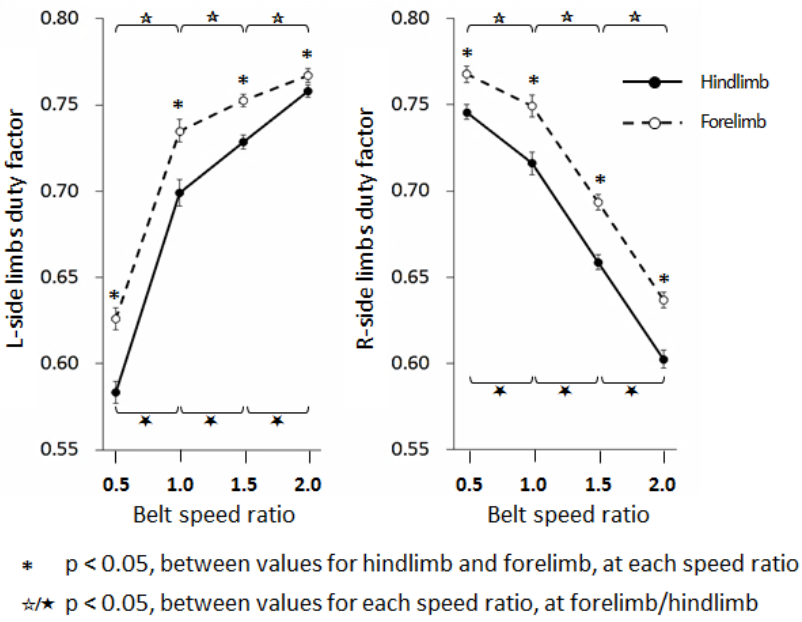

Figure 2.13. Mean (±95% confidence interval) of the duty factor for all four limbs as a function of belt speed ratio.

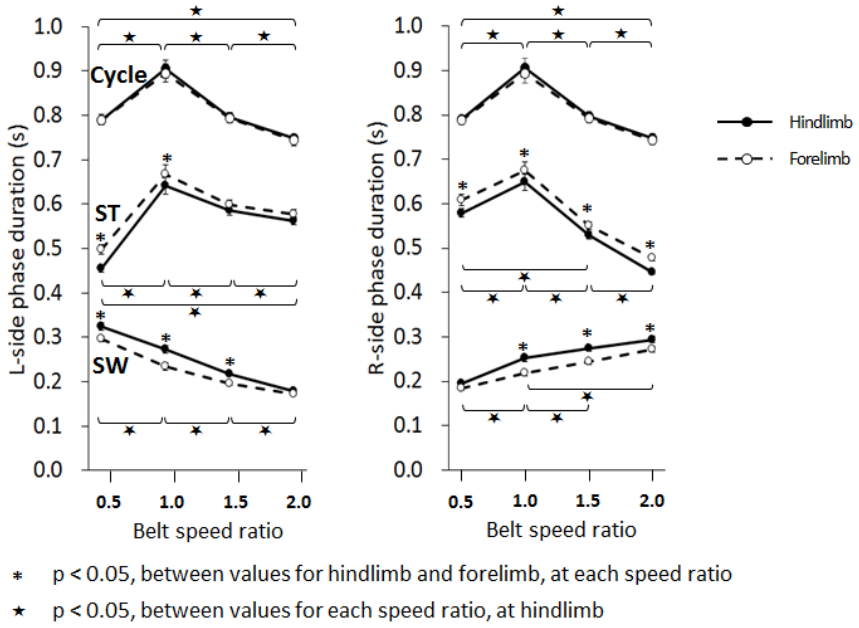

Figure 2.14. Mean (±95% confidence interval) of durations of the cycle, stance phase and swing phase for all four limbs as a function of belt speed ratio.

Changes in the stance phase durations were generally similar to those of the cycle duration with the longest stance duration at speed ratio of 1.0 and the shortest, at ratios

0.5 and 2.0. Stance duration was typically longer for the forelimbs than hindlimbs ($p<0.05$). The range of change in stance duration across all speed ratios was about 0.2 s.

The range of changes in the swing phase duration was smaller, about 0.1 s. Swing durations for left fore- and hindlimbs decreased with the speed ratio, whereas they increased for right fore- and hindlimbs. The effect of the speed ratio was significant ($p<0.05$). At all speed ratios but 2.0, the swing duration of left right hindlimb was larger than that of the left forelimb ($p<0.05$). Similar results were obtained for the right hindlimb, except no difference in the swing duration between the right fore- and hindlimb was observed at speed ratio 0.5.

Temporal step onset symmetry changed relatively little around 0.5 with the speed ratio, although symmetry was significantly smaller at ratio of 0.5 and greater at ratio of 2.0 than at ratios 1.0 and 1.5 for both fore- and hindlimbs ($p<0.05$; Fig. 2.15). The left forelimb was a little more symmetric than the hindlimb at speed ratio 0.5 ($p<0.05$).

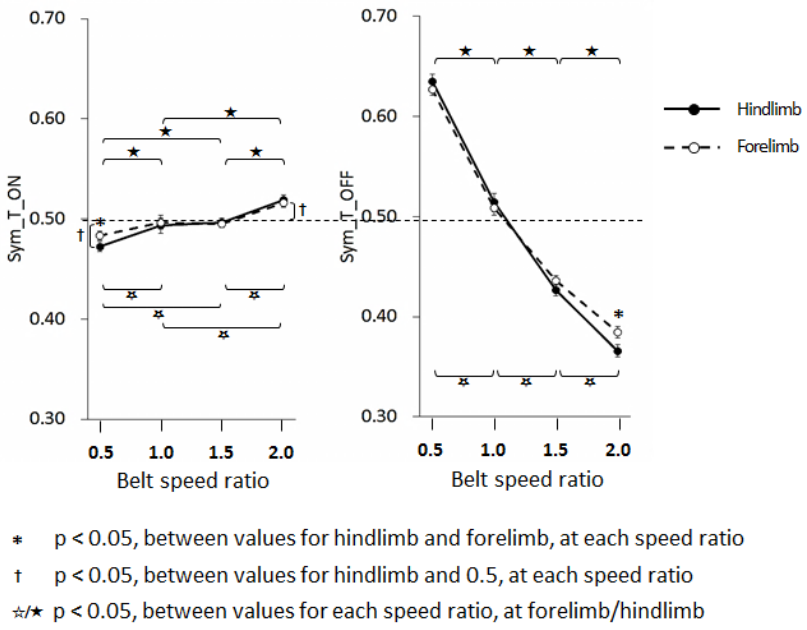

Figure 2.15. Mean (±95% confidence interval) of the temporal step onset and offset symmetry for the fore and hindlimbs as a function of belt speed ratio.

Temporal step offset symmetry was strongly dependent on the speed ratio – it decreased from approximately 0.63 to about 0.35 with increasing speed ratios. That means that the time between right and left limb stance offsets was shorter than that at speed ratio below 1.0, and longer at speed ratios above 1.0. The temporal step offset symmetry of the forelimb was a little better than for hindlimbs at speed ratio 2.0.

Step length and spatial step symmetry. Step length for the left and right limbs demonstrated opposite changes with speed ratios, although with one common rule – limb step length did not change or changed minimally when the speed of the ipsilateral belt increased unilaterally, while it changed substantially when the speed of the contralateral belt increased unilaterally ($p<0.05$; Fig. 2.16). Changes of step lengths of forelimbs and hindlimbs with speed ratios had a similar tendency with the step lengths of hindlimbs longer when the contralateral belt moved faster than the ipsilateral one ($p<0.05$). The step length of the right forelimb was longer than that of the right hindlimb at speed ratio of 2.0 ($p<0.05$).

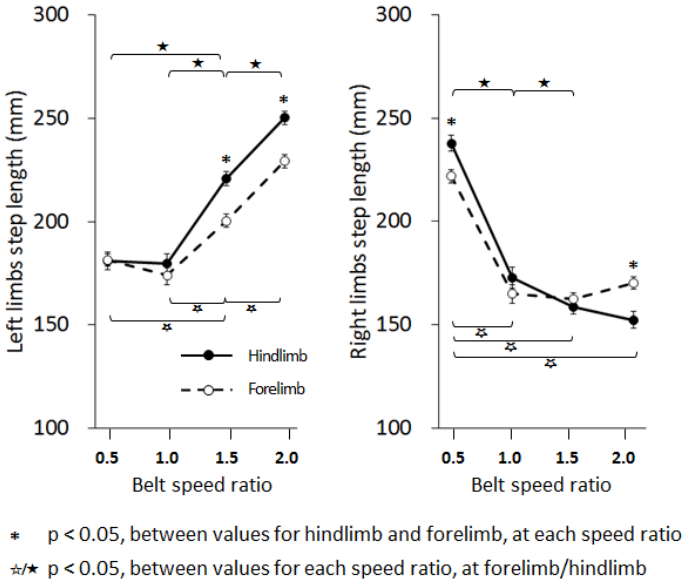

Figure 2.16. Mean (±95% confidence interval) of the step length for left and right fore- and hindlimbs as a function of belt speed ratio.

Spatial step symmetry for fore- and hindlimbs was strongly affected by the speed ratio – the right limb step length was longer than that of the left step length at speed ratio 0.5 by about 7% of the stride length, and it was shorter by approximately 7% – 12% at the ratio of 2.0 (Fig. 2.17). The shorter step length of the right hindlimbs compared to left step lengths at higher speed ratios was due to an earlier stance phase offset of the right hindlimbs (Fig. 2.15, temporal step offset symmetry). Forelimbs had less step length asymmetry than the right forelimbs at all speed ratios except 1.0 ($p<0.01$; Fig. 2.17).

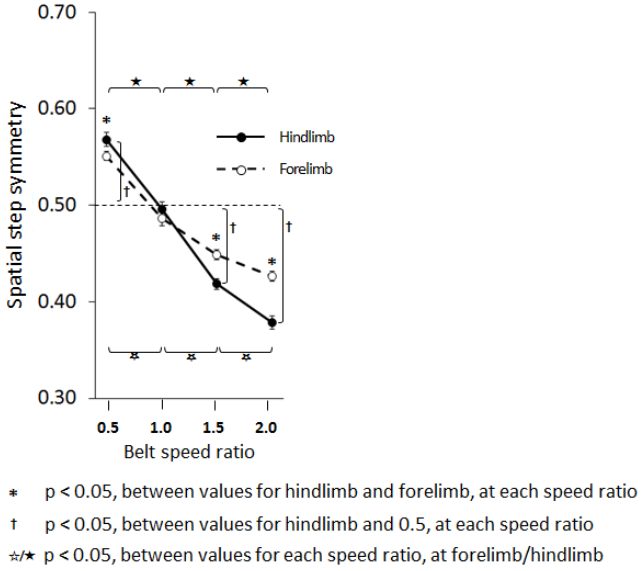

Figure 2.17. Mean (±95% confidence interval) of the step symmetry for fore- and hindlimbs as a function of belt speed ratio.

Pacing (diagonality) of limbs on either side demonstrated opposite changes with increasing speed ratios. Diagonality did not change when the speed of the ipsilateral belt increased unilaterally (Fig. 2.18, left side at speed ratios 0.5 and 1.0), while it decreased (increased pacing) when the speed of the contralateral belt increases unilaterally (speed ratios 1.5 and 2.0; Fig. 2.18). These results demonstrate substantial decoupling between the contralateral limbs and strong coupling of the ipsilateral limbs.

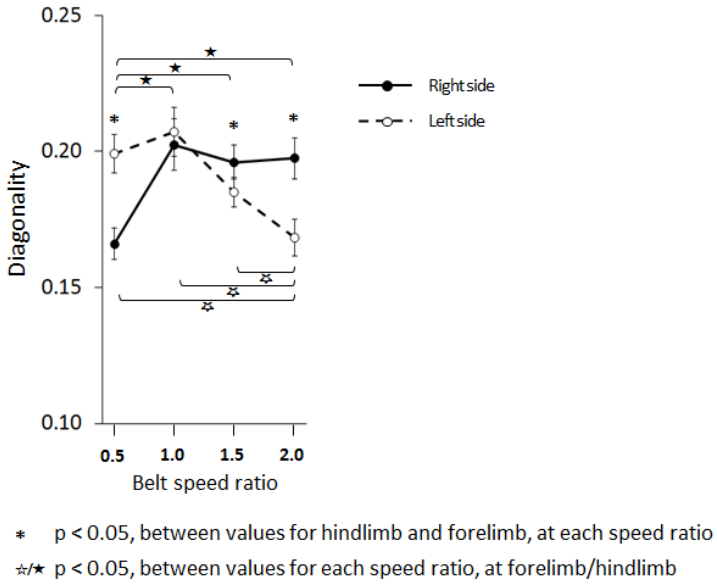

Figure 2.18. Mean (±95% confidence interval) of diagonality (or pacing) for the right and left limbs as a function of belt speed ratio.

Limb angles. There was a relatively small but significant change in the orientation of the fore- and hindlimb angles at stance onset – the forward angle increased up to ~7 deg with increasing the ipsilateral belt speed ($p<0.05$; Fig. 2.19). No changes in this limb angle were observed when the contralateral limb increased speed ($p>0.05$). The forelimb forward angle was several degrees larger than the hindlimb angle ($p<0.05$).

The limb angle at stance offset (the backward angle) increased over 15 deg with increasing speeds of the ipsilateral belt ($p<0.05$; 4.19), however no or little changes occurred in this angle when speed of the contralateral belt increased. Again, the backward angles of the forelimbs were larger than those of the hindlimb ($p<0.05$). The limb angle range for both fore- and hindlimbs increases with increasing speeds of the ipsilateral belt (Fig. 2.19, gray area).

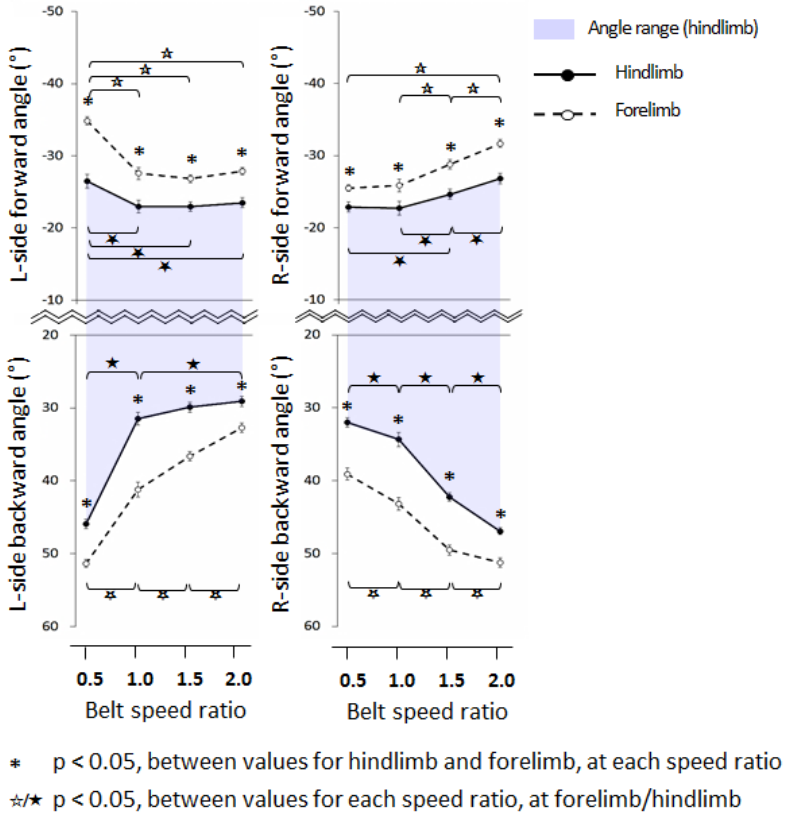

Figure 2.19. Mean (±95% confidence interval) of limb angles at stance onset (forward angle) and offset (backward angle) for left and right fore- and hindlimbs as a function of belt speed ratio.

2.3.2. Effects of Anesthesia of Paw Pad Afferents on Kinematics of Split-Belt Treadmill Walking

COM lateral bias was significantly affected by anesthesia of the right paws ($p<0.05$; Fig. 2.20). The center of mass shifted towards the anesthetized side regardless of the speed ratio, except the ratio of 1.0 at which no COM shift was noticed ($p>0.05$). Stimulation of the right distal-tibial nerve during the stance phase caused a significant reduction of the anesthesia effect

(COM shifted towards the intact condition, $p<0.05$), but only for speed ratios of 1.5 and 2.0, i.e. when the anesthetized paws were moving on a faster right belt. Stimulation effects were not significant for speed ratios of 0.5 and 1.0.

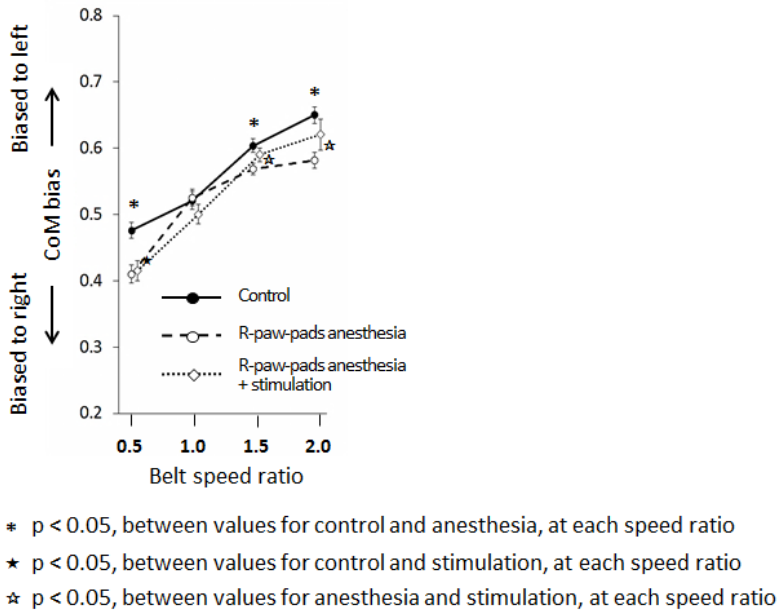

Figure 2.20. Mean (±95% confidence interval) COM lateral shift during split-belt treadmill walking with anesthesia of right fore- and hindpaws and during stimulations of right distal-tibial nerve.

Phase durations. Anesthesia of paw pads in the right fore- and hindlimbs decreased the cycle duration of the ipsilateral forelimbs limbs at all speed ratios but ratio 1.0 ($p<0.05$); the cycle duration of the ipsilateral hindlimb also decreased except at the speed ratio of 0.5 (Fig. 2.21). The stance phase duration of the left and right forelimbs decreased ($p<0.05$) only at speed ratio of 0.5 (forelimb) and 1.0 (hindlimb). The anesthesia effects were stronger for the hindlimbs – the stance duration for the left hindlimb became shorter at speed ratios 1.0, 1.5 and 2.0; for the right hindlimb, it was shorter at ratios 1.0 and 1.5. Paw anesthesia decreased the swing duration of the right fore- and hind-limbs at speed ratios of 1.5 and 2.0 ($p<0.05$) and did not affect the swing duration of the left limbs.

Stimulation of the right distal-tibial nerve while the right hind- and forepaw pads were anesthetized reversed the effects of anesthesia on durations of the walking cycle and its phases at many speed ratios. Stimulation increased the duration of the cycle, stance and swing phases compared to the anesthetized condition for the left and right fore- and

hindlimbs typically for speed ratios of 1.0, 1.5 and 2.0. One noticeable exception was the stance duration of the right hindlimb at ratios of 1.5 and 2.0 – stimulation did not affect the stance duration. In some cases, stimulation increased the cycle duration of the fore- and hindlimbs beyond values of intact walking (at speed ratios of 1.0 and 1.5; $p<0.05$), but did not affect the stance duration (with one exception, it increased beyond control values for the forelimb at speed ratio of 1.5). Stimulation increased the swing duration beyond control values only in the right hindlimb and only at speed ratios of 1.5 and 2.0.

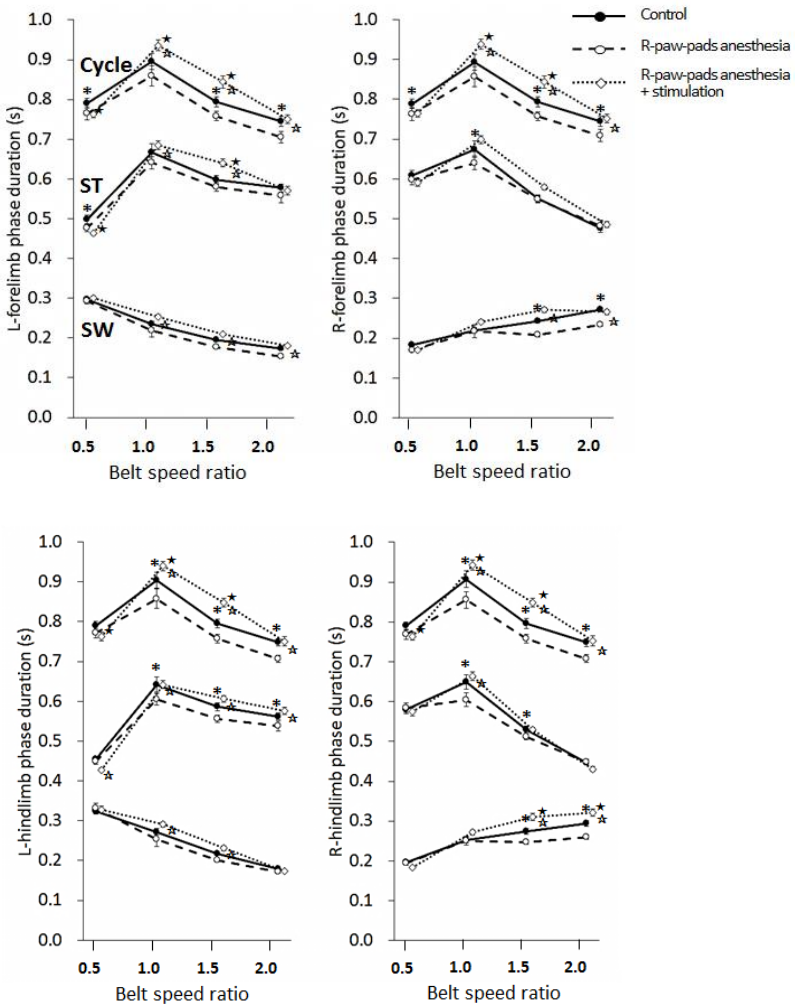

Figure 2.21. Mean (±95% confidence interval) durations of the walking cycle, stance and swing phase during split-belt treadmill walking with anesthesia of right fore- and hindpaws and during stimulations of the right distal-tibial nerve.

Duty factor of right and left fore- and hindlimbs was strongly affected by anesthesia of the right fore- and hindpaws at speed ratios of 1.5 and 2.0. At these speed ratios, anesthesia increased duty factor in the right and left forelimbs and in the right hindlimb ($p<0.05$; Fig. 2.22); anesthesia did not affect duty factor of the left hindlimb ($p>0.05$). Stimulation of the right distal-tibial nerve during stance reduced or reversed the anesthesia effects in the three limbs. For the right hindlimb, stimulation even reduced duty factor beyond the control values ($p<0.05$). Stimulation also reduced duty factor in the left hindlimb except for speed ratio 2.0, in which case duty factor increased.

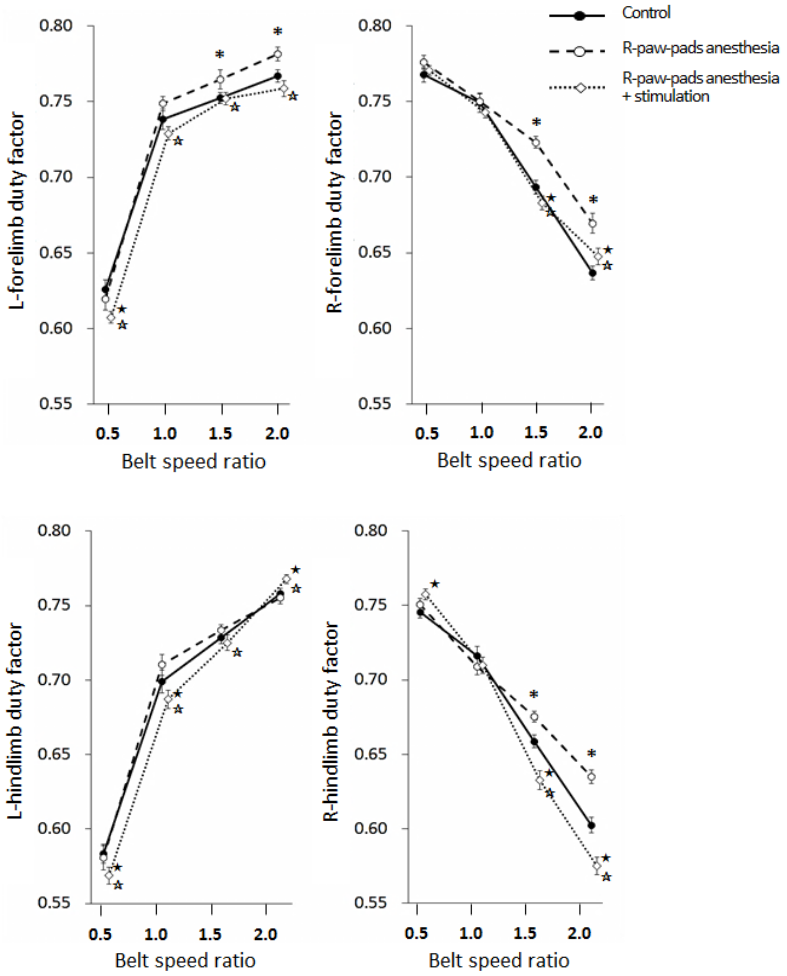

Figure 2.22. Mean (±95% confidence interval) duty factor during split-belt treadmill walking with anesthesia of right fore- and hindpaws and during stimulations of the right distal-tibial nerve.

Temporal step symmetry at stance onset of both forelimb and hindlimb was not significantly affected by anesthesia of the right paws (Fig. 2.23). Temporal step symmetry at stance offset of the right hindlimb increased with anesthesia when the ipsilateral belt moved faster than the contralateral belt. Temporal step symmetry at stance offset of fore- and hindlimbs decreased with anesthesia when two belts moved at the same speed. Tibial nerve stimulation made onset symmetry of both forelimb and hindlimb to

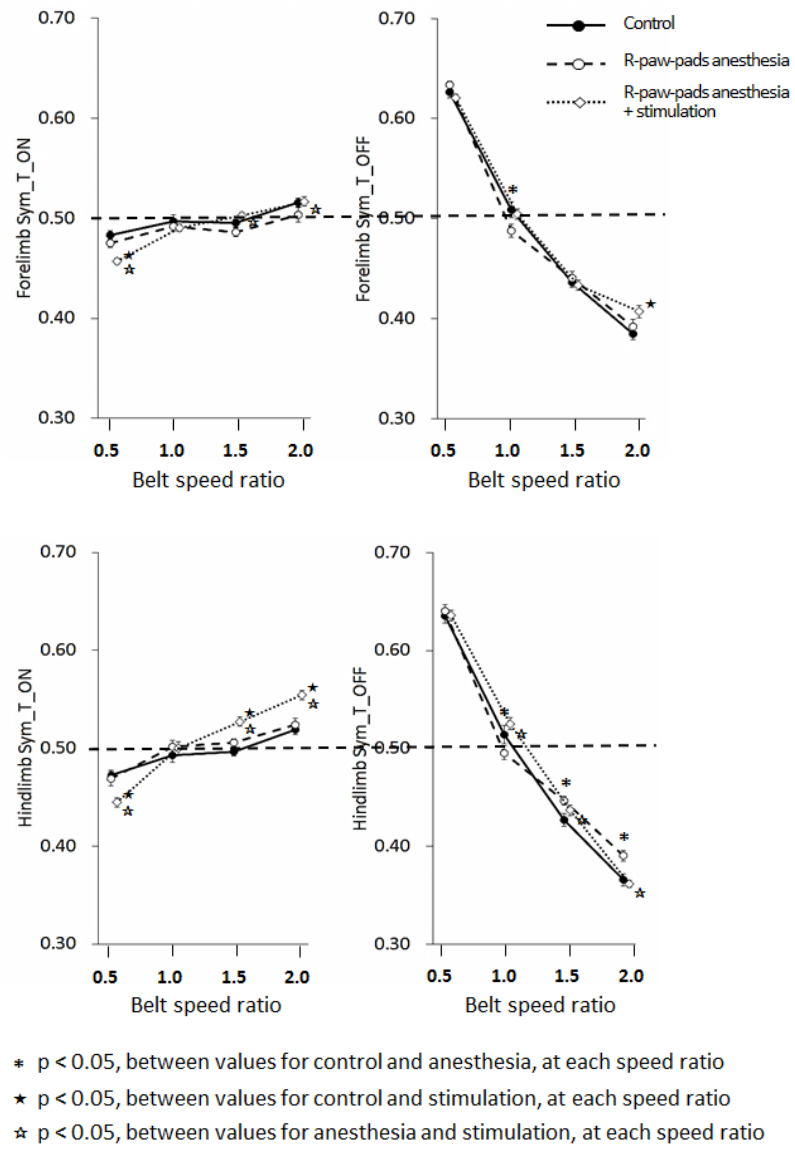

Figure 2.23. Mean (±95% confidence interval) temporal onset and offset symmetry of forelimbs and hindlimbs during split-belt treadmill walking with anesthesia of right fore- and hindpaws and during stimulations of the right distal-tibial nerve.

decrease, i.e. the stance onset timing became more asymmetrical with tibial nerve stimulation. Stimulation reduced or reversed effects of anesthesia on the offset temporal symmetry for the hindlimb at speed ratios 1.0, 1.5 and 2.0.

Step length: Anesthesia of right fore- and hindpaw did not change the right forelimb and hindlimb step length, however it decreased the left hindlimb step length at speed ratios of 1.5 and 2.0 ($p<0.05$; Fig. 2.24). Stimulation of the right distal-tibial nerve

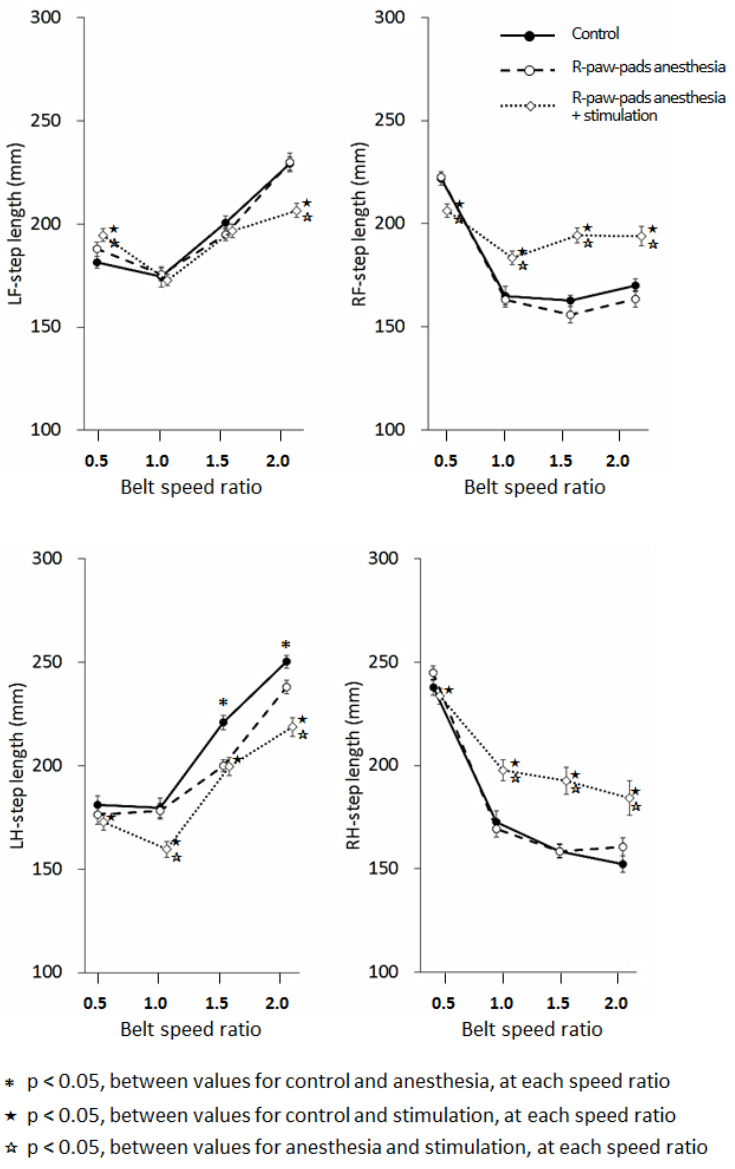

Figure 2.24. Mean (±95% confidence interval) step length of four limbs during split-belt treadmill walking with anesthesia of right fore- and hindpaws and during stimulations of the right distal-tibial nerve. LF, RF, LH and RH are left forelimb, right forelimb, left hindlimb and right hindlimb, respectively.

increased step length of the right fore- and hindlimb at speed ratios 1.0, 1.5 and 2.0 compared to intact and anesthetized conditions. Stimulation effects had the opposite effect on the step length of the left hindlimb (step length became shorter) at speed ratios 1.0 and 2.0, and for the left forelimb at speed ratio of 2.0 ($p<0.05$); step length of the left forelimb increased during stimulation at speed ratio of 0.5.

Spatial step symmetry. Anesthesia of the right forepaw and hindpaw had no effect on the forelimb spatial symmetry ($p>0.05$), where the hindlimb spatial symmetry increased during paw anesthesia at speed ratios 1.5 and 2.0 ($p<0.05$; Fig. 2.25). Tibial nerve stimulation further increased the hindlimb spatial symmetry at speed ratios of 1.5 and 2.0; at speed ratio 1, the hindlimb spatial symmetry decreased above 0.5, i.e. the right hindlimb step length became longer than that of the left hindlimb step length. The same stimulation increased the forelimb spatial symmetry at speed ratios 1.0, 1.5 and 2.0, bringing it closer to almost perfect symmetry.

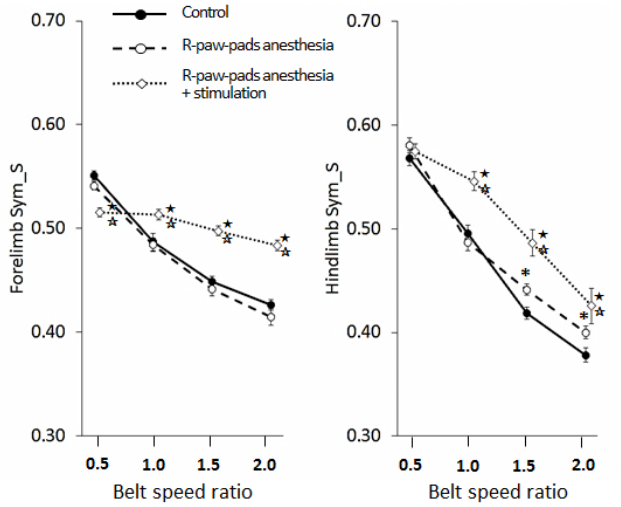

Figure 2.25. Mean (±95% confidence interval) spatial step symmetry of forelimbs and hindlimbs during split-belt treadmill walking with anesthesia of right fore- and hindpaws and during stimulations of the right distal-tibial nerve.

Diagonality (pacing). Anesthesia of right paws reduced diagonality (or increased pacing) of the ipsilateral (right) limbs at speed ratios 1.0, 1.5 and 2.0 ($p<0.05$; Fig. 2.26). There was no change in right side diagonality at ratio of 0.5. Diagonality of the left limbs also decreased during anesthesia but at speed ratios 0.5, 1.0 and 1.5. Stimulation of the right distal nerve substantially decreased diagonality for the right limbs at speed ratio 0.5, and for the left limbs at ratios 0.5 and 2.0 ($p<0.05$). At other speed ratios, stimulation increased diagonality compared to the anesthesia condition ($p<0.05$; Fig. 2.26).

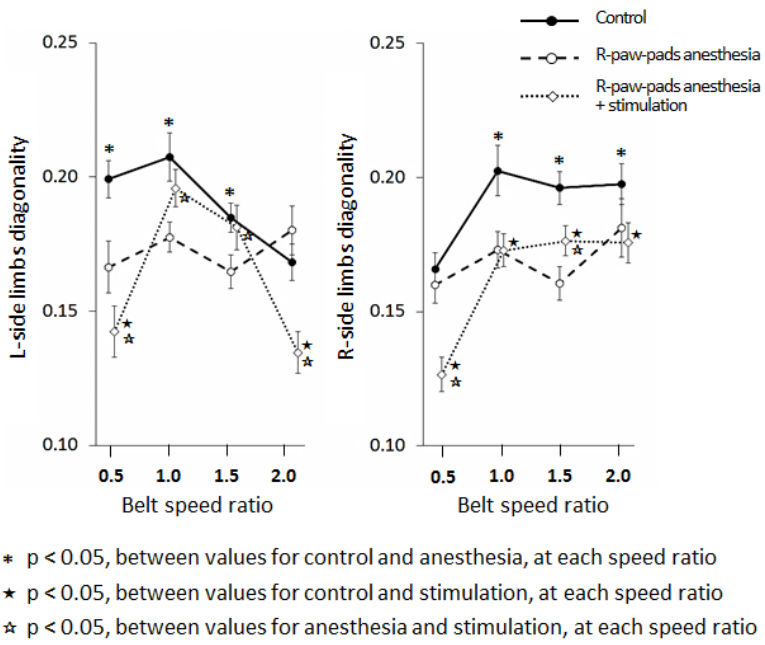

Figure 2.26. Mean (±95% confidence interval) diagonality of the left and right limbs during split-bel treadmill walking with anesthesia of right fore- and hindpaws and during stimulations of the right distal tibial nerve.

Limb angle. Anesthesia of the right paws had opposite effects on the forelimb angle than on the hindlimb angle irrespective of the side. For example, the front angles for both left and right hindlimb increased at speed ratios 1.0, 1.5 and 2.0 (with one exception, $p<0.05$; Fig. 2.26), whereas the front angles of the left and right forelimbs decreased (at all speed ratios for the left forelimb and at ratio 2.0 for right forelimb; $p<0.05$). The backward angles had similar trends. The hindlimb backward angles increased at speed ratios 1.0 and 1.5 for the left hindlimb and 1.5 and 2.0 for the right

hindlimb. The backward angles of the forelimbs increased during right paw anesthesia at most speed ratios ($p<0.05$; Fig. 2.27).

Stimulation of the right distal-tibial nerve had opposite effects on the right and left limb angles. The forward right limb angles of the forelimb and hindlimb increased by stimulation compared to the anesthesia condition, whereas the forward left angles decreased for both forelimb and hindlimb at various speed ratios ($p<0.05$; Fig. 2.27). The backward right limb angles also increased by stimulation at speed ratios 1.0 – 2.0 (right forelimb) and 0.5 and 1.0 (right hindlimb); the backward left angles decreased at ratios 1.5 and 2.0 (left forelimb) and 1.0 – 2.0 (left hindlimb) ($p<0.05$; Fig. 2.27).

Effects of speed ratio, anesthesia and tibial nerve stimulation on EMG of selected muscles. With increasing speed ratio from 1.0 to 2.0 the EMG magnitude of a right ankle extensor (MG) decreased and the right hip flexor (IP) increased ($p<0.05$; Fig. 2.28). EMG burst durations generally decreased with increasing speed ratios from 1.0 to 2.0 ($p<0.05$, not shown). Anesthesia of the right fore- and hindpaw increased the EMG magnitude in SO at speed ratios 0.5 and 1.0, MG at ratios 1.5 and 2.0, and IP at ratios 0.5 – 2.0 ($p<0.05$; Fig. 2.28). Burst durations decreased in SO at speed ratios 1.0 – 2.0, increased in MG at ratio 2.0, increased in IP at ratios 1.0 and 1.5 (not shown).

Stimulation of the right distal-tibial nerve reduced EMG magnitude with respect to the anesthesia condition in SO (speed ratio 1.0), MG (ratio 1.5), and IP (ratio 1.5); it increased EMG magnitude in SO at speed ratios 1.5 and 2.0. Stimulation increased EMG burst duration in SO at peed ration 1.5 and in IP at ration 2.0; it decreased burst duration in MG at speed ratio 1.5 and in IP at speed ratio 1.0 ($p<0.05$; Fig. 2.28).

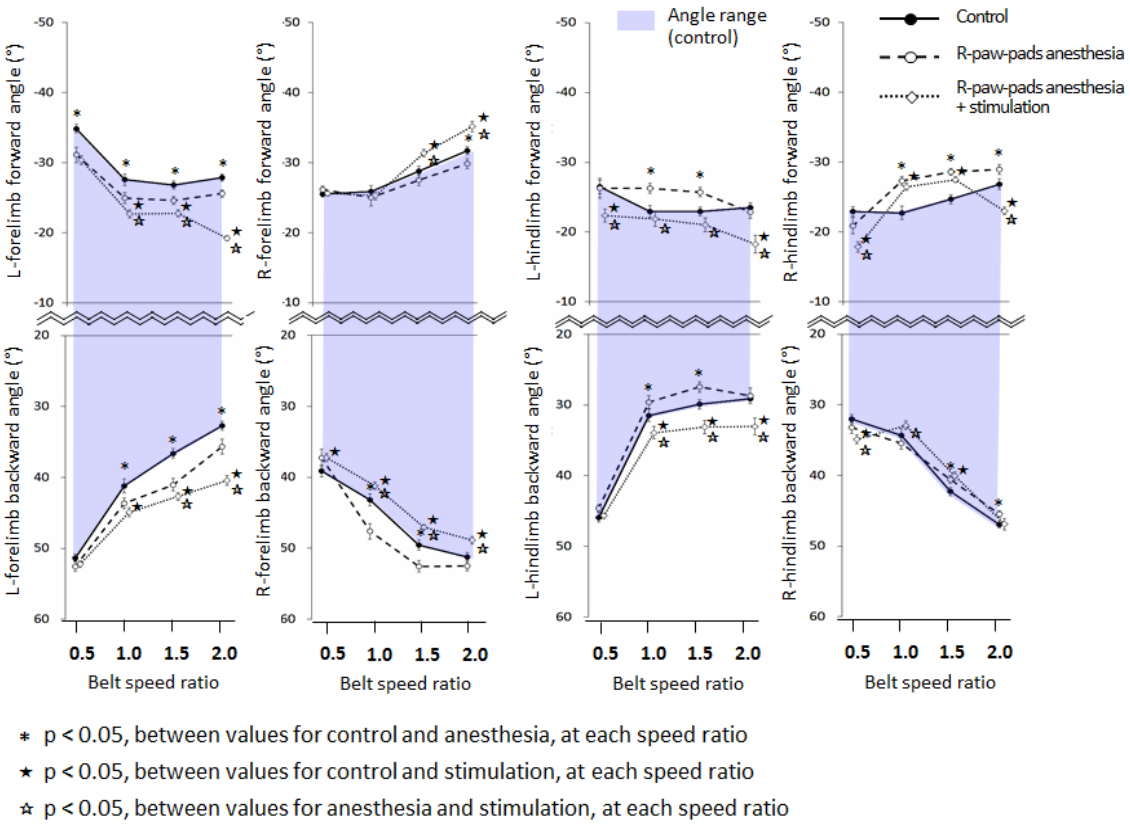

Figure 2.27. Mean (±95% confidence interval) diagonality of the forward and backward angles of the lef and right forelimbs and hindlimbs during split-belt treadmill walking with anesthesia of right fore- and hindpaws and during stimulations of the right distal-tibial nerve.

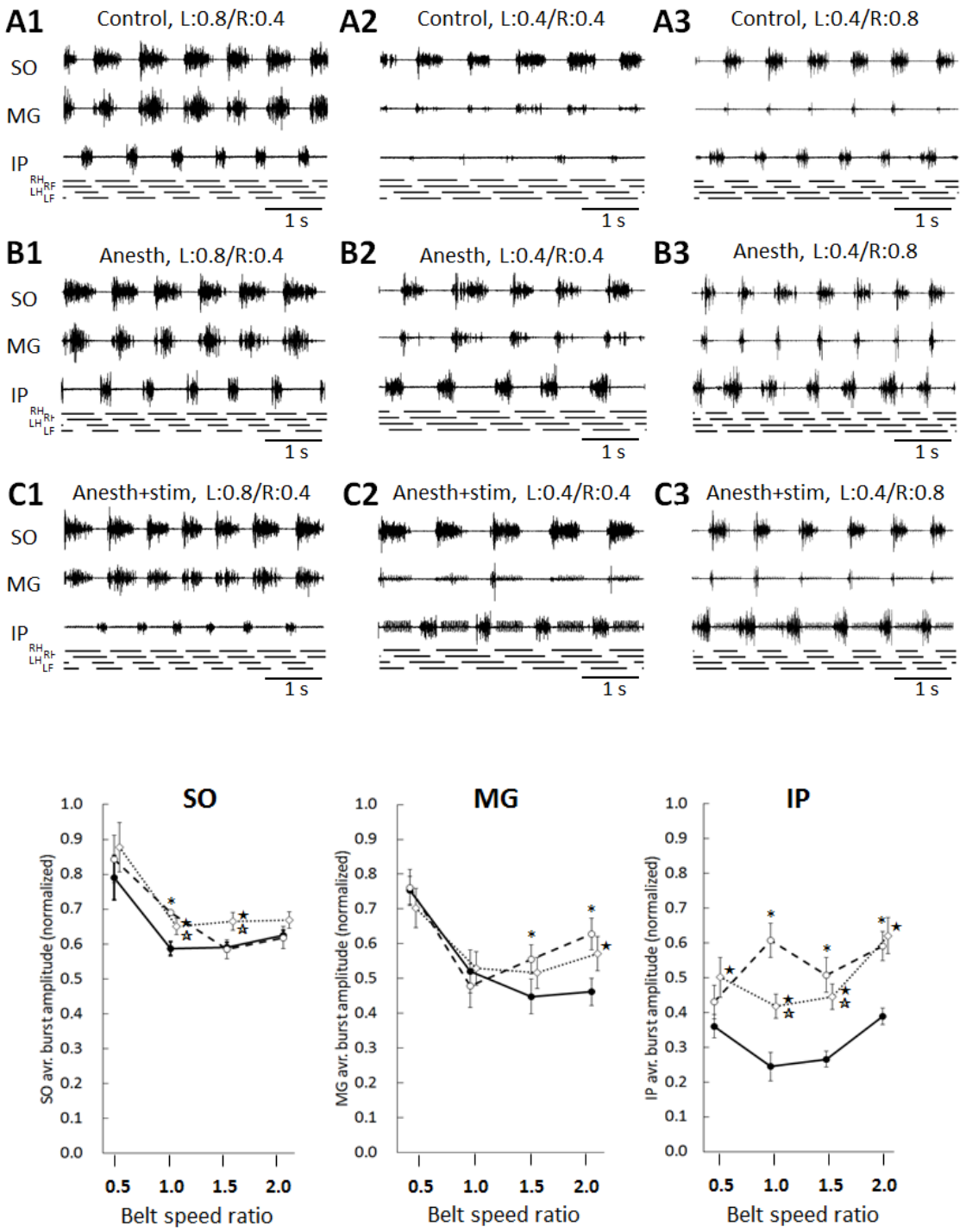

Figure 2.28. EMG activity of soleus (SO), medial gastrocnemius (MG) and iliopsoas (IP) muscles during split-belt treadmill walking with anesthesia of right fore- and hindpaws and during stimulations of the right distal-tibial nerve. **A1, A2, A3**: Intact (control), at each speed ratio, **B1, B2, B3**: anesthesia at each speed ratio, **C1, C2, C3**: anesthesia+tibial nerve stimulation conditions at each speed ratio. **D**: Mean (±95% confidence interval) EMG burst magnitude of SO, MG and IP muscles.

2.3.3. Effects of Stretch Reflex Removal from Quad and Sart on Kinematics of Split-Belt Treadmill Walking

Lateral COM bias was not affected by stretch reflex removal (self-reinnervation) from the right Quad and Sart at any speed ratio. When the right distal-tibial nerve was stimulated during the stance phase, COM shifted towards the affected right side at all speed ratios ($p<0.05$; Fig. 2.29).

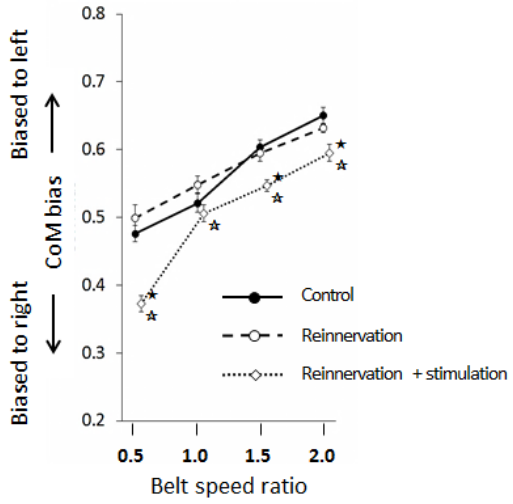

* p < 0.05, between values for control and reinnervation, at each speed ratio
★ p < 0.05, between values for control and stimulation, at each speed ratio
☆ p < 0.05, between values for reinnervation and stimulation, at each speed ratio

Figure 2.29. Mean (±95% confidence interval) COM medial shift during split-belt treadmill walking with self-reinnervated right QUAD and SART and during stimulations of the right distal-tibial nerve.

Cycle and phase durations. Quad and Sart self-reinnervation increased cycle duration in all four limbs at speed ratios 1.5 and 2.0 and decreased it for the right hindlimb at speed ratio 1.0 ($p<0.05$; Fig. 2.30). Self-reinnervation increased the swing duration of the right fore- and hindlimb and the stance duration of the contralateral fore- and hindlimb at speed ratios of 1.5 and
2.0 ($p<0.05$). The stance duration of the right forelimb and swing duration of the left hindlimb were unaffected ($p>0.05$).

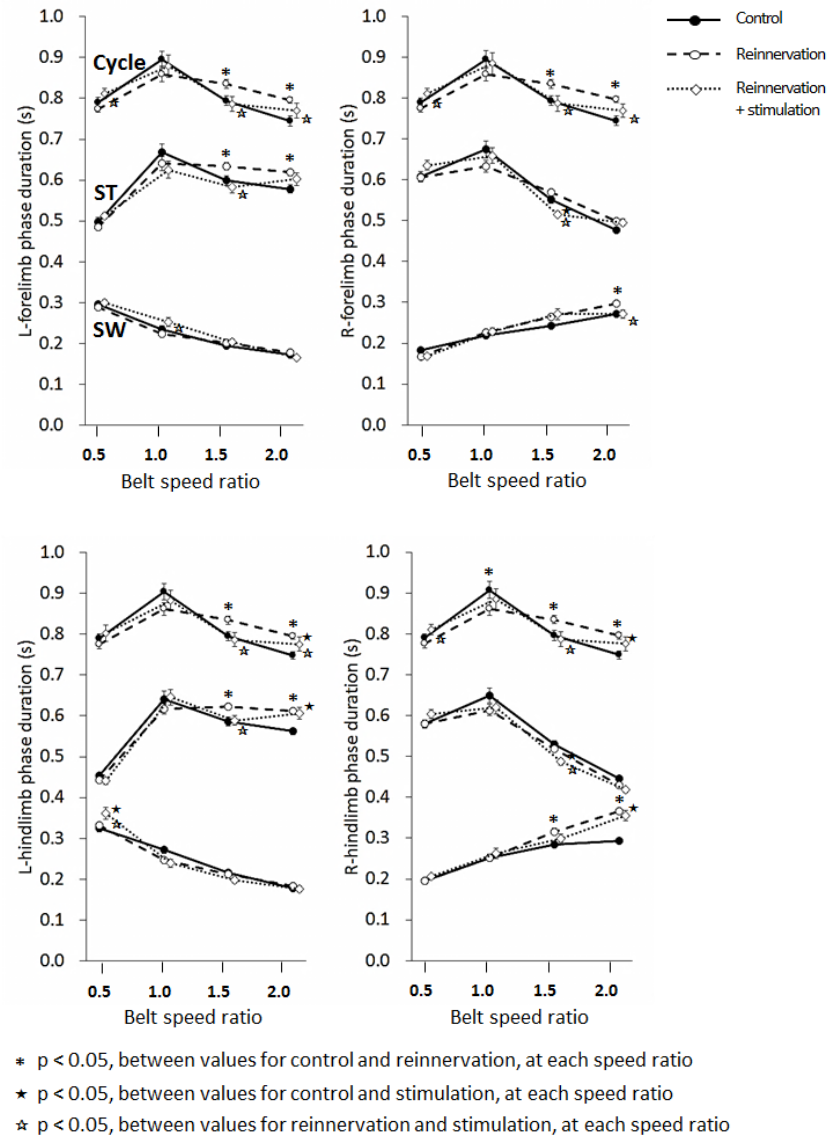

Figure 2.30. Mean (±95% confidence interval) durations of the cycle, stance and swing phases for four limbs during split-belt treadmill walking with self-reinnervated right QUAD and SART and during stimulations of the right distal-tibial nerve.

Stimulation of the right distal-tibial nerve reduced the effect of self-reinnervation on the cycle duration for all four limbs (at speed ratios of 1.5 and 2.0 for the contralateral fore- and hindlimbs and ratio of 1.5 for the ipsilateral hindlimb; $p<0.05$). Stimulation completely reversed the effect of self-reinnervation on the cycle duration of all four limbs at speed ratio 1.5. Stimulation reduced the stance duration compared to the self-

reinnervation condition in the ipsilateral and contralateral fore- and hindlimbs at speed ratio of 0.5 ($p<0.05$). It also had small but significant effects on the swing duration – it was decreased for the right forelimb at speed ratio 2.0 and increased for the contralateral forelimb (speed ratio 1.0), and the contralateral hindlimb (speed ratio 0.5).

Duty factor: Quad and Sart self-reinnervation had the greatest effect on the duty factor of the ipsilateral hindlimb – duty factor decreased by more than 5% at speed ratios of 1.5 and 2.0 ($p<0.05$; Fig. 2.31). The opposite change in duty factor occurred in the contralateral hindlimb, although the increase in duty factor was smaller. There was also a small decrease in duty factor in the ipsilateral forelimb at speed ratios of 1.5 and 2.0, and a small increase in duty factor in the contralateral forelimb at speed ratio of 2.0. Stimulation of the distal-tibial nerve did not generally changed duty factor from the self-reinnervated condition, except there was a decrease in duty factor in the ipsilateral forelimb at speed ratio 1.5 ($p<0.05$). Stimulation had a stronger effect on the duty factor of the contralateral forelimb – it decreased from the self-reinnervation values at speed ratios of 1.0 and 1.5, and increased at ratio 2.0 ($p<0.05$). Stimulation also decreased duty factor of the contralateral hindlimb at speed ratio of 0.5 ($p<0.05$).

Temporal step symmetry: Self-reinnervation of the right Quad and Sart substantially increased the index of temporal step onset symmetry for the hindlimb and made walking asymmetric at speed ratios of 1.0 – 2.0 ($p<0.05$; Fig. 2.32). That means that the step onset by the right hindlimb was delayed with respect to the left hindlimb step onset. A similar delay but with a smaller magnitude occurred for the temporal step onset symmetry of the forelimb ($p<0.05$). No significant effect of the Quad and Sart self-reinnervation was observed for temporal step offset symmetry ($p>0.05$).

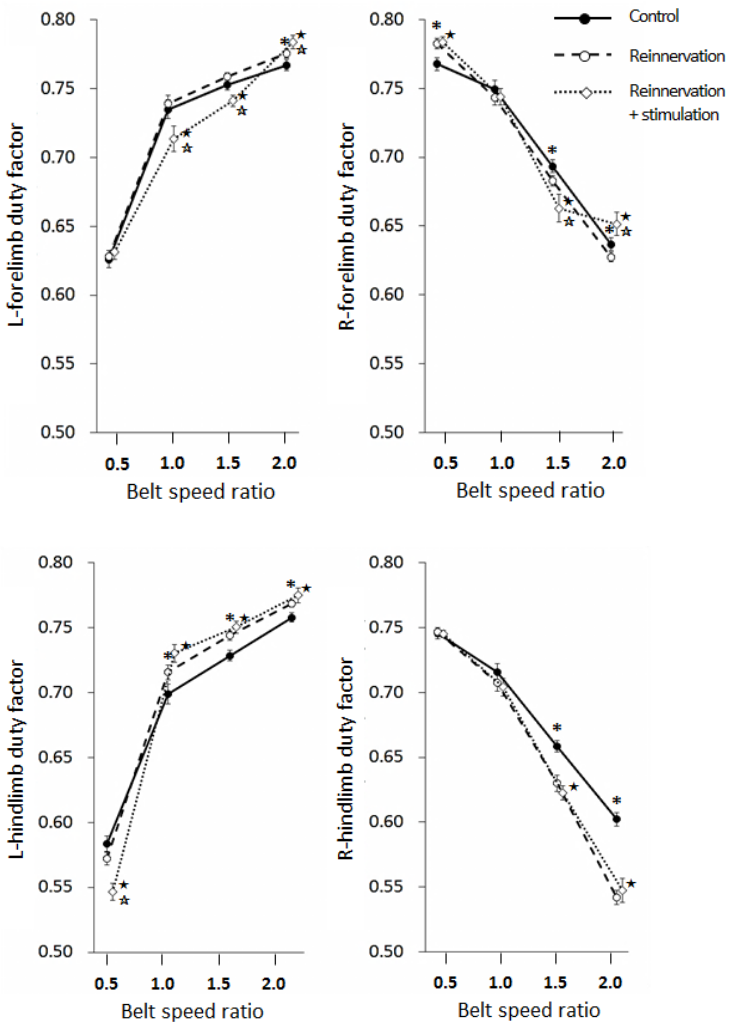

Figure 2.31. Mean (±95% confidence interval) duty factor of four limbs during split-belt treadmill walking with self-reinnervated right QUAD and SART and during stimulations of the right distal-tibial nerve.

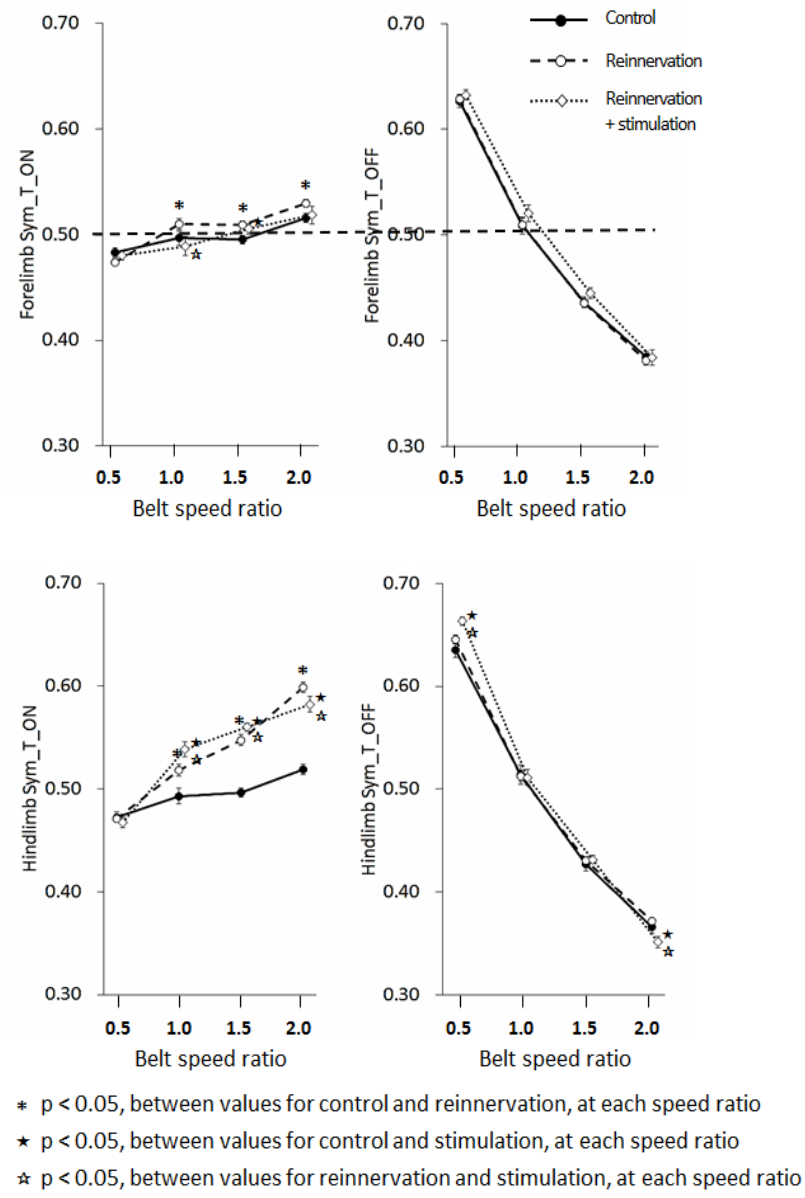

Figure 2.32. Mean (±95% confidence interval) temporal onset and offset symmetry for forelimbs and hindlimbs during split-belt treadmill walking with self-reinnervated right QUAD and SART and during stimulations of the right distal-tibial nerve.

Effects of the distal-tibial nerve stimulation on the temporal symmetry was absent or small. Stimulation decreased the effects of self-reinnervation on hindlimb onset and offset symmetry for hindlimbs at speed ratio of 2.0, decreased the onset symmetry for forelimbs at speed ratio of 1.0, increased the onset symmetry for hindlimbs at speed ratios

of 1.0 and 1.5, and increased the offset symmetry of hindlimbs at speed ratio of 0.5 ($p<0.05$).

Step length. Self-reinnervation of Quad and Sart increased the step length of the ipsilateral hindlimb and decreased the step length of the contralateral hindlimb at all four

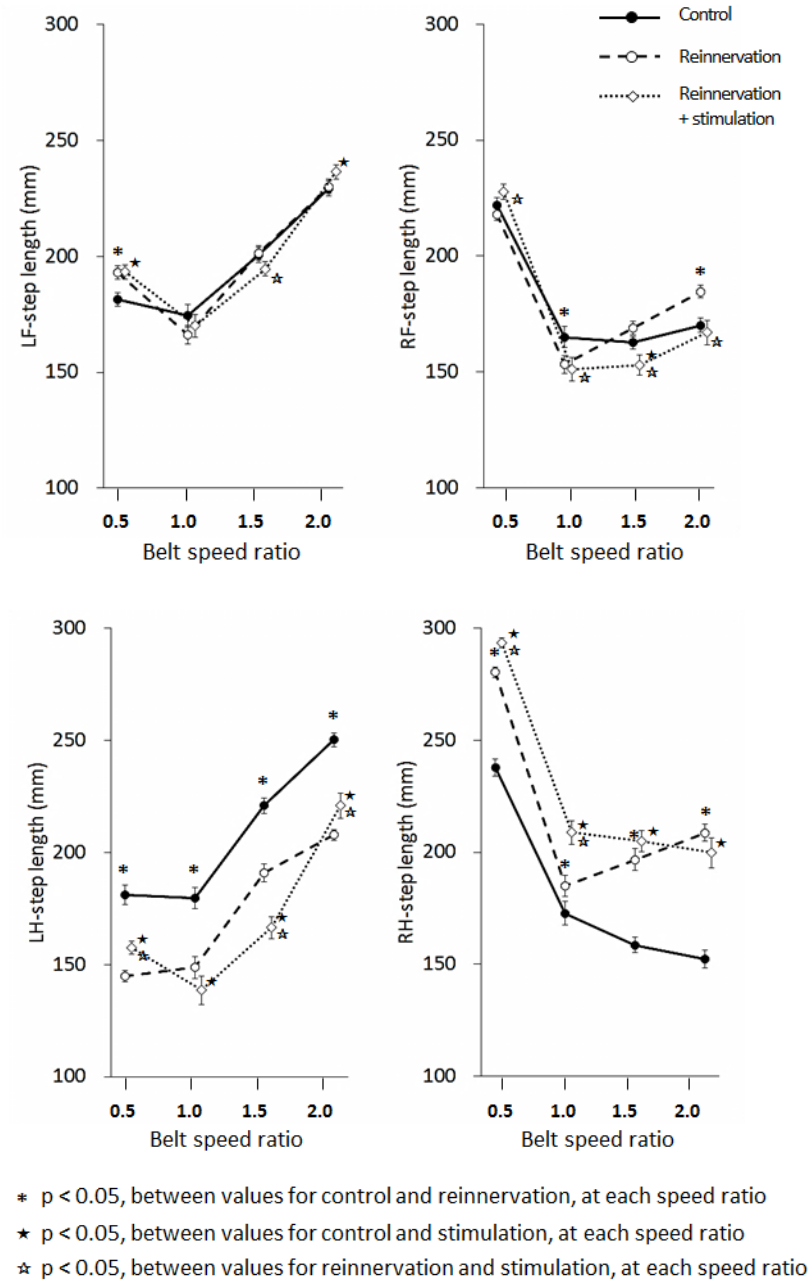

Figure 2.33. Mean (±95% confidence interval) temporal step onset and offset symmetry for forelimbs and hindlimbs during split-belt treadmill walking with self-reinnervated right QUAD and SART and during stimulations of the right distal-tibial nerve.

speed ratios ($p<0.05$; Fig. 2.33). Step lengths of forelimb changed to a much smaller extent. Step length of the ipsilateral forelimb increased at speed ratio of 2.0 and decreased at ratio of 1.0; the step length of the contralateral forelimb increased at speed ratio of 0.5 ($p<0.05$). Tibial nerve stimulation slightly increased the step length of the ipsilateral hindlimb compared to the self-reinnervation condition at speeds ratios of 0.5 – 1.5 ($p<0.05$); decreased the step length of the ipsilateral forelimb at speed ratios of 1.0 – 2.0; decreased step length of the contralateral hindlimb at speed ratio 1.5, and increased the step length of the same limb at speed ratios of 0.5 and 2.0 ($p<0.05$).

Spatial step symmetry. Self-reinnervation shifted the spatial hindlimb symmetry up making walking less symmetric at speed ratios of 0.5 and 1.0, and more symmetric at speed ratios 1.5 and 2.0 ($p<0.05$; Fig. 2.34). These changes in hindlimb symmetry were caused by longer step length of the ipsilateral (right) hindlimb (Fig. 2.33). Spatial

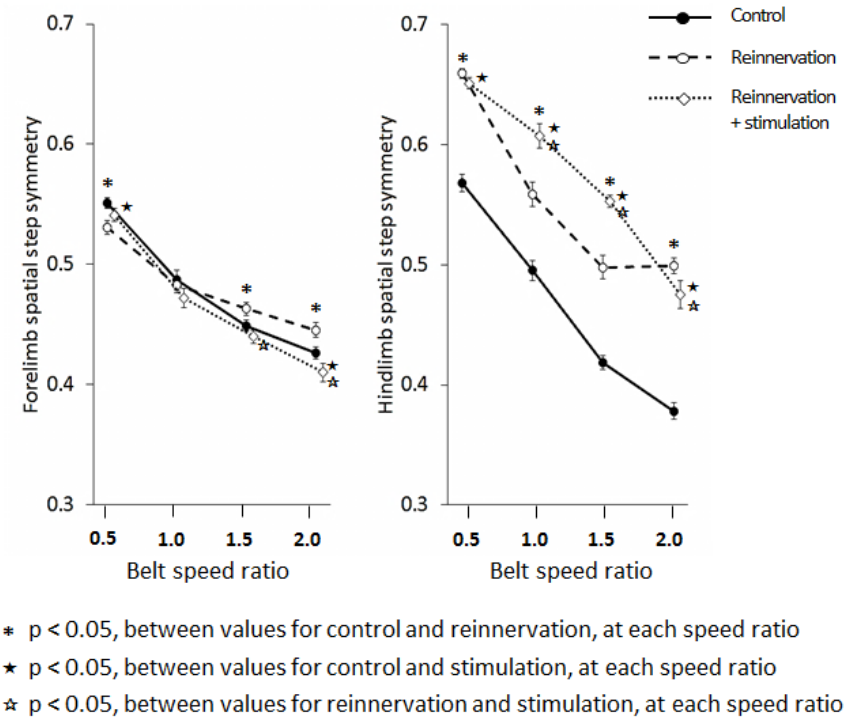

Figure 2.34. Mean (±95% confidence interval) spatial step symmetry for forelimbs and hindlimbs during split-belt treadmill walking with self-reinnervated right QUAD and SART and during stimulations of the right distal-tibial nerve.

forelimb symmetry was also affected by self-reinnervation but to a lesser extent. For example, forelimb symmetry increased at speed ratios of 1.5 and 2.0, did not change at speed ratio of 1.0, and decreased (moved away from 0.5) at speed ratio of 0.5. Tibial nerve stimulation completely reversed the effect of self-reinnervation on the forelimb spatial symmetry at speed ratios of 1.5 and 2.0. Stimulation had the opposite effect on the hindlimb – walking became more asymmetric at speed ratios of 1.0 and 1.5 ($p<0.05$).

Diagonality of both ipsilateral and contralateral limbs was substantially influenced by the Quad-Sart reinnervation. It reduced diagonality of left and right limbs to very low values 0.06 – 0.12 (almost perfect pacing) at all speed ratios ($p<0.05$; Fig. 2.35). Tibial nerve stimulation increased right side diagonality at speed ratios of 0.5 and 2.0, left side diagonality at speed ratios 1.0 and 2.0, and decreased left side diagonality at ratio 1.5 ($p<0.05$).

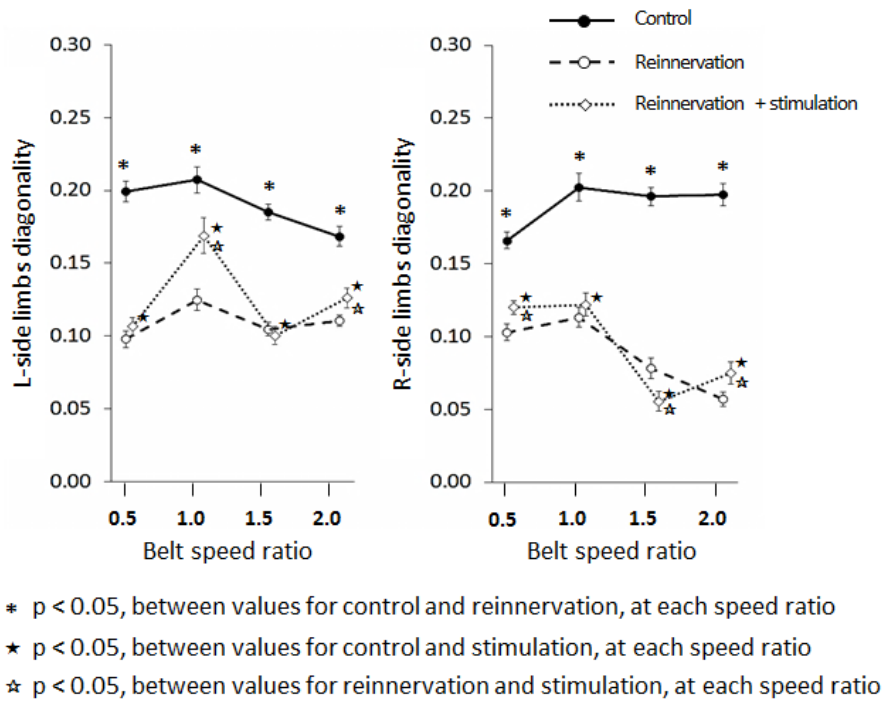

Figure 2.35. Mean (±95% confidence interval) diagonality of the left and right limbs during split-belt treadmill walking with self-reinnervated right QUAD and SART and during stimulations of the right distal-tibial nerve.

Limb angle. The Quad-Sart self-reinnervation increased the forward ipsilateral forelimb angle at speed ratios of 0.5 and 2.0 and the forward hindlimb at ratios 1.0 and 1.5 ($p<0.05$; Fig. 2.36). Contralateral limbs were affected by self-reinnervation in the opposite direction – forward forelimb and hindlimb angles decreased at all speed ratios ($p<0.05$). Backward limb angles had a tendency of opposite response to self-reinnervation. The ipsilateral fore- and hindlimb backward angles decreased at most speed ratios ($p<0.05$) with exception of the contralateral forelimb offset angle at speed ratio of 0.5. The backward angle increased for the contralateral forelimb at speed ratios of 0.5, 1.5 and 2.0 and for the contralateral hindlimb for ratio 2.0 ($p<0.05$).

Stimulation of the right distal-tibial nerve had a greater effect on the limb angles of the contralateral limbs – the contralateral forelimb increased its forward angle at speed ratios of 0.5 – 1.5, whereas the contralateral hindlimb decreased its forward angle at the same speed ratios ($p<0.05$). The ipsilateral forelimb forward angle decreased at speed ratios 0.5, 1.5 and 2.0; the ipsilateral hindlimb forward angle decreased at speed ratio 0.5 m/s. Effects of stimulation on the backward limb angles were typically opposed to those of the forward angles. For instance, ipsilateral backward angle for forelimb decreased at speed ratios of 1.5 and 2.0, but decreased at speed ratio of 0.5 ($p<0.05$). The ipsilateral hindlimb angle increased at speed ratios 0.5 – 1.5 ($p<0.05$). Stimulation had a more modest effect on the ipsilateral limb backward angles – it increased for both fore- and hindlimb at speed ratio of 2.0 ($p<0.05$).

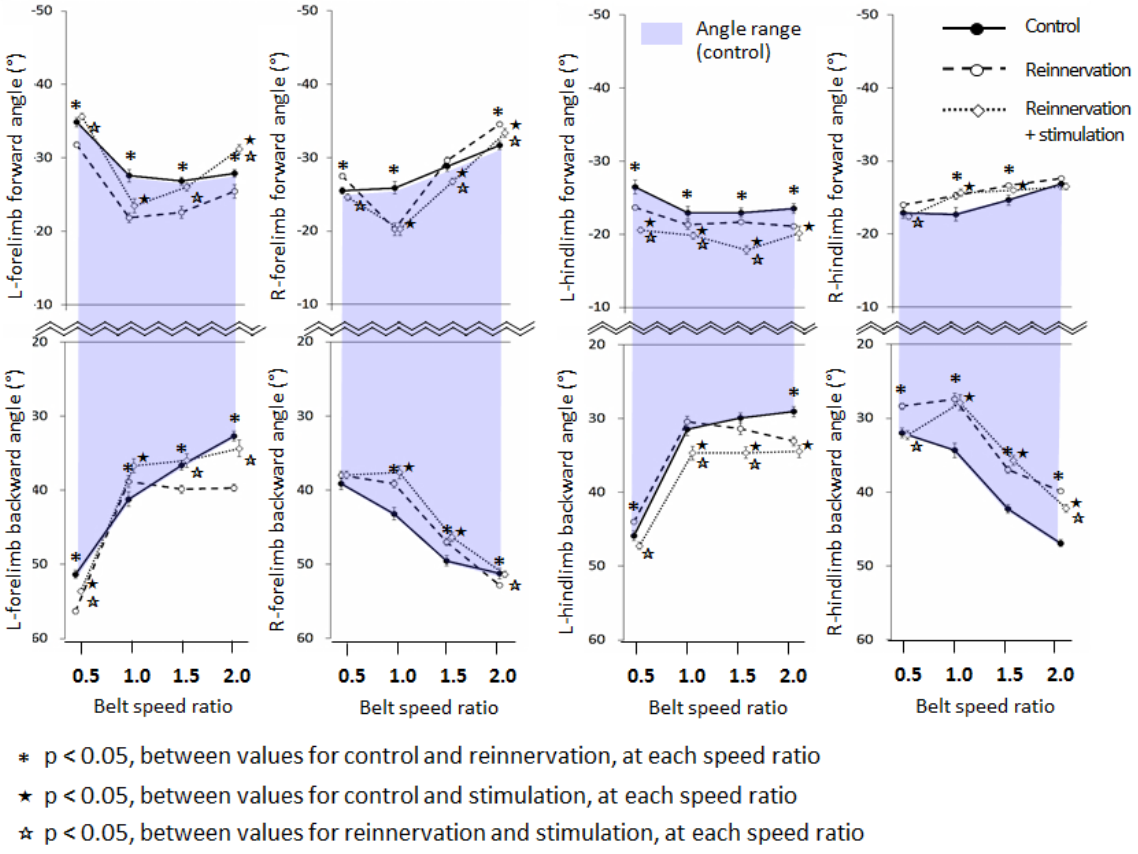

Figure 2.36. Mean (±95% confidence interval) forward and backward angles of left and right forelimbs and hindlimbs during split-belt treadmill walking with self-reinnervated right QUAD and SART and during stimulations of the right distal-tibial nerve.

2.4. Discussion and Conclusions

The goal of these series of experiments was to determine the effects of manipulation of cutaneous feedback from paw pad afferents and muscle stretch-dependent feedback from Quad and Sart on kinematics of walking in the cats.

2.4.1. Effects of Paw Pad Anesthesia

COM lateral shift. After application of anesthesia to the paw pads of the right fore- and hindlimbs, cats shift CoM to the ipsilateral side when two belts moved at different speeds. This shift suggests that the load on the ipsilateral limbs increased, which was confirmed by ground reaction force measurements under each belt in two cats (data are not shown). I expect that cats apply more pressure to the anesthetized limbs to improve the level of tactile sensation from the anesthetized paws (Nowak et al. 2001). Since the CoM did not shift from the control position with anesthesia of the right paws when the two belts moved at the same speed, it can be suggested that CoM moves towards the anesthetized side only during challenging walking tasks. This is consistent with a similar conclusion about the role of paw cutaneous afferents made in (Bouyer and Rossignol 2003).

Duty factor. The change in duty factor agrees with the CoM shift, except when the contralateral belt moved faster than the ipsilateral belt. With the paw pad anesthesia, duty factor of the ipsilateral forelimb and hindlimb increased at speed ratios above 1.0; at the same time, duty factor of the contralateral hindlimb did not change. The changes in duty factor were mainly caused by the reduction in swing phase duration. The reason for the increase of duty factor increase of the contralateral forelimb is unclear.

EMG. The increased duty factor might be related with the increase in the mean EMG amplitude of ankle extensors, either SO or MG muscle. The SO EMG amplitude was higher at low speed ratios 0.5 and 1.0, whereas the MG EMG amplitude increased when the ipsilateral belt moved faster than the contralateral belt (speed ratios above 1.0).

This differential response of SO and MG to increasing speed of the ipsilateral belt is consistent with reports of continuing recruitment of additional motor units and increasing force production with speed of walking in MG but not in SO (Prilutsky et al. 1996; Walmsley et al. 1978). The increased mean IP EMG amplitude is consistent with the shorter swing duration during anesthesia.

Anterior-posterior limb ranges. With paw pad anesthesia, cats placed the hindlimb paws on the ground more rostrally at the stance onset when the speed of the ipsilateral belt was higher than the contralateral one. This forward movement of the hindlimb might be caused by the earlier hindpaw liftoff. During the split-belt walking with a unilateral belt speed increase, the largest spatial change was found for the hindlimb

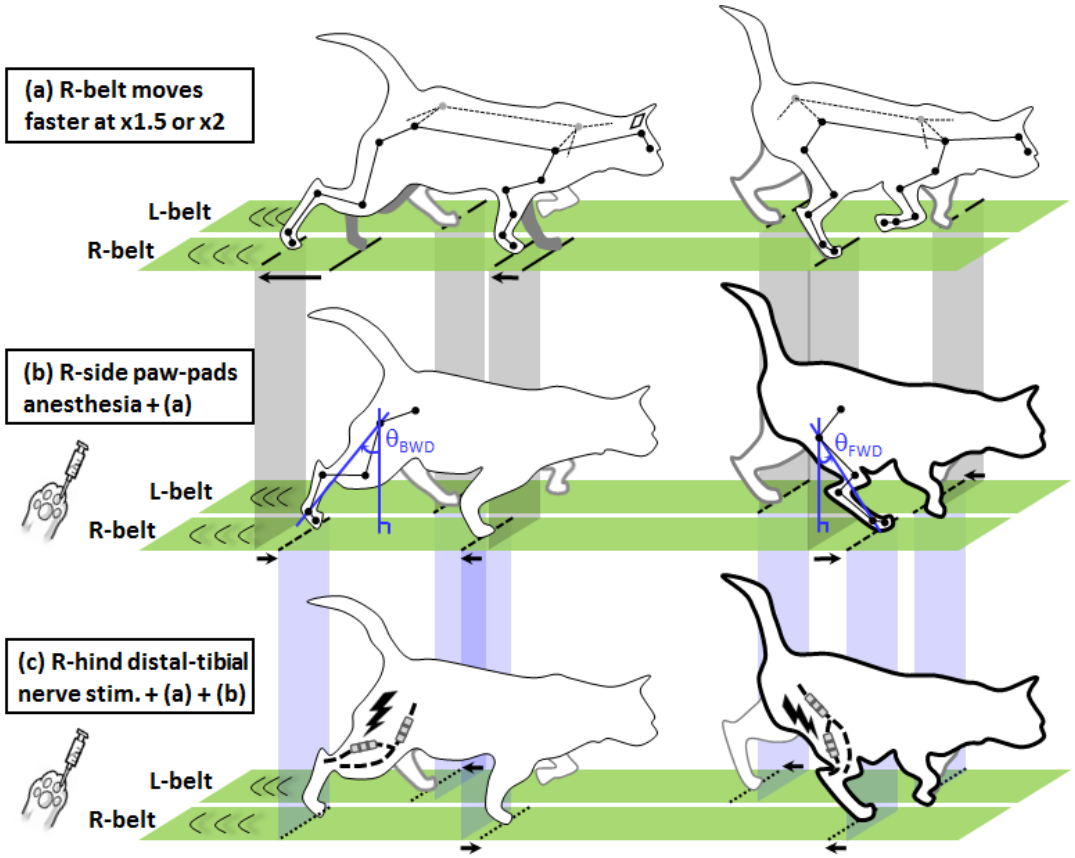

Figure 2.37. Changes of limb positions at right hindlimb stance onset and offset due to the asymmetric belt speed and the cutaneous afferent modulations.

on the faster belt at the stance offset. The right hindlimb traveled more caudally as the ipsilateral belt speed was higher than the contralateral speed (Fig. 2.37a). It has been suggested that the stance offset is influenced by both the length of the hip flexor muscles and by the ankle unloading (Pearson 2008). However, the role of cutaneous feedback in determining the stance offset is still unclear. I suggest that earlier triggering of the stance offset of the affected hindlimb could partially depend on the missing cutaneous feedback from paw pads.

The changes of anterior-posterior limb ranges of movement also contributed to the change of diagonality on both sides. With the paw pad anesthesia, the reduced phase difference between fore- and hindlimb on the ipsilateral side can be the result of an enhanced rostral movement of the ipsilateral hindlimb, and the necessity of the ipsilateral forelimb to avoid the collision, as shown in Fig. 2.37b.

Potential effects of paw pad anesthesia on CPG rhythm generator and pattern formation. With anesthetized right paw pads, cycle duration increased for all four limbs at speed ratios of 1.5 and 2.0. This result suggests that removing or reducing input from paw pad cutaneous afferents affects the rhythm generator level of the locomotor spinal pattern generator (CPG) and modulates the rhythm of the gait cycle. Anesthesia of the right paws did not change the temporal step symmetry at stance onset for both forelimb and hindlimb. This result suggests that cutaneous afferent pathway from the paw pads does not modulate the phases of the gait cycle and thus does not have access to the pattern formation level of CPG (McCrea and Rybak 2008).

With right paw-pad anesthesia, duty factor of the ipsilateral hindlimb increased at speed ratios of 1.5 and 2.0, but did not change for the contralateral hindlimb. This might indicate that cutaneous afferent input from the ipsilateral hindlimb has little influence on motoneurons supplying contralateral hindlimb muscles. The duty factor of the ipsilateral forelimb changed in the way similar to that of the ipsilateral hindlimb and at the same speed ratios of 1.5 and 2.0. This might indicate that, at the pattern formation level,

cutaneous afferents from the hindlimb have a strong excitatory influence on motoneurons supplying ipsilateral forelimb muscles (for review see (Frigon 2017)).

2.4.2. Effects of Distal-tibial Nerve Stimulation Reduces or Reverses some Effects of Paw Pads Anesthesia

Electrical stimulation of the distal-tibial nerve at strength 1.2T presumably activated mostly cutaneous afferents from hindpaw pads and plantar skin since no twitch of hind digit flexors was observed during stimulation. This stimulation during the stance phase while the paw pads were anesthetized resulted in a partial or complete cancellation of anesthesia effects for many kinematic characteristics. First, the swing duration and duty factor of both the right fore- and hindlimb returned to the control values during stimulation. In addition, both the anterior-posterior range of limb motion and phase difference between the ipsilateral forelimb and hindlimb returned to the control values, either partially or completely.

However, the distal-tibial nerve stimulation did not cancel the effect of anesthesia on the step length and on the contralateral forelimb angles. In addition, the phase difference between the contralateral hindlimbs at stance onset (temporal step symmetry at step onset) was clearly deviated from 0.5 due to the stimulation, even though it was minimally deviated from 0.5 with either unilateral belt speed increase or paw pad anesthesia. The phase changed mainly because of the delay in the stance onset by ipsilateral hindlimb. Despite an apparent cancellation of anesthesia effects by stimulation of the distal-tibial nerve, the stimulation could not fully replace the cutaneous afferent feedback from paw pads. The observed effects might be also related with a mismatch between the stance onset and stimulation offset, because only the stimulation onset was synchronized with the stance onset, whereas the stimulation lasted 500 ms.

2.4.3. Effect of Afferent Feedback Modulation from Paw Pads is Amplified when the Ipsilateral Belt Moves Faster than the Contralateral Belt

Each type of afferent feedback modulation from the paw pads (anesthesia of right hind- and forepaw and/or electrical stimulation of the right distal-tibial nerve) affected interlimb coordination during split-belt treadmill walking. The anesthesia changed the interlimb coordination as reflected in several spatial and temporal kinematic parameters. The electrical stimulation of the distal-tibial nerve at the right hindlimb appeared to reduce effects of right side paw anesthesia in most of the interlimb coordination parameters either partially or completely. The effect of the afferent feedback modulation was seen more clearly when the belt speed increased unilaterally on the ipsilateral side. Because the afferent feedback from the paw pads plays an important role in challenging locomotor tasks (Bouyer and Rossignol 2003), it is expected that at a higher speed of the ipsilateral belt, cats will have difficulties to maintain the same strategy of walking with reduced tactile feedback.

2.4.4. Loss of Stretch Feedback from Right Quad-Sart Increases Ipsilateral Hindlimb Swing-Phase Duration and Hindlimb Temporal Step Asymmetry at Stance Onset

Experimental results showed that self-reinnervation of right Quad-Sart increased the swing phase duration of the ipsilateral hindlimb. I could see this effect more clearly when the ipsilateral belt moved faster than the contralateral belt. This change in the right hindlimb swing duration also changed the temporal step symmetry at hindlimb step onset, i.e. the stance onset of the ipsilateral hindlimb was delayed relative to the stance onset of the contralateral hindlimb. It was a very strong effect easily recognizable from the recorded video that the cats unnaturally stopped their ipsilateral hindlimb in midair for a brief moment. It is possible that they were waiting for a certain trigger signal to initiate the swing to stance transition of the reinnervated limb. This result contradicts the initial

hypothesis that removal of stretch-dependent afferent signal from some hip flexors (rectus femoris, a head of Quad and Sart) would delay the stance offset (Kriellaars et al. 1994; Pearson 2008) but not stance onset as observed in this study. Given the obtained results, it appears that group I afferents from the spindles of rectus femoris and Sart are not involved in triggering the stance to swing transition; that trigger signal is likely to come from the spindles of another hip flexor iliopsoas (Kriellaars et al. 1994). Given that removal of stretch reflex from Quad-Sart delayed the swing to stance transition of the ipsilateral hindlimb, an alternative hypothesis can be suggested that the stretch-dependent signal from the medial head of SART participates in regulating the swing to stance transition. This suggestion is supported by the stretch of the knee flexors, including the medial Sart, in late swing due to knee extension (Goslow et al. 1973; Gregor et al. 2006) and the report that electrical stimulation of length sensitive spindle afferents from sartorius at strength 3T – 5T sometimes inhibits the onset of the extensor activity phase in the ipsilateral extensors (e.g., Fig. 4A in (Lam and Pearson 2002)). Since the stimulation strength suggests activation of both group I and group II afferents, the exact mechanisms of the delay of stance onset by the ipsilateral hindlimb after removal of stretch feedback from Quad and Sart remains unclear.

Assuming that intact Sart generates a stretch-dependent signal in late swing as a knee flexor, which can potentially trigger the swing to stance transition, this signal is no longer available after Sart self-reinnervation. Therefore, cats might need another sensory signal to trigger the swing to stance transition. Such a signal could possibly come from the contralateral hindlimb extensor muscles. Instead of the length-dependent sensory signal from the ipsilateral hindlimb, an input from the contralateral hindlimb might trigger the ipsilateral swing to stance transition.

Fig. 2.38 shows simplified hindlimb angle changes for left and right hindlimbs during two cycles of walking. Fig. 2.38a shows hindlimb angle changes before right Quad-Sart self-reinnervation and Fig. 2.38b shows changes after Quad-Sart self-reinnervation. In both examples, the right belt moves faster than the left belt. In the intact condition, the right-hindlimb stance onset happens at the middle of left hindlimb stance phase. In the self-reinnervation condition, the right-hindlimb stance onset is delayed due to the lack of an appropriate sensory trigger. When the contralateral hindlimb initiates ground contact, its load afferents from the paw pads and muscles begin to enhance activity of contralateral extensors that in turn inhibit flexor motoneurons of the right hindlimb via the commissural interneurons (Rybak et al. 2015) and thus can trigger the swing to stance transition in the right hindlimb.

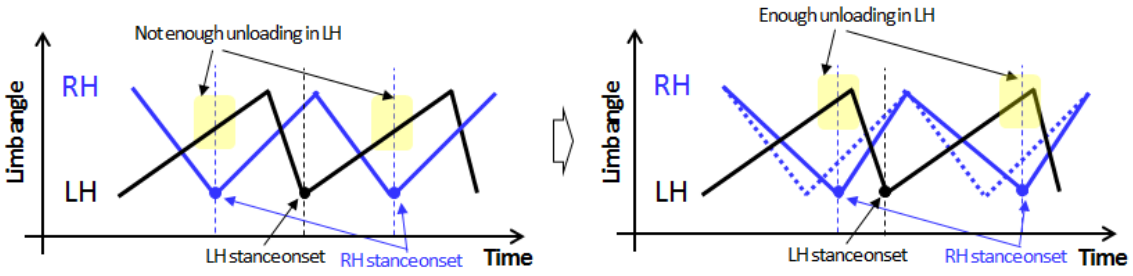

(a) (b)

Figure 2.38. Simplified limb angle changes for left hindlimb and right hindlimb during two cycles of walking.

2.4.5. Removal of Stretch Reflex from Quad-Sart affects Both CPG Rhythm Generator and Pattern Formation Levels with Strong Neural Coupling between Contralateral Limbs

With Quad-Sart self-reinnervation, the cycle duration increases for all four limbs, at speed ratios of 1.5 and 2.0. This result suggests that removal of stretch reflex from Quad and Sart modulates the rhythm of the gait cycle. Removal of stretch reflex from Quad-Sart also changes the hindlimb temporal step onset symmetry. This result suggests that input from Quad-Sart group Ia afferents also modulates the phases of the gait cycle and thus has access to the pattern formation level of the CPG. The changes in the

forelimb temporal step symmetry is minimal at speed ratios of 1.5 and 2.0. This suggests that the forelimb-hindlimb neural coupling at the level of rhythm generators may be weak.

Diagonality (phase difference between the ipsilateral forelimb and hindlimb movement) is another measure of the locomotor kinematics. It decreases significantly for the ipsilateral limbs and contralateral limbs at all four speed ratios. With Quad-Sart self-reinnervation, the swing phase duration of the ipsilateral hindlimb was significantly increased while stance phase duration did not change at speed ratio of 1.5 and 2.0. Therefore, the stance onset of the ipsilateral hindlimb was delayed. The reduced phase difference for ipsilateral limbs indicates that the stance onset of the ipsilateral forelimb is not delayed with respect to the ipsilateral hindlimb. This result also suggests that the fore-hindlimb neural coupling at the rhythm generator level is weak in terms of the phase change. The reduced phase difference between the contralateral limbs could be explained by a strong neural coupling via the commissural interneurons that allows for coordinating contralateral limbs at the rhythm generator level (Frigon 2017; Rybak et al. 2015).

With Quad-Sart self-reinnervation, the duty factor decreases for the ipsilateral hindlimb and increases for the contralateral hindlimb at speed ratios of 1.5 and 2.0. This indicates that group Ia afferents from Quad-Sart have a strong inhibitory influence on motoneurons supplying contralateral hindlimb muscles. The duty factor clearly changed in the same direction for the ipsilateral forelimb. This indicates that, at the pattern formation level, group Ia afferents from Quad-Sart also have a strong excitatory influence on motoneurons supplying ipsilateral forelimb muscles (Miller et al. 1975).

2.4.6. Limited Effect of Distal-Tibial Nerve Stimulation on Selected Spatial and Temporal Gait Parameters

Electrical stimulation of the distal-tibial nerve did not affect the swing phase, therefore the initial hypothesis that this stimulation would reduce the effect of the self-reinnervation needs to be rejected. However, the stimulation reduced or reversed the

effects of Quad-Sart self-reinnervation on cycle duration for all four limbs. In addition, the stimulation reversed the change in the stance phase duration for left fore- and hindlimb at the speed ratio of 1.5. Distal-tibial nerve stimulation minimally affected the temporal step symmetry, diagonality, and step length.

With Quad-Sart self-reinnervation, distal-tibial nerve stimulation did not shift CoM compared to the intact condition. However, with the stimulation, CoM was shifted to the affected side, especially when two belts moved at different speed. This result is hard to explain because it is not consistent with the change in duty factor and phase duration.

CHAPTER 3

EFFECTS OF MODULATING SELECTED PERIPHERAL SENSORY FEEDBACK ON STATIC AND DYNAMIC STABILITY

3.1. Introduction

Undoubtedly, stability is one of very important factors in successful walking because falling caused by stability loss make walking impossible. Postural stability and balance during walking and standing are maintained by a complex system of sensory pathways and reflexes, originating in the visual, vestibular and somatosensory systems (Horak and Macpherson 1996). The fastest reflex responses to postural perturbations are mediated by monosynaptic stretch reflexes that involve muscle spindle group Ia afferents (Hultborn 2006) and two- and polysynaptic pathways from cutaneous afferents from the body but especially from the foot (Duysens et al. 2004). It has been suggested that major functional significance of cutaneous foot reflex responses is to maintain postural stability during locomotion (Zehr and Stein 1999). Loss of proprioceptive and/or cutaneous feedback from lower limb, as a result of neuropathy, peripheral nerve injury or limb amputation, leads to decreased balance and stability and severely complicates movements and especially locomotion (Cole and Paillar 1998; Nardone et al. 2014). On the other hand, balance and stability could be preserved or enhanced even with loss of some somatosensory input by changing a movement strategy (e.g., decreasing walking speed, increasing step width and area of support, lowering the COM height, etc.) or by using artificial sensory signals and neural prostheses that restore sense of touch and movement (Tyler 2015; Weber et al. 2012).

In this chapter, I will discuss changes in walking static and dynamic stability by modulation of somatosensory feedback from cutaneous paw pad afferents and stretch afferents from quadriceps and Sartorius muscles (Quad-Sart).

For the efficient propulsion during walking, ambulatory animals intentionally make some phases of the locomotor cycle unstable. For example, in human walking there is a single limb support phase. During part of this phase, CoM is unstable – it moves beyond the area of support and accelerates forward due to gravity. Although this is a metabolically efficient movement strategy, it is feasible only if the stability can be recovered by the next step. During treadmill walking, cats also have an unstable forward acceleration phase called a diagonal 2-limb support phase. During this phase, the CoM vertical projection leaves the area of support and accelerates in the forward direction, so the cat is unstable in this phase of the walking cycle (Farrell et al., 2014). During most of the walking cycle in the cat, static stability in the frontal plane is much lower than in the sagittal plane due to the configuration of the area of support – it is about 6-10 cm wide and 25 cm long (Bolton and Misiaszek 2009; Farrell et al. 2014; Farrell et al. 2015; Misiaszek 2006).

If either cutaneous sensory feedback from paw pad afferents or muscle length-dependent sensory feedback from muscles crossing the hip joint is removed or reduced, the cat would be less capable of maintaining stability and balance, especially during challenging locomotor tasks like split-belt treadmill locomotion. Accordingly, the cat might be expected in this situation to modify motor strategy to improve balance control and stability. Motor compensations to improve stability of walking include reduction of forward velocity and stride length (Maki 1997; Misiaszek 2006), increasing step width (Dunlap et al. 2012), lowering COM and making the double- or triple-support phases longer (Farrell et al. 2015; Galvez-Lopez et al. 2011). All these modifications in walking kinematics are expected to improve static and dynamic stability of walking. I also expect that this cautious behavior will be more noticeable at higher split-belt speed ratios.

Hof and colleague have found that persons with an above-knee prosthesis have larger margin of lateral dynamic stability than the control healthy group during treadmill walking (Hof et al. 2007). In that study, the participants with the limb loss had obvious deficits of cutaneous and proprioceptive feedback from the prosthetic limb. Thus, they found increased margins of lateral dynamic stability in that study might be a compensation movement strategy to improve stability and reduce probability of falling in people with limb loss. If the cutaneous afferent feedback from paw pads and Quad-Sart stretch reflex were removed (or reduced) from one side of the body, cats would be expected to increase the margin of lateral dynamic stability, especially at the affected side. I expected that this change would be more noticeable when the ipsilateral belt moves faster than the contralateral belt. I also expected that providing an artificial tactile sensation during stance via stimulation of the distal-tibial nerve could improve balance control and reduce the effects of tactile and proprioceptive feedback removal.

The goal of this series of experiments was to examine the effect of manipulation of paw pad cutaneous feedback and stretch-dependent Quad-Sart input on static and dynamic stability of walking on a split-belt treadmill in the cat.

3.2. Materials and Methods

All surgical and experimental procedures were conducted in agreement with the Principles of Laboratory Animal Care (NIH publication No.86-23, revised 1985) and approved by the Georgia Tech Institutional Animal Care and Use Committee. This series of experiments used the same subjects, experimental procedures and afferent modulations as described in Chapter 2 (see Section 2.2 for details). The relevant data analysis related to determining static and dynamic stability is described in the following text.

Data Analysis. To exclude possible effects of motor adaptation to split-belt treadmill locomotion, I excluded the first 10 cycles after each speed change from the analysis. Stability analysis was performed for each walking cycle (see Table 2.1 for the number of cycles analyzed for each cat and experimental condition). Recorded marker coordinates were first low-pass filtered by a 4th order, zero-lag Butterworth filter with a cut-off frequency of 6 Hz. Filtered coordinates were used to determine stability parameters of walking, including step width, margins of static stability, and margins of lateral dynamic stability.

Step width was defined as the mean lateral distance between the center of the left and right limb paws, either forepaws or hindpaws (Fig. 3.1), at the moment of stance onset by the ipsilateral paw. Since body markers were on the lateral aspect of each paw, a half width of the paw and marker diameter was subtracted from the recorded marker position to obtain the position of the paw center for each paw.

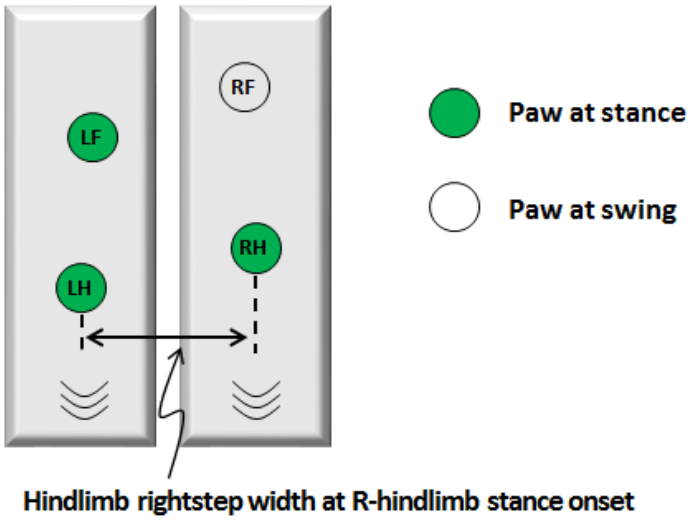

Figure 3.1. Definition of the hindlimb step width of the cat.

Static stability was defined as the shortest distance between CoM and the border of limb support area averaged across all time frames within each walking cycle if the CoM was located inside the limb support area (Fig. 3.2). If CoM was located outside the

limb support area, the same calculation was used and the obtained value was multiplied by -1.

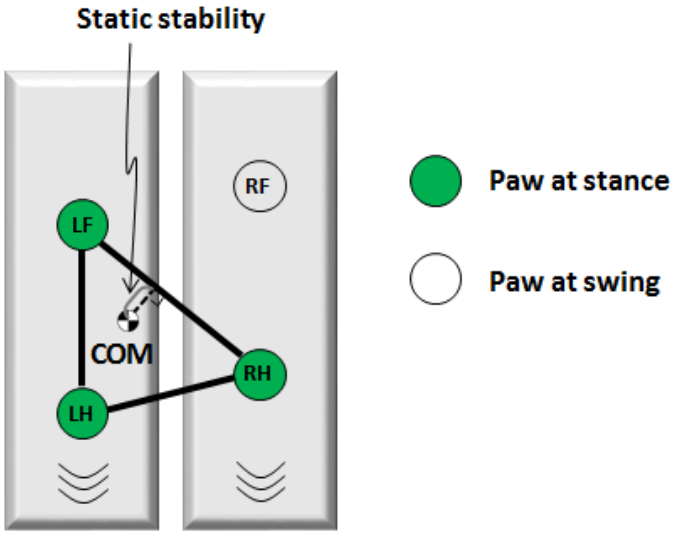

Figure 3.2. Definition of the static stability.

Extrapolated center of mass and center of pressure. The extrapolated center of mass position (xCoM) was defined as a position of the vertical projection of the CoM on the horizontal plane plus its velocity component in the corresponding direction (medial-lateral or anterior-posterior) times a factor $\omega[\sqrt{(g/l)}]$ (Hof et al. 2005).

In the above formula l is the limb length defined as the average length of all four limbs. Length of each limb was defined as the maximum height of either hip or shoulder joint during each cycle. Center of pressure (CoP), or the point of application of the resultant vector of all ground reaction forces acting on each paw in contact with the ground, was defined as the weighted sum of positions of paws on the ground with the corresponding measured magnitude of the vertical ground reaction force (Eq. 3.1).

Margin of lateral dynamic stability was defined as the lateral distance between CoP and xCoM (Fig. 3.3; Hof et al. 2005). I used the margin of lateral dynamic stability calculated at the stance onset of either left hindlimb or right hindlimb, because the margin

of lateral dynamic stability was maximal in the cycle at those instances. I defined the margin of lateral dynamic

stability at each instance of left hindlimb stance onset and right hindlimb stance onset as left margin of lateral dynamic stability and right margin of lateral dynamic stability, respectively. The graphical representation of the margin of lateral dynamic stability is shown in Fig. 3.3.

$$xCoM = CoM + v_{CoM} \cdot 2\pi \cdot f\left[\sqrt{\frac{g}{l}}\right]$$

$(v_{CoM}: velocity\ of\ center\ of\ mass$
$g: gravitational\ accerelation,$
$l: limb\ length, f: gait\ frequency)$

$$CoP = \frac{GRF_L \cdot xL + GRF_R \cdot xR}{GRF_L + GRFR}$$

$(GRF_L: ground\ reaction\ force\ measured\ at\ L\ belt,$
$GRF_R: ground\ reaction\ force\ measured\ at\ R\ belt$
$x_L: mean\ location\ of\ L\ limbs\ in\ contact\ with\ ground,$
$x_R: mean\ location\ of\ R\ limbs\ in\ contact\ with\ ground)$

Eq 3.1. Equations for xCoM and CoP.

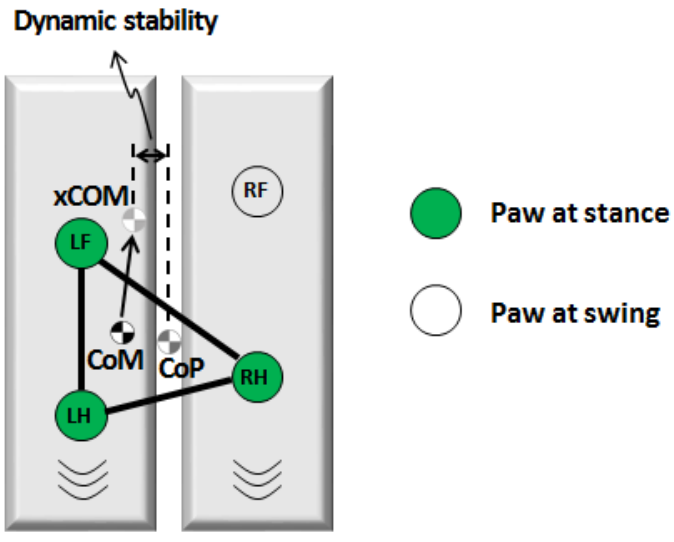

Figure 3.3. Definition of the margin of lateral dynamic stability on right side, at the right hindlimb stance onset.

Relative duration of limb support phases was defined as the ratio of the duration of each limb support phase to the cycle duration. Each limb support phase was defined by the limbs in contact with the ground at each time instant of the walking cycle. During quadrupedal walking, there are 8 limb support phases (4 limbs x 2 phases, stance and swing, for each). Depending on a walking task and speed, the number of limbs on the ground during walking is between 2 and 4 (Farrell et al. 2014; Gray 1968). During intact walking on the split-belt treadmill, the cats had 4 distinct limb support phases: (1) diagonal 2-limb support phase with a diagonal forelimb and hindlimb on the ground, (2) ipsilateral 2-imb support phase with an ipsilateral forelimb and hindlimb on the ground, (3) 3-limb support phase and (4) 4-limb support phase (Fig. 3.5). The number of limbs on the ground generally determine the area of support and thus static stability – the more limbs are on the ground, the better stability.

3.3. Results

3.3.1. Effects of Modulation of Paw Pad Afferent Feedback on Stability of Split-Belt Treadmill Walking

Step width. The hindlimb step width increased when anesthesia was applied to the right fore-and hindpaws at speed ratios of 0.5, 1.5 and 2.0 ($p<0.05$; Fig. 3.4). The step width for forelimbs increased only at speed ratio of 0.5 ($p<0.05$). Stimulation of the right distal-tibial nerve during stance reduced the hindlimb step width at all speed ratios. The stimulation effect on the forelimb step width was less pronounced or consistent – step length decreased for speed ratio of 0.5, and increased for speed ratio of 1.5 ($p<0.05$).

Relative duration of limb support phases. Paw pad anesthesia had different effects on the relative durations of the four limb support phases depending on the speed belt ratio. At ratio of 0.5, anesthesia decreased the ipsilateral 2-limb support phase and increased the 3-limb support phase duration ($p<0.05$). At speed ratios of 1.0 and 1.5, the diagonal 2-limb support and 3-limb support phase duration were decreased, whereas the

4-limb support phase duration is increased ($p<0.05$). Finally, at the highest speed ratio of 2.0, anesthesia of the right paws decreased durations of the two 2-limb phases ($p<0.05$).

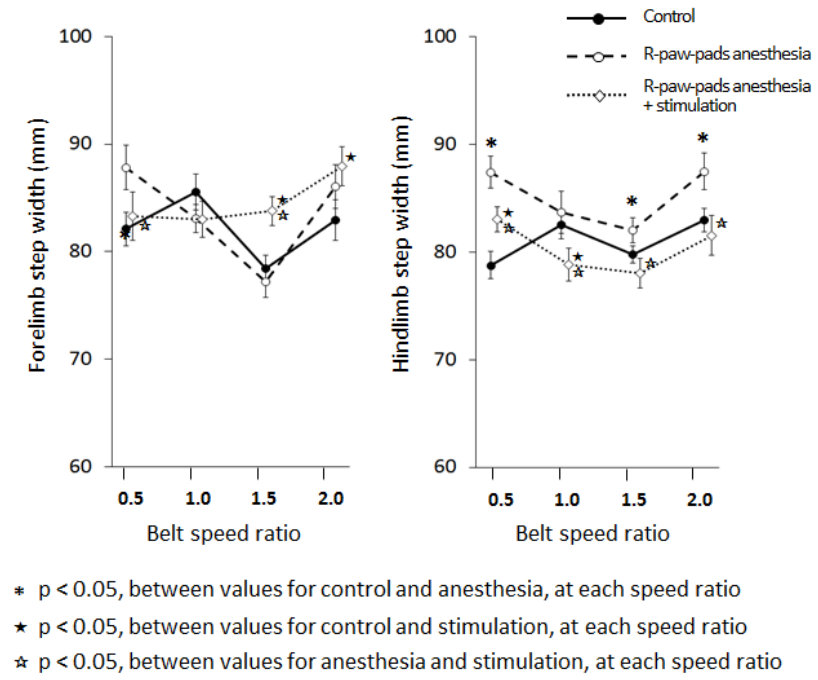

Figure 3.4. Mean (±95% confidence interval) step width of the left and right limbs during split-belt treadmill walking with anesthetized right fore- and hindpaws and during stimulations of the right distal-tibial nerve.

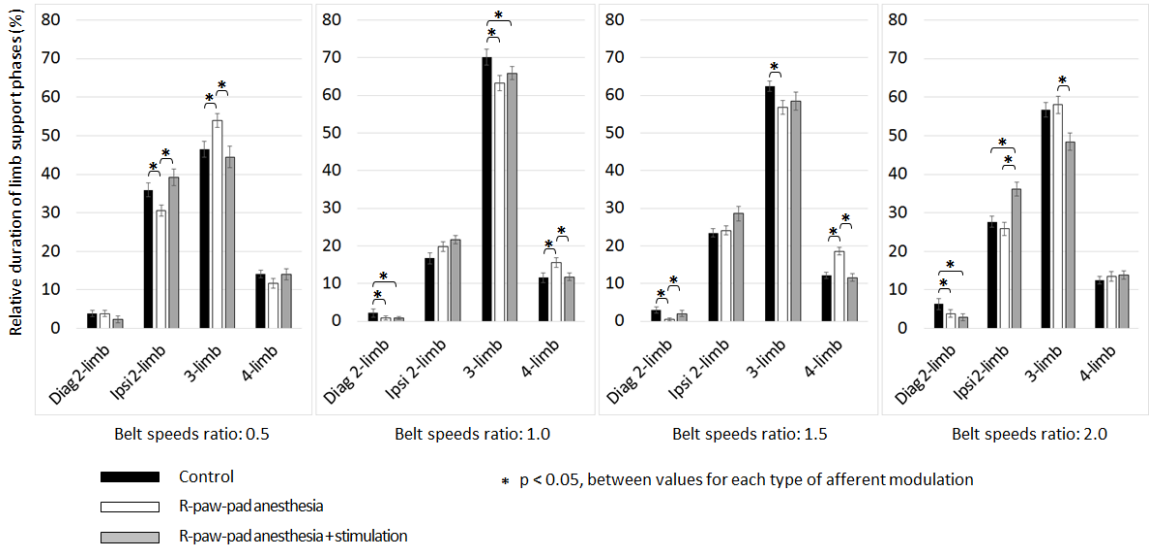

Figure 3.5. Mean (±95% confidence interval) normalized step phase durations of four limb support phases (in %) during split-belt treadmill walking with anesthetized right fore- and hindpaws and during stimulations of the right distal-tibial nerve.

Tibial nerve stimulation during stance reversed the anesthesia effects at speed ratios of 0.5 (for the ipsilateral 2-limb and 3-limb phases), 1.0 (for the 4-limb phase) and 1.5 (for the diagonal 2-limb and 4-limb phase); $p<0.05$ (Fig. 3.5).

Static stability. Margins of static stability increased with application of paw anesthesia at speed ratios 0.5, 1.5 and 2.0 ($p<0.05$) and it did not change at speed ratio of 1.0 ($p>0.05$; Fig. 3.6). Distal-tibial nerve stimulation reversed effects of anesthesia on static stability at speed ratios 0.5, 1.5 and 2.0 (at the latter ratio there was a substantial overshoot beyond the control values). At speed ratio of 1.0 the static stability decreased with tibial nerve stimulation ($p<0.05$). Changes in ipsilateral 2-limb support phase and 3-limb support phase at the speed ratio of 0.5 were reversed, and changes in 4-limb support phase at the speed ratio of 1.0 and 1.5 were reversed.

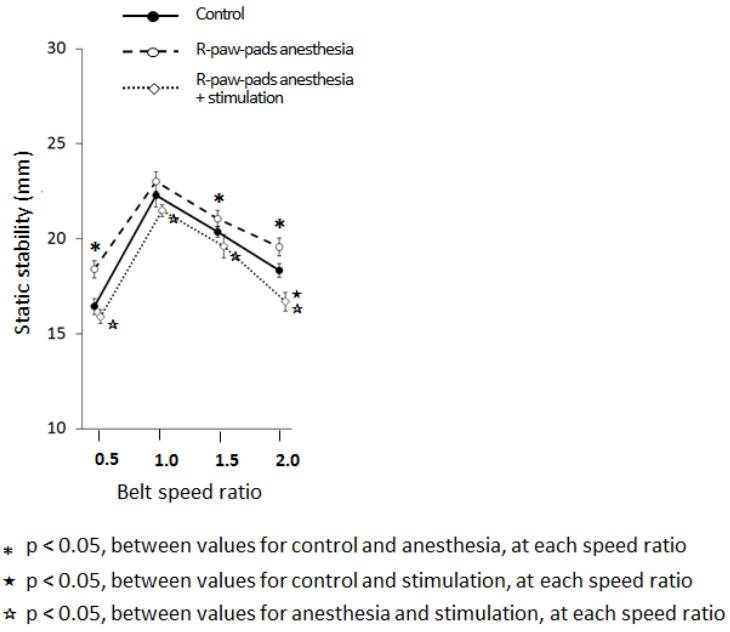

Figure 3.6. Mean (±95% confidence interval) static stability margin during split-belt treadmill walking with anesthetized right fore- and hindpaws and during stimulations of the right distal-tibial nerve.

Lateral dynamic stability. Left margins of lateral dynamic stability decreased with speed ratios, while the right margins increased with speed ratios ($p<0.05$; Fig. 3.7). Anesthesia of the right fore- and hindpaws increased left stability margins at speeds ratios

of 0.5, 1.5 and 2.0 ($p<0.05$) and did not affect right stability margins ($p>0.05$). Fig. 3.8 shows exemplary time-domain graph of lateral CoM, xCoM, and CoP positions for a cat walking on the split-belt treadmill at speed ratio of 2.0. In this figure, cat intact condition and condition with anesthesia of the right paw pads are shown (panels a and b). The figure also shows similar data for an intact human subject (panel c) and a subject with an above-knee prosthesis on the left side (panel d; (Hof et al. 2007)). The cat with right paw-pad anesthesia showed a wider lateral trajectory of CoP, which resulted in larger lateral dynamic stability. The cat data were matched by the human results – the amputee showed a wider lateral trajectory of CoP, which also resulted in larger lateral dynamic stability.

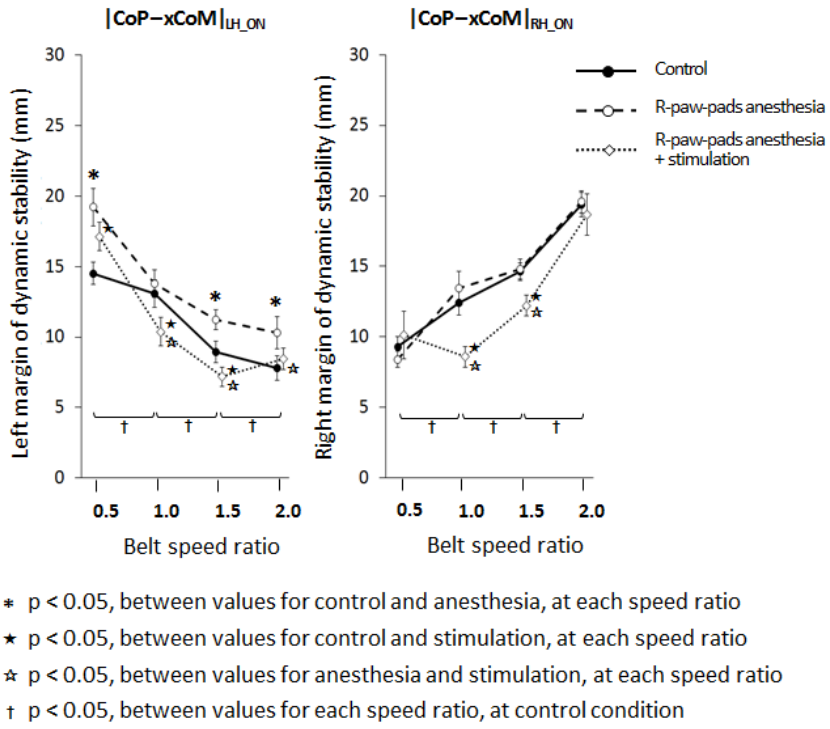

Figure 3.7. Mean (±95% confidence interval) margins of left and right dynamic stability during split-belt treadmill walking with anesthetized right fore- and hindpaws and during stimulations of the right distal-tibial nerve.

Distal-tibial nerve stimulation reduced or reversed the anesthesia effects on the left stability margins at speed ratios of 0.5, 1.5 and 2.0, whereas left stability was reduced by stimulation at speed ratio of 1.0 ($p<0.05$). Distal-tibial nerve stimulation also reduced right stability margins at speed ratios of 1.0 and 1.5 ($p<0.05$).

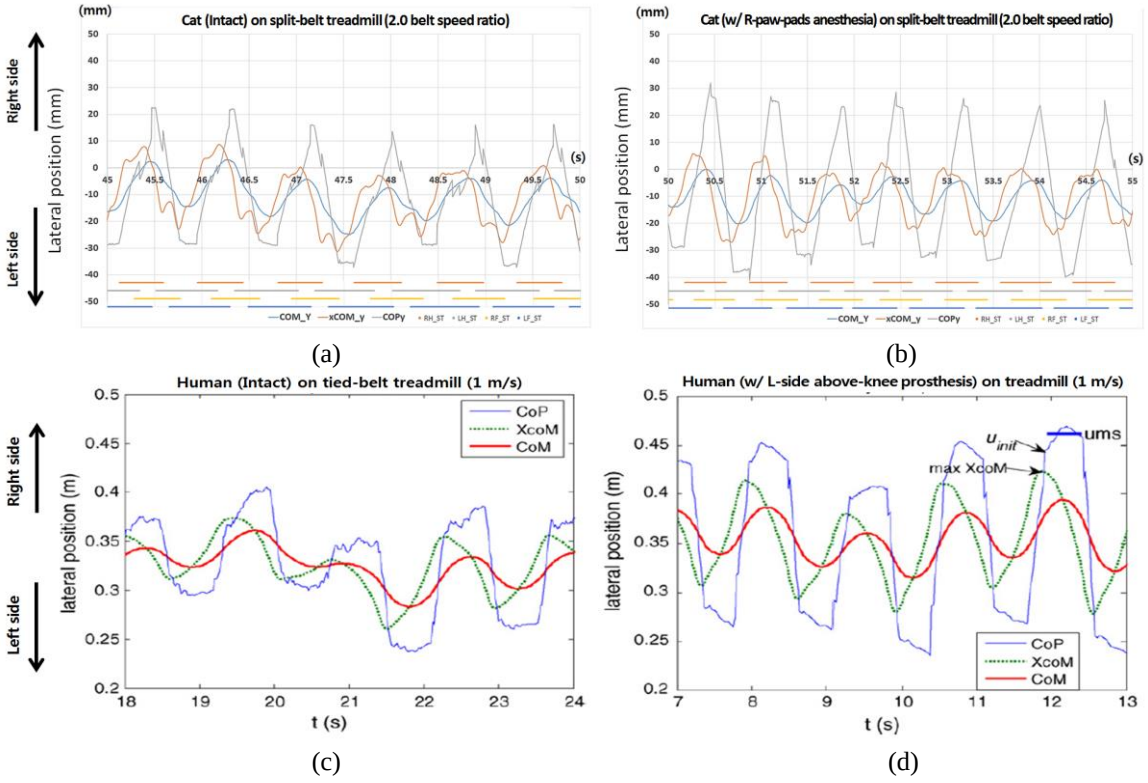

Figure 3.8. Lateral positions of CoM, xCoM, and CoP during (a) intact cat walking on split-belt treadmill (belt speed ratio of 2.0), (b) cat walking with right paw-pad anesthesia (belt speed ratio of 2.0), (c) intact human walking on tied-belt treadmill at speed of 1m/s (Hof et al. 2007), and (d) human walking with a unilateral, left above-knee prosthesis (speed 1m/s; Hof et al. 2007).

3.3.2. Effects of Stretch Reflex Removal from Quad-Sart on Stability of Split-Belt Treadmill Walking

Step width. Stretch reflex removal from the right Quad and Sart by their self-reinnervation substantially reduced step width for forelimbs at speed ratios 1.0, 1.5, and 2.0 ($p<0.05$; Fig. 3.9). The effect of self-reinnervation on the step width of the ipsilateral hindlimbs was rather modest, except a large increase in step length at speed ratio of 0.5

($p<0.05$). Distal-tibial nerve stimulation during stance typically reduced the effects of self-reinnervation on step width of both forelimbs and hindlimbs and in several cases (at speed ratios 1.0 and 1.5) completely reversed them ($p<0.05$).

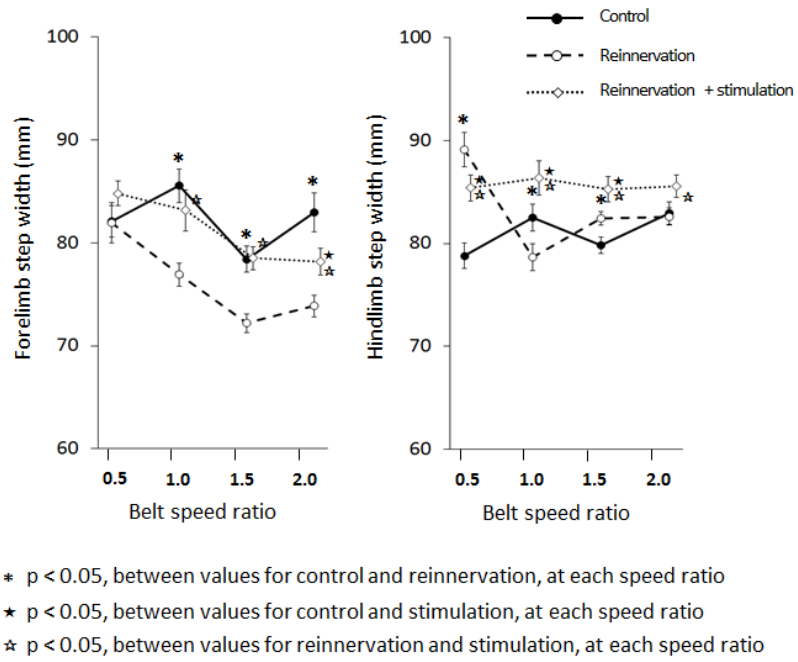

Figure 3.9. Mean (±95% confidence interval) step width of forelimbs and hindlimbs during split-belt treadmill walking with self-reinnervated right QUAD and SART and during stimulations of the right distal-tibial nerve**.**

Relative duration of limb support phases. The main effect of Quad-Sart self-reinnervation was shortening of the relative duration of the ipsilateral 2-limb support phase and a lengthening of the 3-leg support phase at speed ratios of 1.0 – 2.0 ($p<0.05$; Fig. 3.10). In addition, the diagonal 2-limb support phase duration also decreased at all speed ratios ($p<0.05$). Distal-tibial nerve stimulation reduced or completely reversed the effects of self-reinnervation for the diagonal 2-limb phase (speed ratios of 0.5 and 2.0), ipsilateral 2-limb phase (speed ratios of 1.0 and 2.0), 3-limb phase (ratios 1.0 and 2.0) and 4-limb phase (ratio of 1.0) ($p<0.05$). Stimulation also amplified the effect of self-reinnervation by increasing the duration of the ipsilateral 2-limb and 4-limb phases at speed ratio of 1.5 ($p<0.05$).

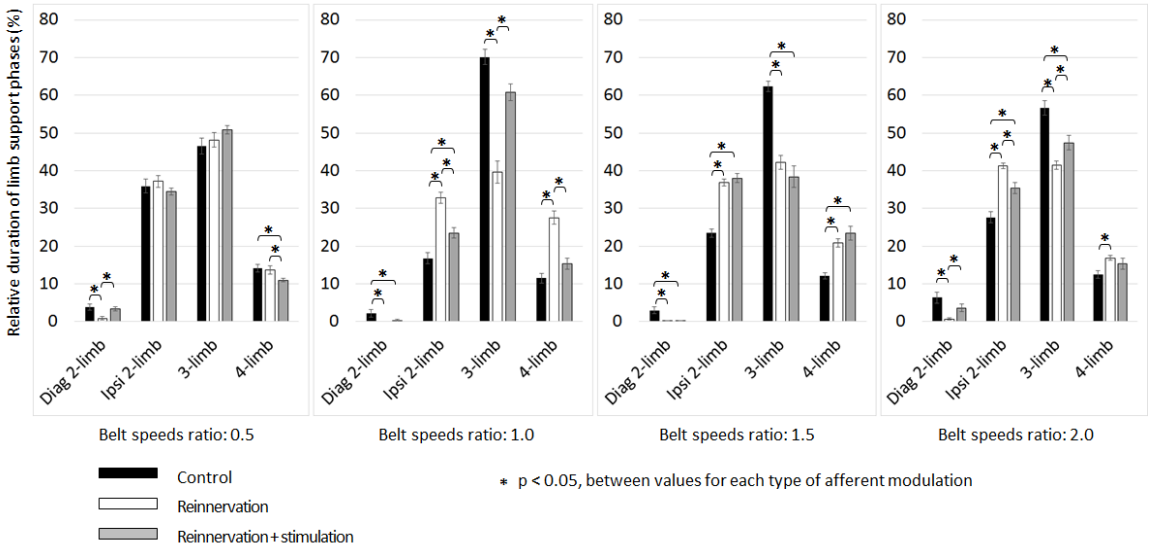

Figure 3.10. Mean (±95% confidence interval) normalized step phase durations of four limb support phases (in %) during split-belt treadmill walking with self-reinnervated right QUAD and SART and during stimulations of the right distal-tibial nerve.

Static stability. Quad-Sart self-reinnervation led to a substantial decrease in margins of static stability at speed ratios of 1.0 – 2.0 ($p<0.05$; Fig. 3.11). Distal-tibial nerve stimulation reduced the effect of self-reinnervation for speed ratios of 1.0 and 2.0 ($p<0.05$).

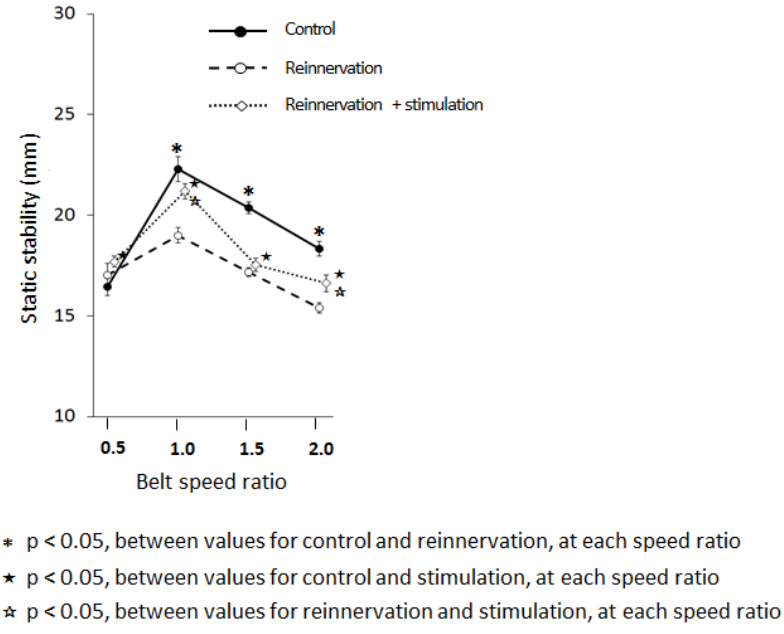

Figure 3.11. Mean (±95% confidence interval) static stability margin during split-belt treadmill walking with self-reinnervated right QUAD and SART and during stimulations of the right distal-tibial nerve.

Lateral dynamic stability. Self-reinnervation of right Quad-Sart reduced the left margins of dynamic stability at speed ratios of 1.0 – 2.0 ($p<0.05$; Fig. 3.12). The right margins were less affected by self-reinnervation – there was an increase in stability at speed ratio of 0.5, and a decrease in stability at speed ratios of 1.0 and 2.0 ($p<0.05$). Stimulation of the distal-tibial nerve increased the margins of left dynamic stability at speed ratios of 0.5 and 1.0; it also increased the right margin of stability at speed ratio of 1.0 and decreased it at speed ratio of 0.5 ($p<0.05$).

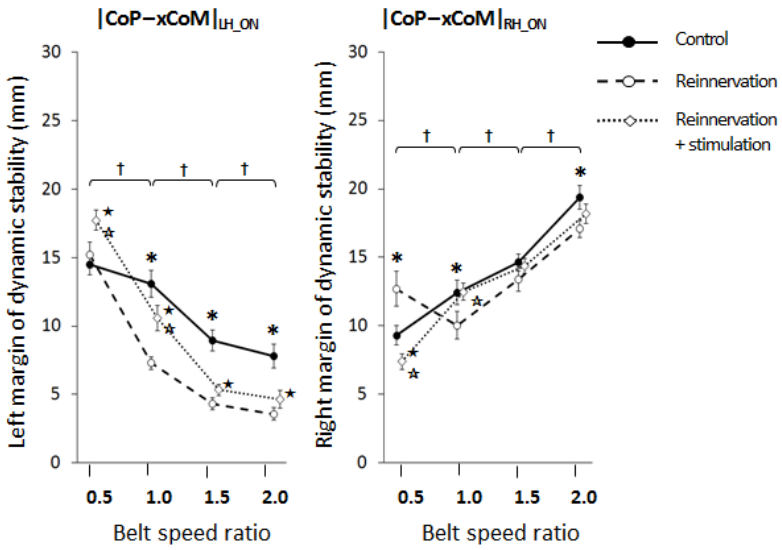

∗ p < 0.05, between values for control and reinnervation, at each speed ratio
★ p < 0.05, between values for control and stimulation, at each speed ratio
☆ p < 0.05, between values for reinnervation and stimulation, at each speed ratio
† p < 0.05, between values for each speed ratio, at control condition

Figure 3.12. Mean (±95% confidence interval) margins of left and right dynamic stability during split-belt treadmill walking with self-reinnervated right QUAD and SART and during stimulations of the right distal-tibial nerve.

3.4. Discussion and Conclusions

3.4.1. Paw Pad Anesthesia Decreases Duration of Diagonal 2-Limb Support Phase

Farrell and colleagues have found that the smallest area of support and substantial instability has been observed during the diagonal 2-limb support phase of the walking cats (Farrell et al. 2014). On the other hand, this diagonal 2-limb support phase helps cats to propel the body forward. With anesthesia of the right fore- and hindpaws, the relative duration of the diagonal 2-limb support phase shortened when the ipsilateral belt moved faster than or at the same speed as the contralateral belt. This result suggests that cats might be more cautious maintaining stability in this phase and select a motor strategy to avoid it.

3.4.2. Paw Pad Anesthesia Increases Margins of Lateral Dynamic Stability with Larger Step Width and CoM Shift

Cats increased the left dynamic stability with anesthesia of the paws on the right side. This result agrees with the increase in step width, especially the hindlimb step width. The margin of left and right lateral dynamic stability changed asymmetrically because the margin at the contralateral side increased and the margin at the ipsilateral side did not change. It would make more sense if the margin of dynamic stability increased on the ipsilateral side rather than the contralateral side, considering that the ipsilateral paw pads were anesthetized. This unexpected result could be explained by the CoM shift to the ipsilateral side, because the lateral dynamic stability was defined as the lateral distance from the xCoM to COP at the limb stance onset. If CoM was not shifted to the ipsilateral side, the stability margin at the ipsilateral side would have been increased at the contralateral side instead.

3.4.3. Changes in Step Width, Step Length, and Cycle Duration are Consistent with Stability Change during Paw Pad Anesthesia

Hak and colleagues have found that people increase step width and decrease step length and cycle duration with increasing perturbation intensity (Hak et al., 2013). I expected that cats would show a similar behavior with the loss of cutaneous input from paws if the loss affected stability of walking. Interestingly, cats showed the same behavior as humans when the ipsilateral belt speed increased unilaterally. In other words, paw pad anesthesia increased step width and decreased both step length and cycle duration when the ipsilateral belt moved faster than the contralateral belt. My interpretation of this result is that anesthesia of ipsilateral paws reduced walking stability and the cats adjusted the walking mechanics to compensate for stability metrics.

The decrease in step length with paw anesthesia needs a closer look because it occurred only on the contralateral side. This result is expected because the step length of the contralateral side was much longer than that of the ipsilateral side when the ipsilateral belt speed increased unilaterally. Cats would be expected to decrease the longer step length first to improve stability. The forward movement of the ipsilateral hindlimb with increasing speed ratios could be also related with the change in the step length, because the forward movement of the ipsilateral hindlimb could reduce the anterior-posterior distance between hindlimbs at stance onset of the contralateral hindlimb (i.e. reduce the step length of the contralateral hindlimb).

3.4.4 Distal-Tibial Nerve Stimulation Reduces or Reverses Effects of Paw Pad Anesthesia on Stability

Distal-tibial nerve stimulation reduced effects of anesthesia on stability measures. First, stimulation reversed changes in static stability (decreased static stability) and even showed an overshoot at the speed ratio of 2.0. It also reversed changes in lateral dynamic stability and step width, and had an overshoot of these two measures when two belts moved at the same speed. Distal-tibial nerve stimulation also reduced or reversed changes in the durations of stride phases, especially at speed ratio of 0.5, 1.0, and 1.5. In chapter

2, I have already observed that distal-tibial nerve stimulation reduced or reversed most of the changes in spatiotemporal gait parameters caused by paw pad anesthesia. The changes in stability due to stimulation further support the notion that tibial nerve stimulation partially substitute the missing natural cutaneous input.

3.4.5. Loss of Stretch Reflex from Right Quad-Sart Shortens the Diagonal 2-limb Support Phase, and Decreases Static and Dynamic Stability Too

With loss of stretch reflex from the right Quad-Sart, the relative duration of the diagonal 2-limb support phase was decreased at all speed ratios. This result agrees with the initial hypothesis that this most unstable phase of the walking cycle would be reduced with reduced proprioceptive input. However, the static stability and the margin of the contralateral dynamic stability decreased at the speed ratios of 1.0, 1.5, and 2.0 as a result. The latter observations appear to contradict the hypothesis.

First, I will discuss the stability decrease by analyzing other walking parameters. The forelimb step width decreased with loss of stretch-dependent feedback from the right Quad-Sart at the speed ratios of 1.0, 1.5, and 2.0. The decrease in step width would decrease the area of support in all limb support phases and thus decrease the static stability. Furthermore, the decreased step width would decrease the distance between the CoM and limb contact and thus COP, which would also decrease the lateral dynamic stability.

Next, I would focus on the remarkable increase of the ipsilateral 2-limb support phase. Although the ipsilateral 2-limb support phase is not as unstable as the diagonal 2-limb support phase, it still has a very small area of support compared to the 3-limb and 4-limb support phases (Farrell et al. 2014; Farrell et al. 2015). The remarkable increase of the ipsilateral 2-limb support phase duration might be related with the delayed stance onset of the ipsilateral hindlimb, as discussed in section 2.3.5. The 3-limb support phase also decreased significantly. Although the 4-limb support phase increased, the effect of

expending ipsilateral 2-limb support phase and shortening the 3-limb support phase would be enough to decrease static stability.

The potential reason for the decreased stability after removal of Quad-Sart stretch reflex could be that cats change walking strategies to compensate for the reduced proprioceptive input, but the changes are not necessarily directed to improve stability. Another explanation could be that the lost proprioceptive input is critical for maintaining stability, and the observed compensatory changes in walking kinematics were the best the animals could do to maintain stable locomotion.

3.4.6. Changes in Step Width, Step Length, and Cycle Duration are Consistent with Stability Change after Removal Stretch Reflex from Quad-Sart

In accordance with the decrease in static and dynamic stability, cats would decrease step width, increase cycle duration, and decrease step length (Hak et al., 2013). First, cats decreased forelimb step width at the speed ratio of 1.0, 1.5, and 2.0. I also observed that cats increased cycle duration when the ipsilateral belt moved faster than the contralateral belt. The change in step length does not agree with the stability changes. The step length increased on the ipsilateral side, while it decreased on the contralateral side. Considering that the step length on the contralateral side is much longer than that on the ipsilateral side in intact condition, these changes appear to improve static stability.

3.4.7. Distal-Tibial Nerve Stimulation Reduces or Reverses Effects of Quad-Sart Stretch Reflex Removal on Walking in Selected Conditions

Tibial nerve stimulation reduced or reversed effects of stretch reflex removal from the right Quad-Sart on several parameters of walking kinematics. This effect was clear and could be observed in many stability measures, including static stability, lateral dynamic stability, step width, and durations of limb-support phases.

The fact that stimulation of the right distal-tibial nerve affected only some kinematic parameters and measures of stability and at specific speed ratios can be

potentially explained by task and phase dependent effects of stimulation of foot cutaneous afferents. The responses to this stimulation differ if stimulation is delivered in early stance, mid-stance, late stance and early swing (Duysens et al. 2004; Zehr and Stein 1999). In this study the stimulation duration was constant (500 ms) and started at the onset of stance, but the stance duration of the right hindlimb varied with speed ratios (Fig. 2.21). Thus, it is expected that at relatively long stance phases of the right hindlimb at speed ratios of 0.5 and 1.0 (~580 – 650 ms, Fig. 2.21) right paw pad afferents would not be stimulated at late stance; at speed ratio of 1.5 (~500 – 520 ms), they will be stimulated during most of the stance; and at speed ratio 2.0 (~450 ms), they will be stimulated during the whole stance plus early swing. This variability of the stimulation phase is expected to lead to variable responses (Duysens et al. 2004; Zehr and Stein 1999).

CHAPTER 4

CLOSED-LOOP CONTROL SYSTEM TO CORRECT FOR ASYMMETRY OF PROSTHETIC WALKING

4.1. Introduction

Amputees with passive unilateral prosthetic legs frequently show asymmetric gait, which can cause undesirable compensation and subsequent degenerative musculoskeletal changes (Jeagers et al. 1995; Burke et al. 1978). Among the variety of underlying reasons causing gait asymmetry, the lack of a muscular system below amputation and the lack of peripheral sensory feedback from the missing limb are two fundamental problems that differentiate the prosthetic leg from the intact leg. To correct motor and sensory deficits, it is necessary to establish a communication interface between the body and the prosthesis. In addition, it is important to find a map for both the ascending sensory pathway and the descending motor pathway, to translate electrical signals to neural signals and vice versa.

The idea of locomotor control by modulating somatosensory feedback is supported by prior studies that investigated the effect of sensory feedback on walking (Van de Crommert et al. 1998; Pearson 2008). Those studies have suggested that sensory feedback from moving limbs plays an important role in control of locomotion. For example, chronic spinal cats lacking supra-spinal control can adapt to different speeds of the treadmill belt by changing gait patterns (Grillner 1981). Additionally, electrical stimulation of either the distal-tibial or sural nerves could modulate activity of leg extensors or flexors during locomotion depending on the strength and phase of stimulation (Pearson, 2008; Ollivier-Lanvin et al. 2011). Although human locomotion seems to depend more on the supra-spinal control, it is widely accepted that sensory feedback also contributes to the control of human walking (Gervasio et al. 2013; Sinkjær

et al. 2000). The role of sensory feedback can be seen more clearly during walking in novel and complex environments, where sensory feedback contributes to correcting locomotion by providing information about the state of the moving limbs with respect to the environment (Jacobs et al. 2000; Bouyer et al. 2003).

Recent studies have shown the feasibility of replicating tactile sensations from the amputated, phantom limb by applying electrical stimulation to residual cutaneous nerves. For example, the electrical stimulation of peripheral nerves in the arm could activate variety of tactile sensations from the phantom hand (Tan et al. 2014; Ortiz-Catalan et al. 2014; Oddo et al. 2016). These studies suggest that electrical stimulation of sensory nerves with the appropriate stimulation parameters and movement phases can evoke a compound action potential in sensory nerve fibers and partially restore the missing sensory feedback (Tan et al. 2014).

It has been shown that a myoelectric signal with a built-in pattern recognition algorithm enables fine motor control in the arm prosthesis, even without any sensory feedback (Ortiz-Catalan et al. 2013; Ortiz-Catalan et al. 2014). Likewise, we might be able to control locomotor outputs (e.g. gait symmetry) by control of the active ankle joint, using myoelectric signals from ankle extensor/flexor muscles and a built-in pattern recognition algorithm. The myoelectric signals could be mapped onto control parameters of the motor driving an active ankle joint. Prior work on an active ankle joint has proved its efficacy for correcting gait abnormalities (Herr et al. 2012; Takahashi et al. 2015).

Although we can find the ascending and descending maps to elicit a tactile sensation using electrical nerve stimulation and to control ankle joint for walking using myoelectric signals from ankle extensor/flexor muscles, the map should have a range of adjustment considering individual difference and adaptiveness of the bio-system to various environments. The adjustment can be performed by a closed-loop optimization of the map, by monitoring selected gait metrics in real time. The closed-loop optimization could be done either on the sensory map of the afferent pathway or on the motor map of

the efferent pathway. In this chapter, I will discuss the development of a closed-loop control paradigm of the bi-directional neural pathway in the bone-anchored transtibial prosthesis of the cat, with a closed-loop optimization of either sensory nerve stimulation parameters or feedforward motor control parameters.

The following hypotheses were tested. (1) A closed-loop control of the stimulation parameters of distal-tibial nerve stimulation will control spatial step symmetry of intact walking cats on a split-belt treadmill. (2) Cat transtibial prosthesis with an active ankle joint and artificial sensory feedback will produce ground reaction force patterns similar to the intact hindlimb.

4.2. Materials and Methods

4.2.1. Animal Model for the Optimization of Sensory Nerve Stimulation Parameters

An adult cat has been involved in the experiments, which were approved by the Georgia Tech Institutional Animal Care and Use Committee. The cat was sufficiently trained to naturally walk on the split-belt treadmill for two minutes using food reward. The cat walked on the split-belt treadmill with two different split-belt treadmill speed settings: (1) both left and right belts moved at 0.4 m/s (04-04 speed, belt speed ratio 1.0) and (2) left belt moved at 0.4 m/s while right belt moved at 0.6 m/s (04-06 speed, belt speed ratio 1.5), as shown in Fig. 2.1. The cat had cuff electrodes implanted on both the distal-tibial nerve and the sciatic nerve of the right hindlimb. The cuff electrode on the distal-tibial nerve was used for electrical stimulation of cutaneous afferents on the plantar surface of the foot and paw during walking to modulate walking characteristics. The cuff electrode on the sciatic nerve was used to establish a stimulation threshold of the distal-tibial nerve that causes the smallest compound action potential of cutaneous afferent fibers in the sciatic nerve in a sedated animal (Ollivier-Lanvin et al. 2011).

4.2.2. Real-Time Gait Monitoring System and a Closed-Loop Optimization of Stimulation Parameters

Fig. 4.1 shows the entire system used in the experiment. A cat walked on a split-belt treadmill and a pressure sensor array under the belts monitored walking phase duration in real time. A control box electronics read sensor data from a pressure sensor array, sent it to the external computer, updated the stimulation parameters from outside, and generated a stimulus. An external computer analyzed the sensor data in real time, optimized stimulation parameters, and sent the updated parameters to the control box electronics (Park et al. 2016). The actual implementations of a pressure sensor array and a control box electronics are shown in Fig. 4.1.

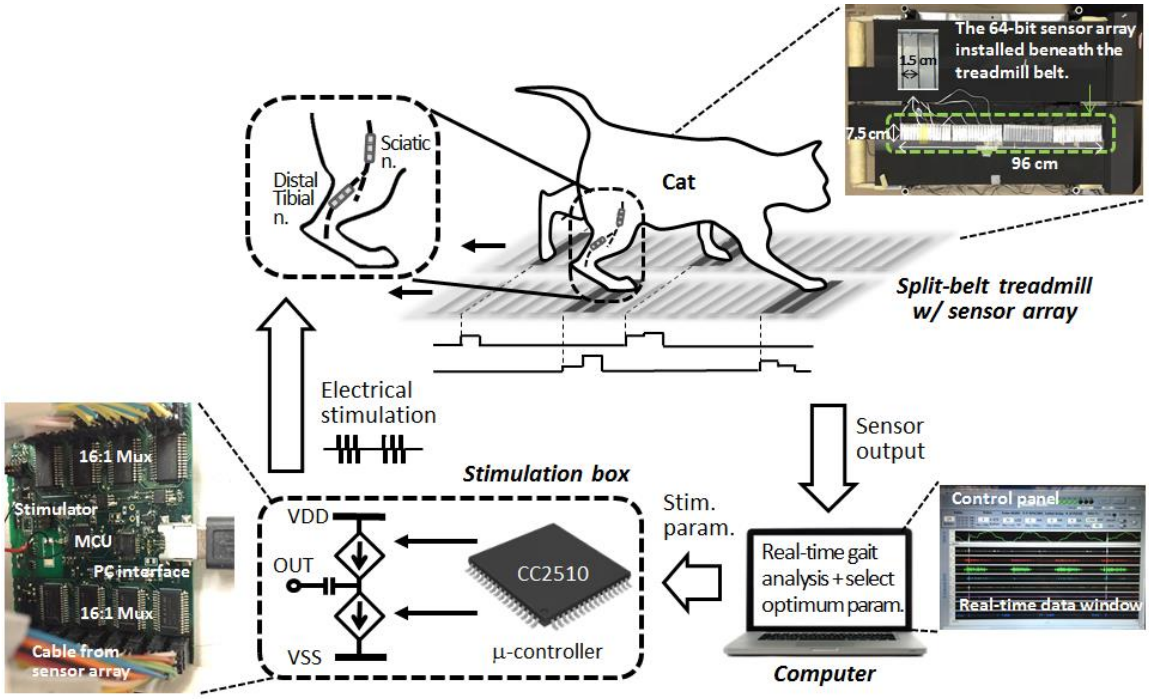

Figure 4.1. A real-time gait monitoring system with a pressure sensor array

The pressure monitoring system consisted of a 2-channel 64-bit pressure sensor array with 12-bit analog-to-digital converters at 100 Hz sampling. Digitized data from each channel were delivered to the computer in real time. I selected the pressure monitoring system over the optical recording system to decrease the timing error of stance onset and offset (Pantall et al. 2012). The timing error is caused by the processing time of the optical recording system to calculate stance onset and offset from optically

recorded kinematics. However, the pressure monitoring system could have a lower spatial resolution for recording the paw position at ground contact compared to optical recording system. To validate the spatial resolution of the pressure monitoring system, full-body kinematics was simultaneously recorded using the Vicon motion capture system (UK).

The computer processed the pressure sensor data to convert them to the spatiotemporal information of paw contacts, and calculated gait metrics. The computer also derived tailored stimulation parameters based on the measured gait metrics and the target gait metrics. The control box electronics generates an electrical stimulus according to the selected stimulation parameters. The CC2510 (Texas Instrument, TX, USA) microcontroller in the control box electronics communicated with the computer and tuned the stimulus accordingly.

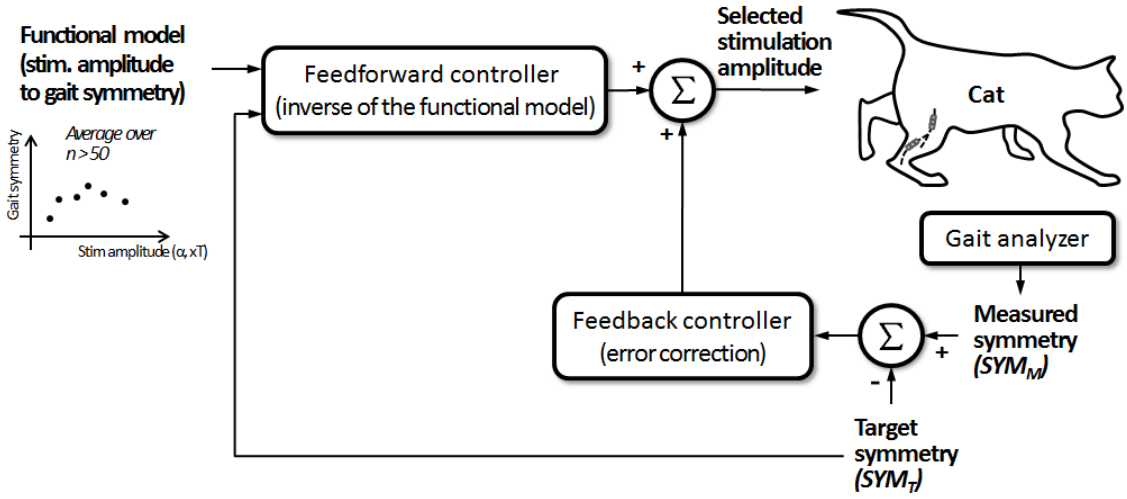

Figure 4.2. A functional block diagram of the real-time closed-loop gait control system using the optimization of stimulation amplitude at ascending pathway (SYM_M: measured spatial step symmetry, SYM_T: target spatial step symmetry) with feedforward and feedback controllers.

4.2.3. Functional Model (between simulation amplitude and gait symmetry)

The functional model of gait symmetry metrics described a statistical relationship between input of the model (i.e., the stimulation amplitude), and its output (i.e., the recorded spatiotemporal information of paw contacts) (see Fig. 4.2). This model was established experimentally. Although multiple stimulation parameters were desired to fully

utilize the effect of sensory nerve stimulation, I only investigated the effects of the stimulation amplitude on gait symmetry to simplify the experiment and provide a proof of concept.

4.2.4. Gait Analyzer

A gait analyzer generated gait metrics that were used for the stimulus optimization. Several gait metrics were used to describe locomotor behavior on the split-belt treadmill, such as the ratio of stance duration over swing duration, spatial step symmetry, and temporal step symmetry (Malone et al. 2012; Frigon et al. 2013). In this work, the spatial step symmetry was selected as the output gait metric, considering its prevalence in the abnormal gait with sensorimotor deficits. The spatial step symmetry (SYM_M) was defined as the ratio of the the right step length to the sum of the left and right step lengths (see Fig. 2.6). The right step length was defined as the anterior-posterior distance between the two hindpaws at the moment when the right hindpaw contacted the ground; the left step length was defined similarly, as the anterior-posterior distance between paws at stance onset of the left hindlimb (Malone et al. 2012).

4.2.5. Feedforward and feedback Controller

Fig. 4.2 illustrates a block diagram of the feedforward and feedback controllers used to select the optimum stimulation amplitude based on the measured spatial step symmetry (SYM_M), the target spatial step symmetry (SYM_T), and the statistical relationship between the stimulation amplitude and the spatial step symmetry. The controller first selects appropriate stimulation amplitude using the input-output relationship obtained from the functional model of gait symmetry. Because input-output relationships are complex and adaptive in biological systems, the controller also employs a feedback controller having the error between SYM_M and SYM_T as an input. The role of the feedback controller is to stabilize the output, and to correct for the adaptive change of the neural circuitry. We expect the adaptive change could be compensated via the statistical training of the system using actual input/output data (Afshar et al. 2013).

4.2.6. Design of Transtibial Prosthesis with an Active Ankle Joint, for the Cat

As an active ankle joint, I selected a linear actuator instead of a rotary actuator because we can implement a closer mechanism to actual ankle joint operation using the linear actuator. Several human transtibial/transfemoral prostheses/orthoses have been developed with linear actuators, as shown in Fig. 4.3. Because of the bi-directional controllability of the linear motor arm, a linear actuator can work both as an ankle extensor (like the Soleus muscle) and as an ankle flexor (like the Tibialis Anterior muscle). As shown in Fig. 4.4, a linear motor can work as either an extensor muscle or a flexor muscle, by decreasing or increasing its arm length, respectively.

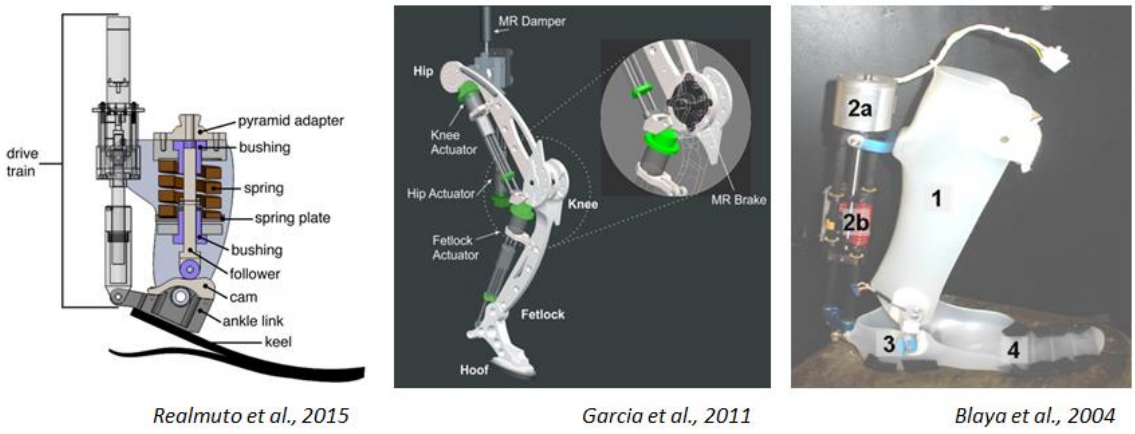

Figure 4.3. Exemplary human transtibial/transfemoral prosthesis/orthosis with linear actuators.

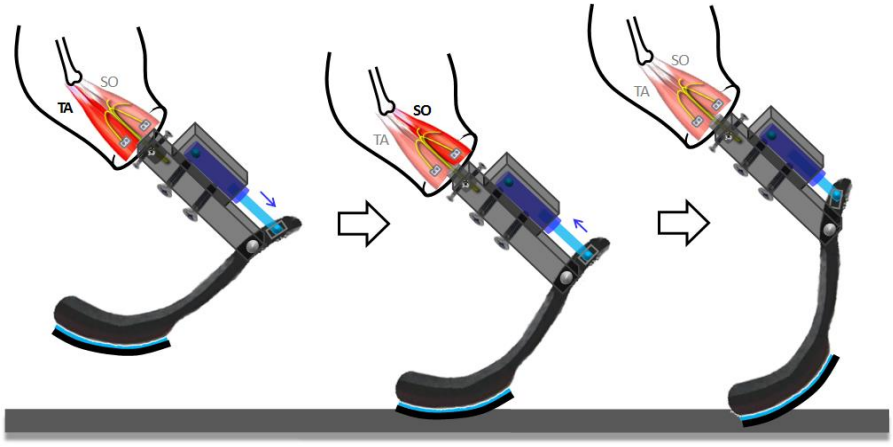

Figure 4.4. Graphical operating diagram of the transtibial prosthesis: (a) at the middle of the swing phase with inactive SO and active TA, (b) at the beginning of the stance phase with active SO and inactive TA, and (c) at the end of the stance phase with inactive SO and inactive TA.

4.2.7. Transtibial Prosthesis with Active Ankle Joint and Artificial Sensory Feedback

Fig. 4.5 shows the overall operating diagram of the transtibial prosthesis with active ankle joint and artificial sensory feedback (I will call it "active sensing transtibial prosthesis" in the following paragraphs). The active sensing transtibial prosthesis communicates with the nervous system via bi-directional neural interface with ascending/descending maps. Both ascending and descending maps are updated externally. The external gait monitoring system analyzes the gait in real time and the external processor updates both ascending and descending maps by a closed-loop optimization to achieve a target value of gait metric.

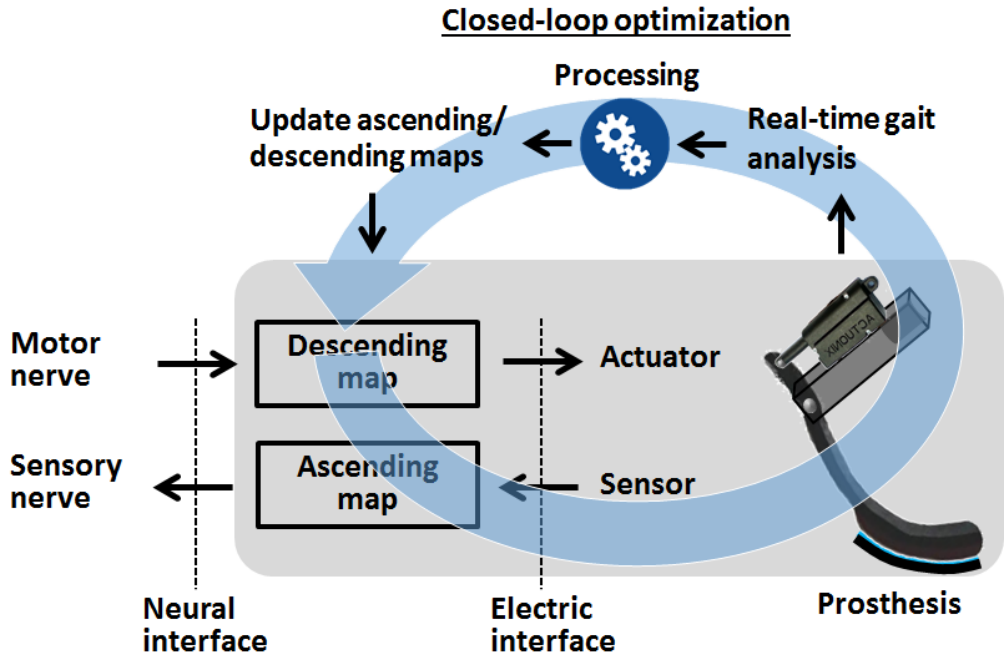

Figure 4.5. Overall operating diagram of the transtibial prosthesis having active ankle joint and artificial sensory feedback. The external gait monitoring system optimizes both ascending and descending maps and updates them as by the closed-loop optimization.

Fig. 4.6 shows the actual implementation of the active sensing transtibial prosthesis. Because the small size of the cat hindlimb, a major challenge was the system integration onto the limited area with limited weight (< 100 g, assuming the weight of the cat as 3 kg) (Hoy and Zernicke, 1985). All electronics have been integrated onto two

separate printed circuit boards. The electronics on one side of the linear motor takes care of the bi-directional neural pathway and another on the J-shape foot takes care of the wireless communication and battery recharging. A finger-sized small linear motor was selected to act as an active ankle joint, and a rechargeable Li-ion battery was selected to supply power to the entire system. The weight of the implemented active sensing transtibial prosthesis is ~60 g, which satisfies the design specification.

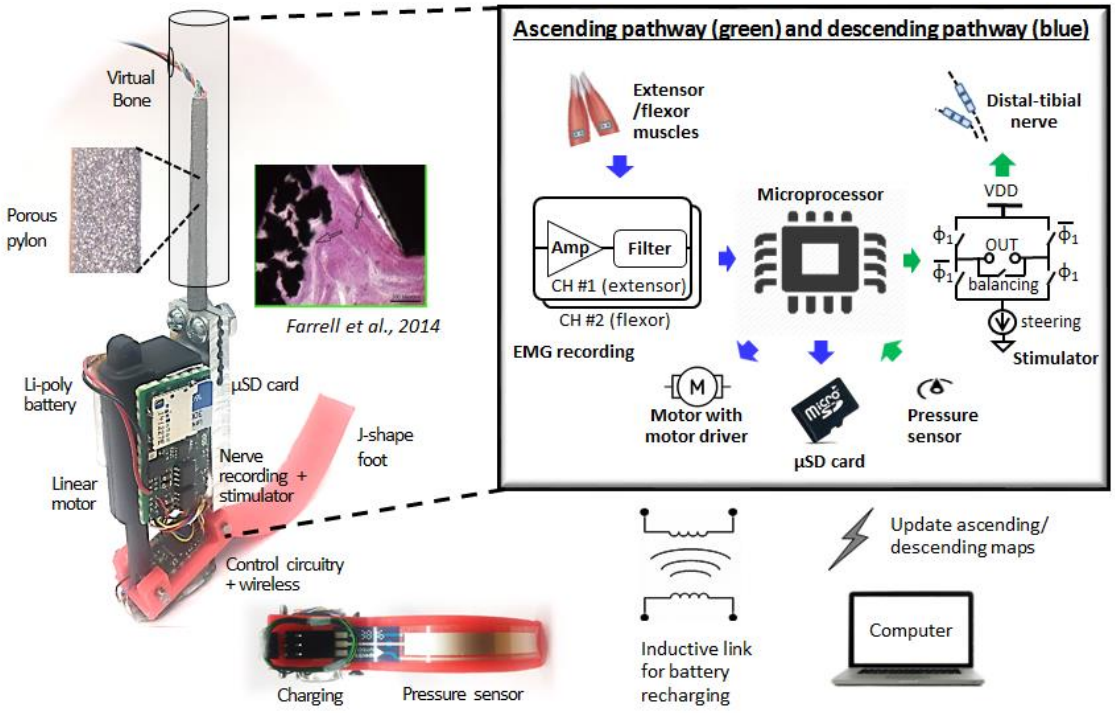

Figure 4.6. Implementation of the active sensing transtibial prosthesis and the block diagram of ascending/descending pathway.

4.2.8. System Description and Implementation of Active Sensing Transtibial Prosthesis

In this section, I will describe the actual implantation of the active sensing transtibial prosthesis, by categorizing its six functional blocks: (1) actuator and sensor, (2) ascending map and stimulator to generate artificial sensory feedback, (3) amplifier to record EMG signal and descending map, (4) battery and wireless recharging, (5) skin and bone integrated pylon with a peripheral nerve interface (SBIP-PNI), and (6) signal

processing in the external computer. I will explain each functional block in the above order.

First, as an actuator for the ankle joint, the PQ12 miniature linear motor (Firgelli, BC, Canada) was selected to be integrated onto the limited area and to generate a necessary torque for the ankle joint (Gregor et al. 2006). As a pressure sensor, a ThinPot linear position sensor (Spectra symbol, UT, USA) is located on the bottom of the J-shape foot, between the foot and the rubber.

Second, the ascending map converts the pressure sensor data to the form of electrical stimulus. The 12-bit analog-to-digital converter (ADC) and ultra-low-power 16-bit MSP430FR5738 MCU (Texas instruments, TX, USA) generate digital on/off signal of the stimulator based on the pressure information. The ascending map, which determines stimulation parameters (e.g. frequency, pulse width), is updated by the external signal processing via wireless link. The stimulator is composed of two P-channel MOS transistors and two N-channel MOS transistors, along with a charge balancing circuit and a current steering circuit on the bottom (Shulyzki et al. 2010). It was designed to generate a biphasic constant current stimulus under a single supply voltage, and to remove accumulated charge in the vicinity of the electrodes. Because the gates of the MOS transistors are controlled by the MCU, this stimulator can generate arbitrary forms of stimulus with user-defined frequency, pulse width, and pulse spacing. Additionally, the MCU controls the current steering circuit on the bottom of the stimulator, to set the amplitude of the stimulus as programmed by the user.

Third, the descending map converts the EMG signal to the form of a motor control signal. The INA128 instrumentation amplifier (Texas Instruments, TX, USA) amplifies the EMG signal with a gain of 1000 V/V and a Sallen-key off-chip bandpass filter removes motion artifact and high frequency noise with 30 Hz low-pass cutoff frequency and 5 kHz highpass cutoff frequency. The 12-bit ADC and the MSP430™ CPU receives amplified and filtered EMG signal and generates motor control signal

based on the built-in descending map. The built-in descending map is updated by the external signal processing via wireless link and motor control signal is delivered to the DRV8837 motor driver (Texas instruments, TX, USA). The motor driver generates voltage output with pulse-width modulation and switches polarity of voltage output by H-bridge according to the direction of movement.

Fourth, a 400 mAh Li-polymer rechargeable battery is mounted on one side of the linear motor. It can generate current up to 800 mA to handle the stall current of 550 mA for the PQ12 linear motor. Considering that the motor consumes ~200 mA to generate force of 20 N and the other electronics consumes less than 20mA in total, the battery will generally last more than 4 hours considering the duty of less than 50% in the ground reaction force curve of walking. The inductive coil for wireless recharging is located at the proximal end of the J-shape foot. Note that wireless recharging is required for the prosthesis, because it will be fully covered to avoid potential damage from the cat.

Fifth, skin and bone integrated pylon with a peripheral nerve interface (SBIP-PNI) is used to anchor the prosthesis onto the bone of the residual tibia. SBIP-PNI provides a wired pathway for a bi-directional neural communication between the electronics in the prosthesis and the peripheral nervous system on the distal end of the amputated limb (Pitkin et al., 2012). A porous surface of the pylon helps skin to penetrate the surface and seals the skin-pylon interface that can potentially cause a skin infection (Farrell et al. 2014).

Sixth, an external computer monitors the gait in real time, using the external pressure sensor array as shown in Fig. 4.1, and optimizes parameters for both the electrical stimulation and linear motor control. The updated parameters are sent to the electronics on the active sensing prosthesis, to update the ascending/descending maps programmed in the MCU. The update rate of the ascending/descending maps will be every 5-10 cycles of the gait, to minimize the effect of intra-individual biological variability. A user will set the target gait metric on the computer screen and a built-in

proportional-integral (PI) controller in the Labview (National Instrument, TX, USA) will change the parameters automatically, based on the open-loop relationship between gait parameters and target gait metric.

4.2.9. Modeling of Bi-directional Neural Pathway in Transtibial Prosthesis

To control an active, sensing transtibial prosthesis, I developed mathematical equations for each neural pathway. These mathematical equations are necessary to optimize both motor control parameters and nerve stimulation parameters, through a closed-loop control paradigm of a bi-directional neural pathway. I will call the mathematical equations as model equations because they are used to model the relationship (mapping). Each model equation has been obtained using the previous experimental results of intact cats. In the following paragraph, I will explain how I derived each model equation, with a graphical description shown in Fig. 4.7.

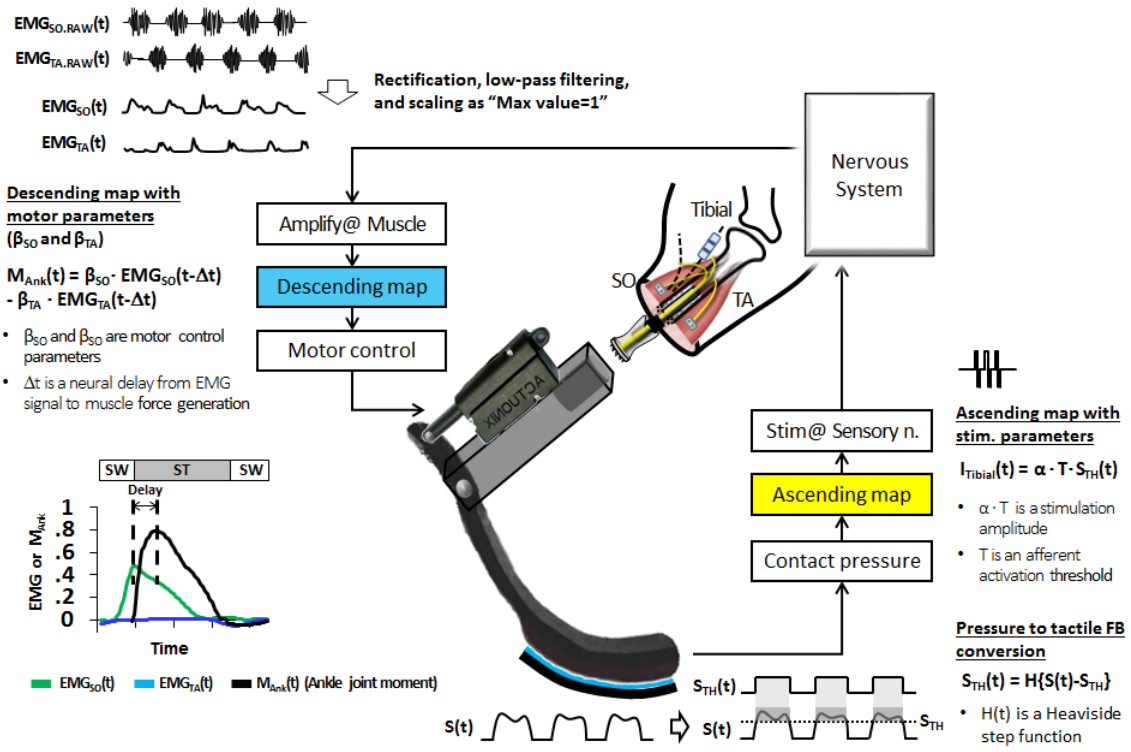

Figure 4.7. Modeling of the neural pathways in the active sensing transtibial prosthesis.

There are three model equations that describe the operation of the whole closed-loop system of the prosthesis. First, the tactile sensation is modeled as a unit step function $S_{TH}(t)$, as shown in the bottom right side of Fig. 4.7. The pressure information is measured using the pressure sensor mounted on the bottom of the prosthesis. I set a threshold for this pressure output and the $S_{TH}(t)$ is defined based on the comparison between the pressure output and the threshold. Accordingly, the first model equation for the tactile sensation is $\underline{S_{TH}(t) = H\{S(t)-S_{TH}\}}$, where H(x) is a Heaviside step function that is "1" if $x \geq 0$ and "0" otherwise and S_{TH} is a threshold value of pressure.

Second, the stimulation current amplitude generating the compound action potential to deliver tactile sensation is modeled as a step function $I_{tibial}(t)$, as shown in the right side of Fig. 4.7. Because the action potential is generated with the active tactile sensation, the stimulation is turned on when the $S_{TH}(t)$ is "1". The amplitude of the stimulation, $\alpha \cdot T$, is determined by the experimental results, where T is the afferent threshold of each cat based on the sciatic nerve recording. Accordingly, the second model equation for the stimulation amplitude is $\underline{I_{Tibial}(t) = \alpha \cdot T \cdot S_{TH}(t)}$, where T is the afferent threshold of each cat. Note that the other stimulation parameters (e.g. frequency, pulse width) are fixed with the values used in the experiment described in chapter 2, because the values are already verified by the experimental results.

Third, the ankle joint moment is modeled as a step function with a dual polarity. The reason for the dual polarity is to express the bi-directional movement of the ankle joint. I modeled the ankle joint moment with the activity of Soleus and Tibialis Anterior, as the major ankle extensor flexor muscle, respectively. Accordingly, the fourth model equation for the ankle joint moment is $\underline{M_{Ank}(t) = \beta_{SO} \times EMG_{SO}(t-\Delta t) - \beta_{TA} \times EMG_{TA}(t-\Delta t)}$, where β_{SO}, β_{TA} are fixed constant of motor gain to reflect characteristics of muscles of each cat and Δt is a neural delay from EMG signal to muscle activation. I assumed that neural delay for Soleus and Tibialis Anterior is the same. This model equation is not applicable for the special case when both Soleus and Tibialis Anterior are active, because

those two muscles “hold” the ankle joint instead of changing angle. I defined this status as “brake” because the linear motor brakes its arm movement and maintains its arm length.

In sum, I modeled the sensorimotor loop between the neuromuscular system of the residual limb and the active sensing transtibial prosthesis. By implementing the model equations onto the MCU on the prosthesis, the linear motor replicates the actions of ankle extensor/flexor muscles, the pressure sensor replicates tactile receptors on paw pads.

4.2.10. Laboratory Test Setup of Active Sensing Transtibial Prosthesis

Fig. 4.8 shows the laboratory test setup of the active sensing transtibial prosthesis with the test rig. The test rig has been made with aluminum rods, L-shaped connectors, a zinc-plated compression spring, and a locking pivot. First, the prosthesis is hanging in the air with a fully compressed spring, as in Fig. 4.9a, with the assistance of the hand as in Fig. 4.8. When the hand releases the prosthesis, it touches the ground with the linear motor reducing its arm (ankle extension), as in Fig. 4.9b. The prosthesis then pushes off the ground as the motor arm further reduces, as in Fig. 4.9c. The prosthesis lifts off the ground again and comes back to the position in the air, with the assistance of the hand, to iterate the cycle.

To verify the operation of the active sensing transtibial prosthesis, I need to compare gait parameters between the intact walking and the prosthetic walking. However, there are several limitations on collecting gait parameters from the active sensing transtibial prosthesis using the test rig. First, the active sensing transtibial prosthesis itself does not have any interlimb coordination. Second, the test rig cannot emulate the proximal part of the body, because the spring and locking pivot have limited degrees of freedom to imitate the movement of the proximal part of the body. Therefore, I decided to focus on the prosthesis’s capability of replicating ground reaction force profile, which can be verified by placing a force plate on the bottom of the prosthesis, as in Fig. 4.8.

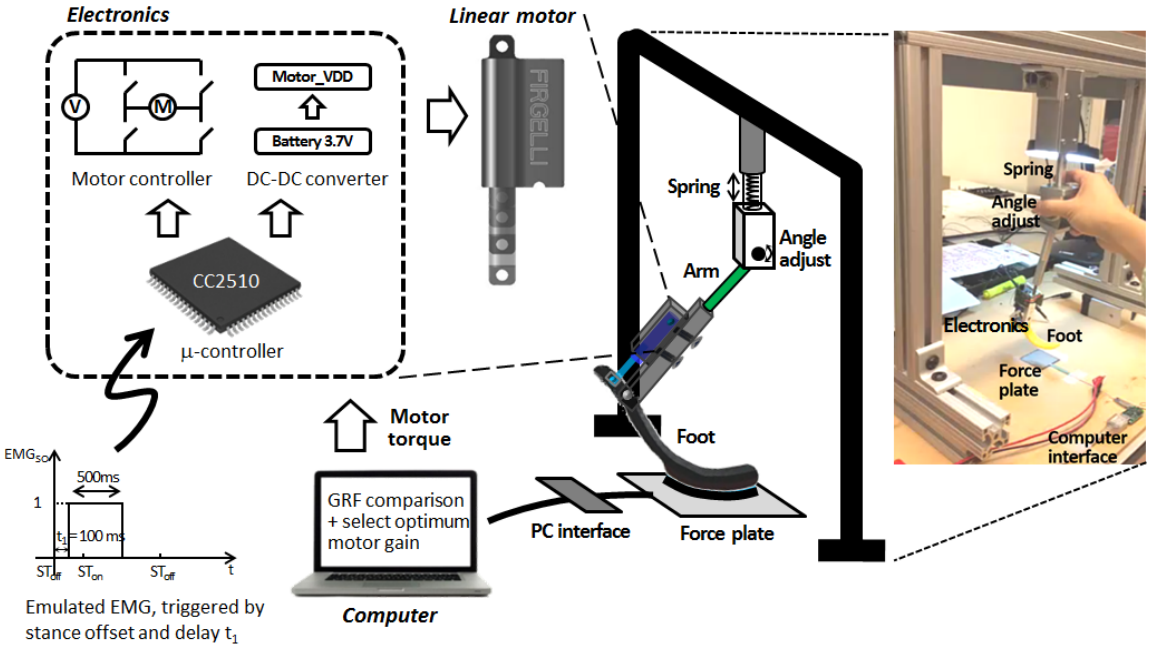

Figure 4.8. Laboratory test setup of the active sensing transtibial prosthesis with a test rig.

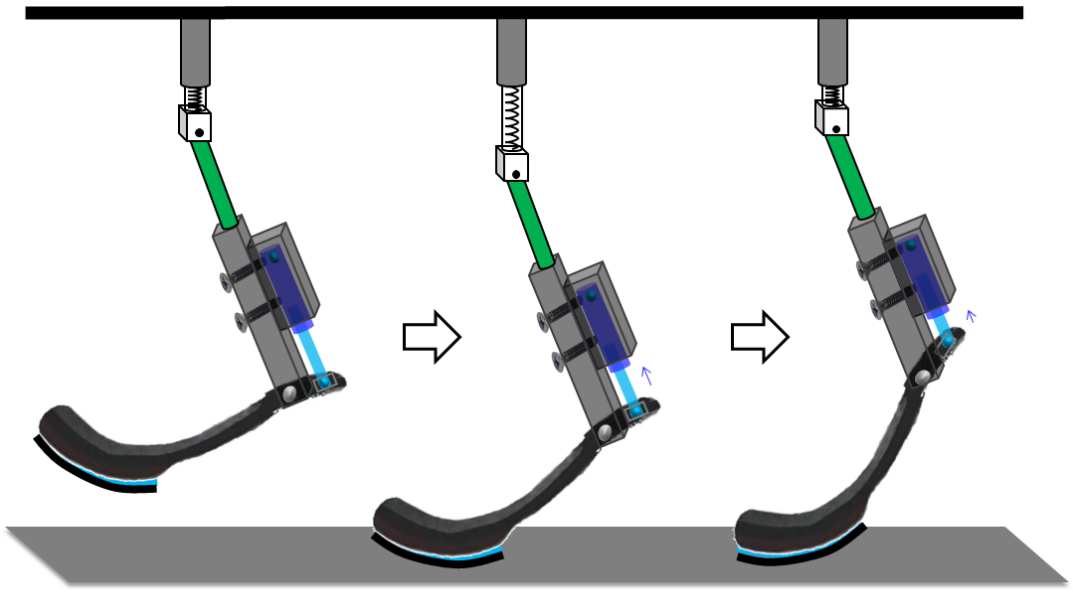

(a) (b) (c)

Figure 4.9. Operation phase of the active sensing transtibial prosthesis based on the contact to the ground: (a) before touchdown at maximum height from the ground (at the mid of the swing), (b) right after touchdown (at the beginning of the stance), and (c) right before liftoff (at the end of the stance).

4.2.11. Closed-Loop Optimization of Motor Gain

The developed models described in section 4.2.9 will be eventually verified by the gait analysis of the cats walking with the active sensing transtibial prosthesis. Prior to the cat experiments, I had to verify the operation of the active sensing transtibial prosthesis with the laboratory test setup. For the test of the closed-loop operation, I bypassed the nervous system and therefore emulated EMG signals from the built-in MCU.

EMG is modeled as a unit step function to represent the timing of EMG activity. I am interested in two muscles: Soleus as an ankle extensor muscle and Tibialis Anterior as an ankle flexor muscle, and I model EMG of those two muscles. First, EMG_{SO}, EMG activity of Soleus muscle, is modeled as $EMG_{SO}(t) = H(t-t_1) - H\{t-(t_1+T_{SO})\}$, where t_1 is a lagging phase duration to the stance offset and T_{SO} is an active duration of EMG_{SO}. Note that $EMG_{SO}(t)$ is defined at every stance offset, because EMG activity of Soleus muscle begins after stance offset and prior to stance onset. For the actual test, t_1=100ms and T_{SO}=500ms were selected from the experimental data of intact cats, as shown in Fig. 4.8. Second, EMG_{TA}, EMG activity of Tibialis Anterior muscle, is modeled as $EMG_{TA}(t) = H(t-t_2) - H\{t-(t_2+T_{TA})\}$, where t_2 is a lagging phase duration to the stance onset and T_{TA} is an active duration of EMG_{TA}. Note that $EMG_{TA}(t)$ is defined at every stance onset, because EMG activity of Tibialis Anterior muscle begins between stance onset and stance offset. For the actual test, t_2=400ms and T_{TA}=200ms were selected from the experimental data of intact cats.

The linear motor was driven by the amount of torque determined by the model equation of the ankle joint moment, with βSO and βTA selected based on the previous measurement data of intact cats. The model equation of the tactile sensation, based on the pressure output, was used to re-synchronize the EMG signals. The EMGSO(t) was re-synchronized at stance offset and the EMGTA(t) was re-synchronized at stance onset, considering the onset timing of each EMG signal.

To apply appropriate load comparable to the weight applied to the hindlimb in the intact walking of the cat, the spring on the top of the prosthesis needs to have a proper spring constant. I selected a zinc-plated compression spring considering its moderate resistance. It has a spring constant of 0.35 N/mm, and it applies 11~14 N to the prosthesis with its vertical displacement of 30~40 mm. The weight of the aluminum rods (~100 g) also applies ~1N, to make a total applied force as 12~15 N.

To regulate the ground reaction force (GRF) pattern of the prosthetic limb to be close to that of the intact limb, the controller has been designed to optimize βSO and generate appropriate amount of torque, as shown in Fig. 4.10. Because βTA is not related with generating GRF pattern, it is set as the maximum value and excluded from the optimization. First, the feedforward controller selects appropriate βSO from the open-loop relationship between the βSO and the measured peak GRF. Second, in every cycle, the feedback controller increases or decreases the βSO by the pre-defined step magnitude, based on comparison between the peak GRF measured from the force plate and the target peak GRF.

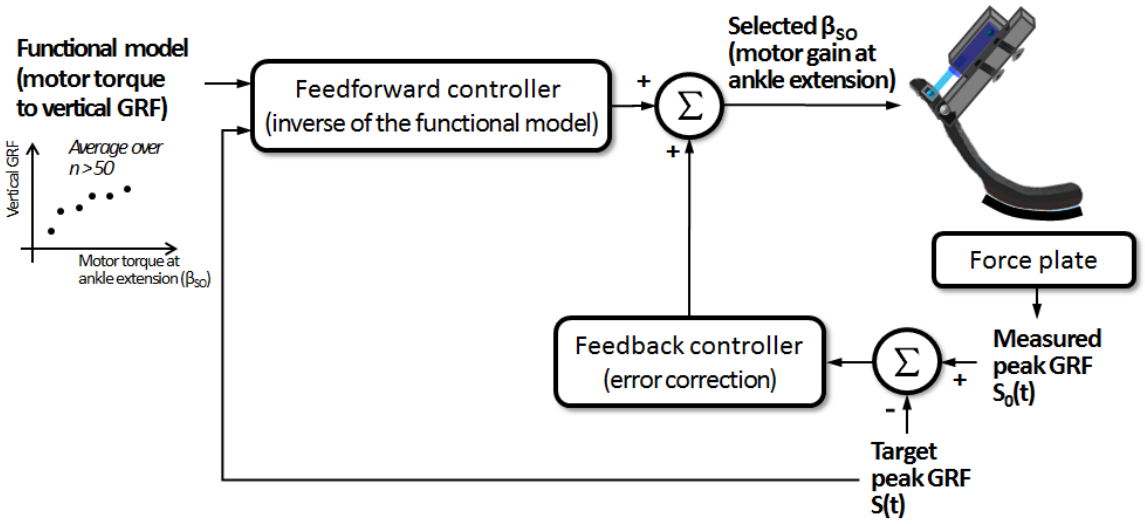

Figure 4.10. A functional block diagram of the real-time closed-loop gait control system using the optimization of motor gain at descending pathway with feedforward and feedback controllers.

4.3. Results

4.3.1. Open-Loop Relationship Between Stimulation Amplitude and Spatial Step Symmetry

I first observed the open-loop behavior of the system by monitoring the spatial step symmetry in response to sensory nerve stimulations with multiple amplitudes. The amplitude range was determined based on both activation threshold (T) of cutaneous paw pad afferents and muscle twitch threshold (25T) in plantar flexors of hind digits. The afferent threshold was determined by stimulating the distal-tibial nerve and monitoring the compound action potential in the sciatic nerve. The muscle twitch threshold was determined by observing the movement of the toes while the cat was sedated. I selected five values of the stimulation amplitude in logarithmic scale, from 1.2T to be just above the afferent threshold to 16T to be just below the muscle twitch threshold. The stimulation was applied during the stance period of the right hindlimb to modulate the tactile feedback from paw pads. Stimulation onset and offset times were triggered based on the paw contact times measured by the pressure monitoring system (Park et al. 2016).

Five selected stimulation amplitudes were applied to the distal-tibial nerve in the right hindlimb during two series of walking experiments on the split-belt treadmill. In the first series, the speeds of the two treadmill belts were the same, 0.4 m/s (04-04 condition). The speed of 0.4 m/s was selected through the treadmill training as a comfortable walking speed for the cat. In the second series, the speeds of the two belts were different, left belt moved at 0.4 m/s and right belt moved at 0.6 m/s (04-06 condition).

Fig. 4.11 shows the spatial step symmetry at different stimulation amplitudes and two walking conditions measured either by the pressure monitoring system or the Vicon motion capture system (Pantell et al., 2012). There was no statistically significant difference in the spatial step symmetry between the two measurement systems (t-test,

p<0.05), which directly validated the performance of the pressure monitoring system. In the 04-04 condition, the step lengths were symmetric without sensory nerve stimulation but became asymmetric with stimulation (see Fig. 4.11). As the amplitude of the stimulation increased, the step length asymmetry also increased; that is, the right step length became increasingly longer than the left step length. In the 04-06 condition without nerve stimulation, the step lengths were asymmetric, in agreement with a previous study (Malone et al., 2012). The asymmetry of the step length decreased with increasing the stimulation amplitude up to 8T (see Fig. 4.11).

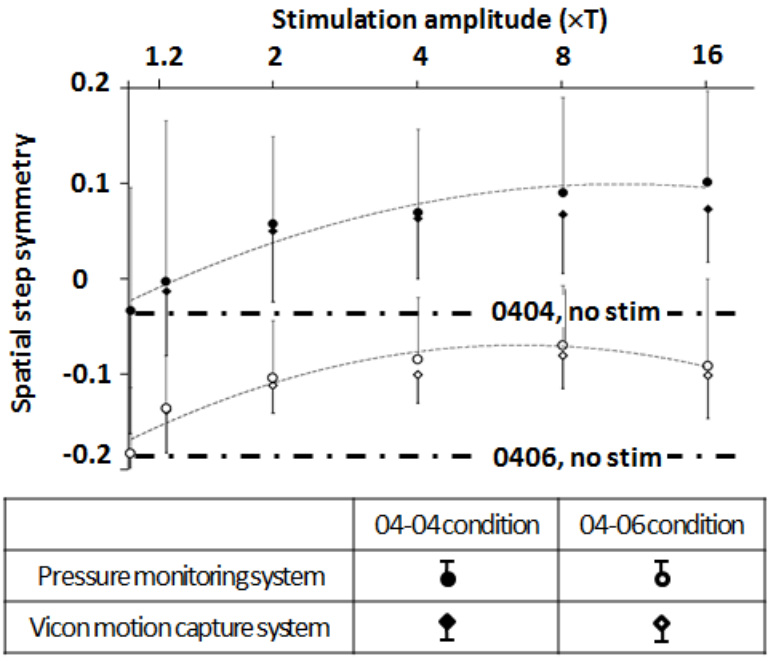

Figure 4.11. Open-loop relationship between stimulation amplitude and spatial symmetry

4.3.2. Spatial Step Symmetry with a Closed-Loop Electrical Nerve Stimulation

Since the stimulation amplitude modulated the spatial step symmetry, as demonstrated in Fig. 4.11, we could design a closed-loop system that would maintain the step spatial symmetry in the vicinity of a specific target value. The stimulation controller (see Fig. 4.2) selects an optimum stimulation amplitude to make the SYM_M to approach

the SYM_T. Considering the complexity of the biological system, we started from a very simple closed-loop experiment with only two stimulation amplitudes. In this experiment, the 04-06 condition was tested, and the SYM_T was set as -0.1, so that sensory nerve stimulation would make walking more symmetric (see Fig. 4.11). The averaged values of the SYM_M over 4 consecutive strides (large diamond dots in Fig. 4.12) were used as the value of the spatial step symmetry fed into the stimulation controller as shown in Fig. 4.2a. This closed-loop experiment was designed to demonstrate that the transient response to sensory nerve stimulation was consistent with the open-loop response and was fast enough for the real-time control.

Fig. 4.12 shows the measured spatial step symmetry with a closed-loop optimization of stimulation amplitude. The controller selected the stimulation amplitude of either 1.2T or 8T, which resulted in either the minimum or the maximum change in spatial step symmetry metric in the open-loop operation (see Fig. 4.11). Based on the open-loop experiment, we expected that stimulation at 1.2T and 8T would result in the spatial step symmetry of -0.14 and -0.07, respectively (see Fig. 4.11). The controller selected the stimulation amplitude of either 1.2T or 8×T depending on the sign of the difference (SYM_M - SYM_T). That is, the magnitude was 8T if the (SYM_M - SYM_T) < 0 and it was 1.2T when (SYM_M - SYM_T) > 0. The difference (SYM_M - SYM_T) was updated every 5 walking cycles, by averaging the last 4 cycles and skipping the first cycle that could be affected by transition between different stimulation amplitudes. The initial stimulation amplitude value was set at 1.2T. Stimulation at 8T increased SYM_M above the SYM_T (-0.1) in 5-10 cycles, whereas stimulation at 1.2T decreased SYM_M below SYM_T more slowly (see Fig. 4.12). The slow change in the SYM_M in response to the lower stimulation amplitude (1.2×T) might have been caused by the aftereffect of the higher stimulation amplitude (8T).

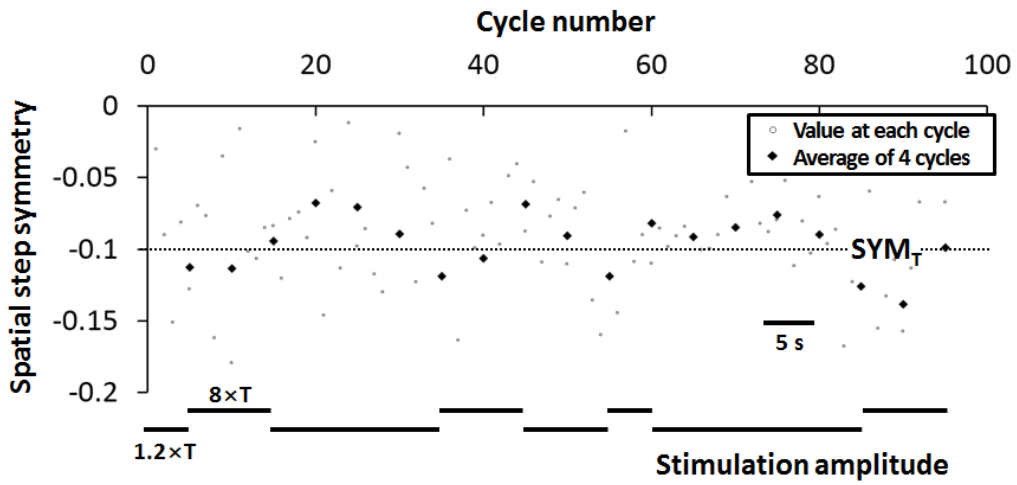

Figure 4.12. Measured spatial step symmetry over time with sensory nerve stimulation in a closed-loop operation (SYM_T: target spatial step symmetry).

4.3.3. Aftereffect of Closed-Loop Electrical Nerve Stimulation

Fig. 4.13 shows measured hindlimb duty factor and spatial symmetry without any sensory modulation, before & after the experiment of the closed-loop electrical nerve stimulation. First, hindlimb duty factor on the ipsilateral hindlimb (R-hindlimb) increased at the speed ratio of 1.5, while other values did not change. I could see the exact same change at the experiment with R-paw-pads anesthesia, as shown in Fig. 2.22. Second, spatial step symmetry increased at both speed ratios. I could see the same change at the experiment with R-paw-pads anesthesia, at speed ratio of 1.5, as shown in Fig. 2.25. From the above results, I conclude that, after the stimulation experiment, a cat walked as if R-side paw pads were anesthetized. However, this result should be verified with subsequent experiments because the experiment was done with only one cat.

It is possible that multiple nerve stimulations used to obtain the results in Fig. 4.11 damaged the axons of the cutaneous paw pad afferents, and that led to changes in the duty factor and spatial step symmetry similar to those observed after anesthesia of the right hindpaw and forepaw pads.

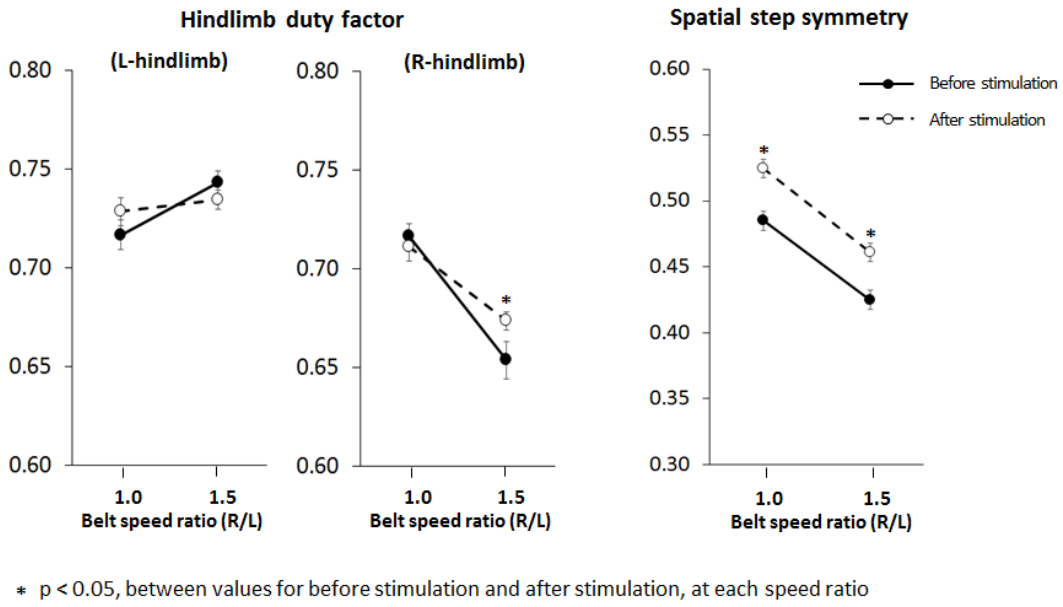

Figure 4.13. Measured hindlimb duty factor and hindlimb spatial step symmetry, before and after the stimulation experiment.

4.3.4. Measured Ground Reaction Force with Closed-Loop Motor Control

Fig. 4.14a shows mean vertical GRF measured from the right hindlimb of four intact walking cats with five sessions for each cat, and Fig. 4.14b shows vertical GRF obtained from the prosthesis on the test rig, respectively. Although the amplitude of the GRF obtained from the prosthesis is a bit smaller than that of the cat, it shows comparable amplitude and two peaks at the beginning and end of the stance phase.

Fig. 4.15 shows the closed-loop operation of the prosthetic leg, to optimize the β_{SO}, with the change of both GRF and β_{SO} in time domain. The initial value of the β_{SO} is set as 0.5 (N·m) and the step magnitude is set as 1/30 (N·m). Because the measured peak GRF is smaller than the target peak GRF, the feedback controller increases the β_{SO} by 1/30 (N·m) and after 3 cycles, the β_{SO} is saturated to 0.6 (N·m) as the maximum capacity of the selected PQ12 miniature linear motor (Firgelli, BC, Canada). To replicate the target peak GRF, a motor should be replaced with the one with higher torque rating. However, the PQ12 is the best choice among the currently available linear motors, to satisfy strict limitations in the size and weight to be worn on the cat hindlimb.

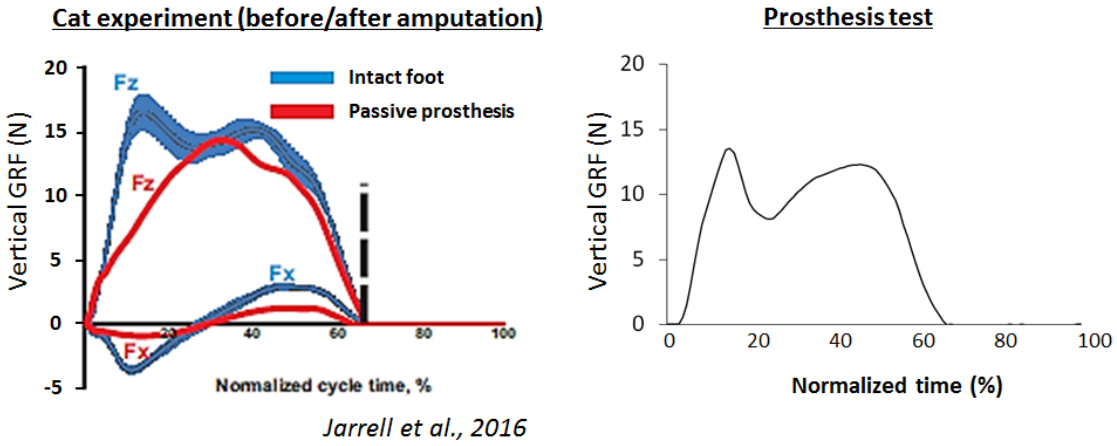

(a) (b)

Figure 4.14. Measured ground reaction force from (a) a right hindlimb of four intact walking cats and (b) an active sensing transtibial prosthesis operated with a test rig.

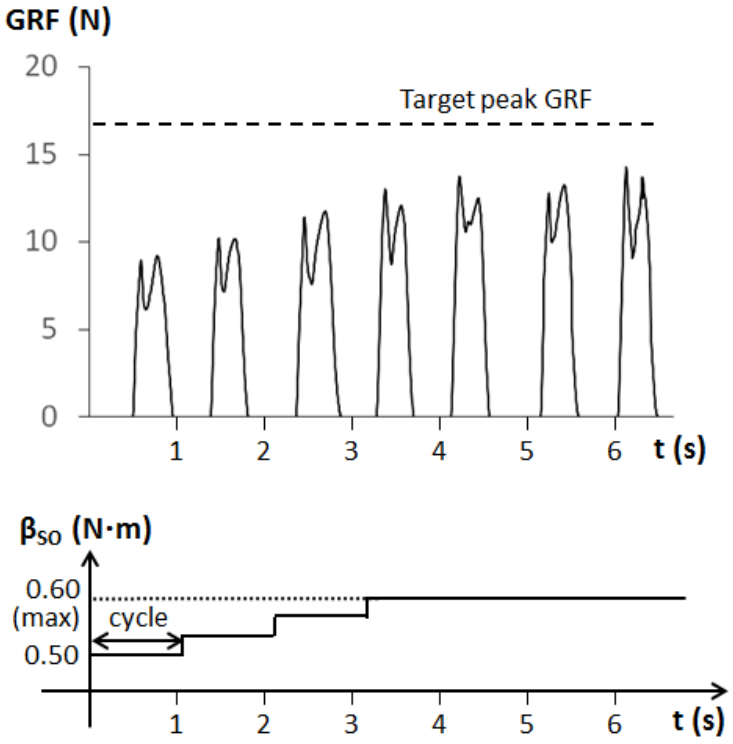

Figure 4.15. Measured ground reaction force from the force plate, during the closed-loop operation of the prosthetic leg to optimize the β_{SO}.

4.4. Discussion and Conclusions

4.4.1. A Spatial Step Symmetry can be Controlled by Real-Time Closed-Loop Optimization of Electrical Nerve Stimulation

I have developed a real-time closed-loop gait control system and tested it in the intact walking cat. The electrical stimulation was applied to the distal-tibial nerve to modulate the tactile feedback from paw pads and control the spatial step symmetry. The open-loop relationship between the stimulation amplitude and the spatial step symmetry showed that the spatial step symmetry could be controlled by the stimulation amplitude. Results of the closed-loop control experiment demonstrated that the spatial step symmetry could be controlled by stimulation of a sensory nerve in real time by the developed system. This system could be used, for example, for correcting gait asymmetry during walking in people with motor deficits.

4.4.2. Aftereffect of Closed-Loop Electrical Nerve Stimulation

After multiple sessions of stimulations of the distal-tibial nerve necessary to obtain the data for the model (~20 sessions with stimulation), the studied cat walked without stimulation as if the right hind- and forepaw pads were anesthetized. I expect this aftereffect could be caused by the damage of the distal-tibial nerve that I stimulated for too long during the experiment. I could think of two potential reasons: (1) I applied wide range of stimulation amplitudes to find out the relationship between stimulation amplitude and spatial symmetry. Even though the maximum stimulation amplitude 16T was smaller than the muscle twitch threshold (25T), repetitive application of the large amplitude of stimulation could have caused nerve damage. (2) The damage could be caused by the accumulated residual charge on the nerve. Because I did not implement a charge balancing circuitry in the stimulator, the change could be unbalanced, although I used a bi-phasic stimulus. The accumulated residual charge on the nerve could have generated a large potential to break the cellular protection and damage the nerve. In the

subsequent experiments with stimulation, I will decrease the maximum stimulation amplitude and include a charge balancing circuitry.

I would not exclude the possibility that the aftereffect can be caused by the learning effect (or the plasticity) of the nervous system. Note that the aftereffect could be also seen with a stimulation amplitude of 1.2T, at the spatial step symmetry of hindlimb, as in Fig. 2.11. To clarify the cause of the aftereffect, more experiments with a long-term observation are necessary.

4.4.3. Active Sensing Transtibial Prosthesis Can Generate Vertical GRF Comparable to that of the Intact Hindlimb

I verified the hypothesis that the active sensing transtibial prosthesis can produce similar GRF profile as the intact hindlimb. I could verify both the prosthesis's capability of generating forces in a right time window and a closed-loop operation of the prosthesis by controlling the efferent pathway with the model equations (more specifically, the motor gain β_{SO}) and the emulated EMG signal from the MCU.

4.4.4. Active Sensing Prosthesis will be Implemented in Cats

I implemented the active sensing transtibial prosthesis using a linear motor, a pressure sensor, a J-shape foot, a SBIP-PNI, and electronics including MCUs. The active sensing transtibial prosthesis has an active ankle joint controlled by the muscle activity and a pressure sensor with stimulator delivering the cutaneous sensory feedback from the bottom of the foot to the nervous system. With a bi-directional neural pathway provided by the SBIP-PNI and model equations embedded on the MCUs, the active sensing transtibial prosthesis will communicate with the neuromuscular system of the residual limb. Effectiveness of the designed prosthesis and close-loop control system will be tested in cat in the future experiments.

CHAPTER 5

CONCLUSIONS AND FUTURE WORK

In this chapter, I will summarize my work on peripheral sensory modulations and development of the active sensing transtibial prosthesis with a closed-loop optimization. I will also describe future work related with my research. A cat experiment with the active sensing transtibial prosthesis will begin soon, and thus I will describe it with a proper detail.

5.1. Conclusions

From the cat locomotor behavior on the split-belt treadmill, I found that modulating somatosensory feedback could change their gait, especially when the ipsilateral belt moves faster (i.e., in challenging walking environment). The range of effects is not limited to spatial and temporal gait parameters, but also includes stability metrics. I also found that electrical nerve stimulation can evoke peripheral sensory feedback and reverse changes caused by the missing sensory feedback. These results confirm the basic assumption of my research that the gait parameters (e.g., spatial step symmetry) can be controlled by modulating somatosensory feedback.

Experimental results with a closed-loop electrical nerve stimulation in the walking cat showed that we can improve the quality of gait by a closed-loop somatosensory modulation. This result can be applied to the leg prosthesis because amputees have hard time to achieve a decent gait quality with their leg prosthesis, partly because of the missing sensory feedback from the prosthesis. In addition, I showed that active joint of the prosthesis could be controlled by the motor commands derived from the activity of residual ankle extensor/flexor muscles. I believe that the closed-loop optimization with both afferent and efferent pathways will improve asymmetric walking.

5.2. Future work

5.2.1. Cat Experiment with Developed Active Sensing Transtibial Prosthesis

Preparation of the active sensing transtibial prosthesis for cat experiment. I am preparing two active sensing transtibial prostheses for each cat, considering the charging time of the battery in the prosthesis. Considering we are planning to have eight cats in the experiment, we need 16 prostheses in total. I will make 20 prostheses including four backup prostheses. Cats will wear the prosthesis in their daily lives at the animal facility to adapt to it, and change it with the fully-charged prosthesis right before the experiment.

Cat experiment with the active sensing transtibial prosthesis. The experiment will be done in three stages: (1) training the cat on the split-belt treadmill before surgery, (2) surgery of cats with implantation of the SBIP-PNI, (3) split-belt treadmill walking sessions with three different belt speed ratios and four different modes of the prosthesis. Three different split-belt speed ratios will help us to see the effect of active joint and artificial sensory feedback, i.e. if it is amplified at more challenging walking environment. Four different modes of the prosthesis will help us to see the effect of artificial sensory feedback on prosthetic walking and the synergistic effect of active ankle joint on top of artificial sensory feedback.

Fig. 5.1 describes stage (3) in detail. The first mode of the prosthesis is necessary to record the prosthetic gait with a typical J-shape passive prosthesis. The second mode of the prosthesis, active sensing transtibial prosthesis with both motor and sensor turned off, might look redundant because the first mode of the prosthesis is a J-shape passive transtibial prosthesis. However, it is necessary to test the second mode to get the baseline data for the active sensing transtibial prosthesis. The third mode of the prosthesis, without active joint and with sensory feedback, will help us to find out how the artificial sensory feedback improves the prosthetic gait. Finally, at the fourth mode of the prosthesis, with

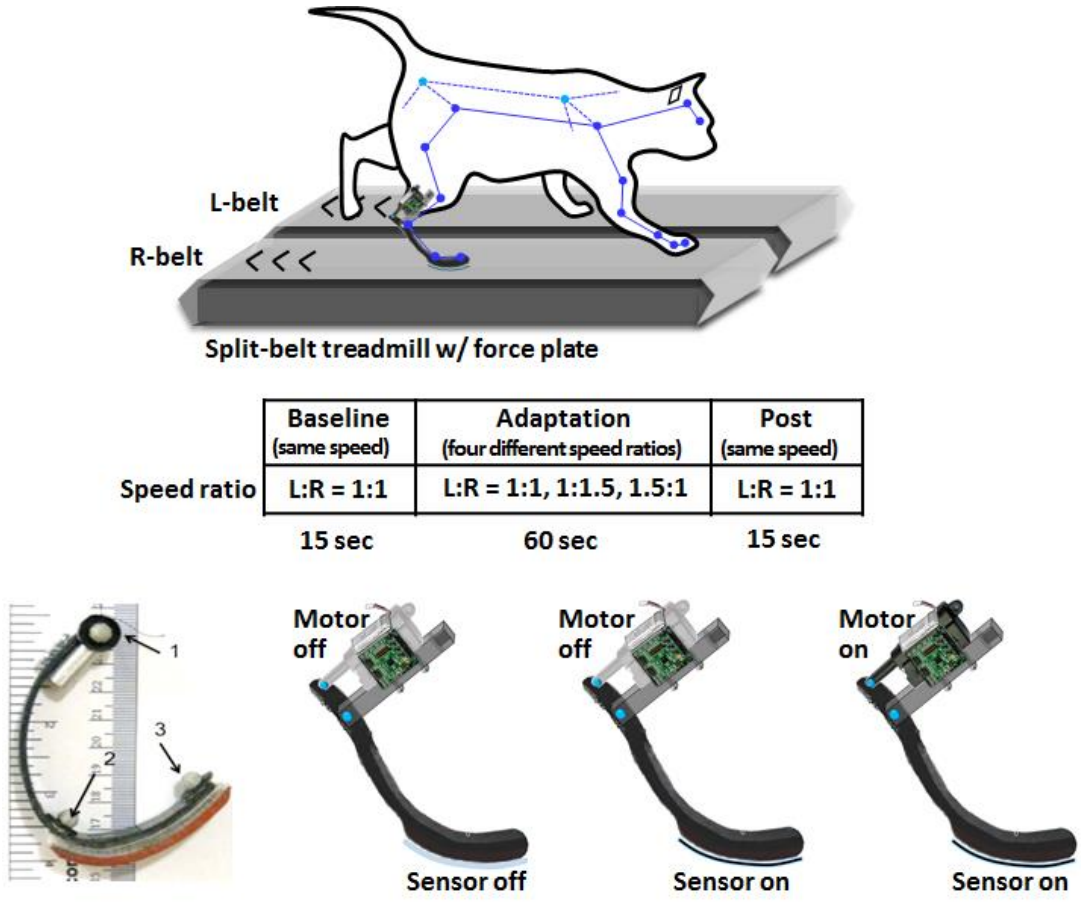

(a) (b) (c) (d)

Figure 5.1. Cats will walk on the split-belt treadmill with three belt speed ratios, after finding a comfortable default walking speed: (1) two belts will move at the same default speed, (2) R-belt will increase its speed 1.5 times faster after 15 seconds and will come back to default speed after 60 seconds, while L-belt keeps its speed at default speed, and (3) L-belt will increase its speed 1.5 times faster after 15 seconds and will return to default speed after 60 seconds, while R-belt keeps operating at default speed. In combination with three different belt speed ratios, four different prosthesis settings will be used: (a) J-shape passive transtibial prosthesis, (b) active sensing transtibial prosthesis with motor off and sensor off, (c) active sensing transtibial prosthesis with motor off and sensor on, and (d) active sensing transtibial prosthesis with motor on and sensor on.

both active joint and sensory feedback, we will find the synergistic effect of a bi-directional neural pathway on prosthetic gait.

Fig. 5.2 describes both the integration of the active sensing transtibial prosthesis with the amputated limb and the bi-directional neural pathway with both on-board and off-board optimization. As shown in Fig. 5.2b, the SBIP-PNI will be implanted inside the residual Tibia of the cat and the active sensing transtibial prosthesis will be integrated

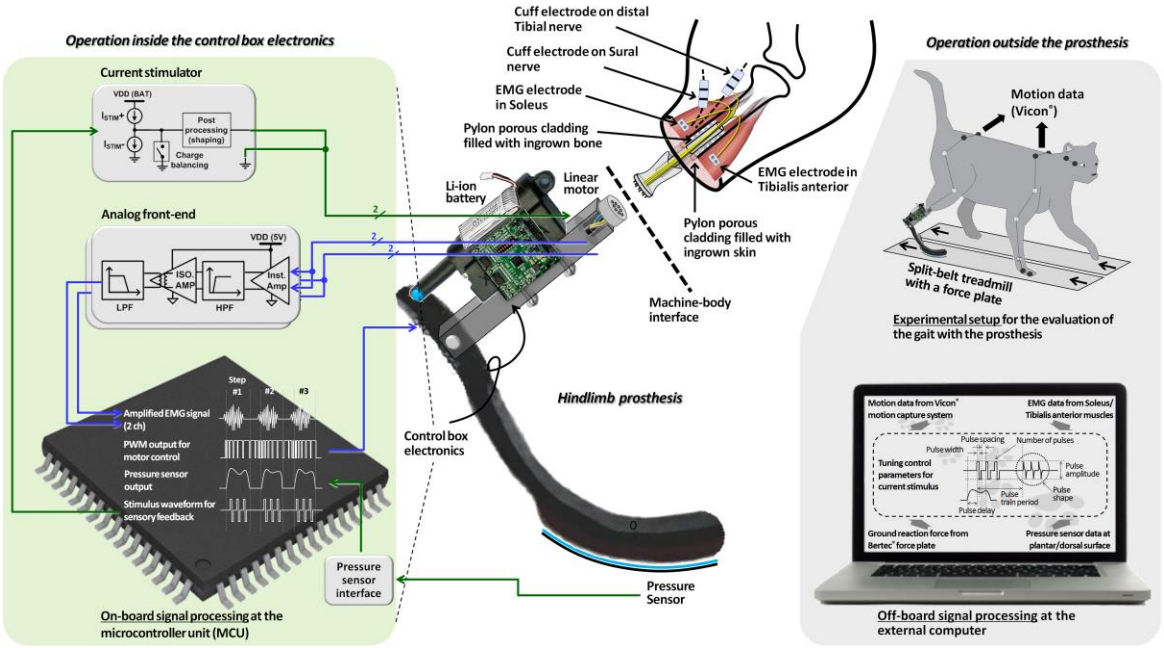

(a) (b) (c)

Figure 5.2. Overall system description of the active sensing transtibial prosthesis: (a) control box electronics, which is composed of a current stimulator, an analog front-end, and a MCU, (b) the active sensing transtibial prosthesis composed of a linear motor, electronics, and a J-shaped carbon fiber, which interfaces with the body of the cat through the pylon implanted in the residual hindlimb, and (c) cat walking with a prosthesis and an external gait analysis system with the off-board signal processing to adjust motor control parameters and stimulation parameters to release the burden of the on-board signal processing.

with the SBIP-PNI. Both the on-board signal processing (Fig. 5.2a) and the off-board signal processing (Fig. 5.2c) will analyze gait metrics in real time and adjust parameters for motor control and electrical nerve stimulation. During split-belt treadmill walking of the cat, kinematic and kinetic data will be collected by pressure sensors under the belt and fed back to the system for the real-time optimization. Vicon motion capture system will also record the kinematic data for a further gait analysis.

5.2.2. Potential Future Works

Osseointegrated limb prosthesis for humans. The results will be applied for design of novel osseointegrated limb prosthesis for humans that can provide an active joint and an artificial tactile feedback to the user. I expect the combination of the active powered ankle joint and the artificial tactile feedback would result in the best possible

spatiotemporal gait symmetry between left and right limbs. It would be not just a summation of two effects but also a synergetic integration of ascending and descending pathways via the closed-loop operation.

Gait rehabilitation. Prostheses with a bi-directional neural pathway, called neuroprostheses, will help gait rehabilitations. Note that the prosthesis is not limited to the device replacing the missing body, but includes all devices helping the function of the body. Neuroprostheses will help gait rehabilitation by modulating the gait in a preferred direction. For example, I expect neuroprostheses will help damaged nervous system, such as injured spinal cord, to regain its functionality by assisting its operation with a closed-loop optimization. I also expect that neuroprostheses will help damaged nervous system to find an alternative route to perform the original function by motor adaptation and learning. For example, people post stroke may regain their motor function and improve gait symmetry by the gait training with a neuroprosthesis.

Diabetic foot. The artificial sensory feedback may help diabetic patients who lost plantar cutaneous sensation, to reduce the asymmetry in their gait. Further, it will help avoiding complications on the sole of the foot caused by the abnormal pressure distribution (e.g. skin ulcer), if the spatial resolution of the plantar cutaneous feedback can be increased to a proper level.

REFERENCES

Abelew TA, Miller MD, Cope TC, and Nichols TR. Local loss of proprioception results in disruption of interjoint coordination during locomotion in the cat. *J Neurophysiol* 84: 2709-2714, 2000.

Afshar P, Khambhati A, Stanslaski S, Carlson D, Jensen R, Linde D, Dani S, Lazarewicz M, Cong P, Giftakis J, and Stypulkowski P. A translational platform for prototyping closed-loop neuromodulation systems. *Frontiers in neural circuits 6.* 2012.

Andersson O, and Grillner S. Peripheral control of the cat's step cycle. II. Entrainment of the central pattern generators for locomotion by sinusoidal hip movements during "fictive locomotion.". *Acta Physiol Scand* 118: 229-239, 1983.

Birke JA, Novick A, Hawkins ES, and Patout Jr C. A Review of Causes of Foot Ulceration in Patients with Diabetes Mellitus. *J Prosthetics and Orthotics* 4: 13-22, 1991.

Blaszczyk J and Loeb GE. Why cats pace on the treadmill. *Physiology & behavior* 53: 501-507, 1993.

Blaya JA and Herr H. Adaptive control of a variable-impedance ankle-foot orthosis to assist drop-foot gait. *IEEE Trans Neural Systems and Rehabilitation Engineering* 12:24-31,2004.

Bolton DA, and Misiaszek JE. Contribution of hindpaw cutaneous inputs to the control of lateral stability during walking in the cat. *J Neurophysiol* 102: 1711-1724, 2009.

Bouyer LJ, and Rossignol S. Contribution of cutaneous inputs from the hindpaw to the control of locomotion. I. Intact cats. *J Neurophysiol* 90: 3625-3639, 2003.

Brown TG. The intrinsic factors in the act of progression in the mammal. *Proc R Soc B* 84: 308-319, 1911.

Burke MJ, Roman V, and Wright V. Bone and joint changes in lower limb amputees. *Annals of the rheumatic diseases* 37: 252-254, 1978.

Cartmill M, Lemelin P, Schmitt D. Support polygons and symmetricalgaits in mammals. *Zoological J. Linnean Society* 136: 401-420, 2002.

Cole J, and Paillar J. Living without touch and peripheral information about body position and movement : studies with deafferented subjects. In: *The Body and the Self*, edited by Bermúdez J. Cambridge, MA: MIT Press, 1998.

Conway BA, Hultborn H, and Kiehn O. Proprioceptive input resets central locomotor rhythm in the spinal cat. *Exp Brain Res* 68: 643-656, 1987.

Cope TC, Bonasera SJ, and Nichols TR. Reinnervated muscles fail to produce stretch reflexes. *J Neurophysiol* 71: 817-820, 1994.

Cope TC, and Clark BD. Motor-unit recruitment in self-reinnervated muscle. *J Neurophysiol* 70: 1787-1796, 1993.

Corriveau H, Prince F, Hebert R, Raiche M, Tessier D, Maheux P, and Ardilouze JL. Evaluation of postural stability in elderly with diabetic neuropathy. *Diabetes Care 23*:1187-91, 2000.

Davis TS, Wark HAC, Hutchinson DT, Warren DJ, O'Neill K, Scheinblum T, and Greger B. Restoring motor control and sensory feedback in people with upper extremity amputations using arrays of 96 microelectrodes implanted in the median and ulnar nerves. *J Neural Engineering* 13: 036001, 2016.

Dietz V, Zijlstra W, and Duysens J. Human neuronal interlimb coordination during split-belt locomotion. *Experimental brain research* 101: 513-520, 1994.

Dunlap P, Perera S, VanSwearingen JM, Wert D, and Brach JS. Transitioning to a narrow path: the impact of fear of falling in older adults. *Gait Posture* 35: 92-95, 2012.

Duysens J, Clarac F, and Cruse H. Load-regulating mechanisms in gait and posture: comparative aspects. *Physiol Rev* 80: 83-133, 2000.

Duysens J, Clarac F, and Cruse H. Load-regulating mechanisms in gait and posture: comparative aspects. *Physiol Rev* 80: 83-133, 2000.

Duysens J, and Pearson KG. The role of cutaneous afferents from the distal hindlimb in the regulation of the step cycle of thalamic cats. *Exp Brain Res* 24: 245-255, 1976.

Ekeberg O, and Pearson KG. Computer simulation of stepping in the hind legs of the cat: an examination of mechanisms regulating the stance-to-swing transition. *J Neurophysiol* 94: 4256-4268, 2005.

English AW. Enhancing axon regeneration in peripheral nerves also increases functionally inappropriate reinnervation of targets. *The Journal of comparative neurology* 490: 427-441, 2005.

Fan RE, Culjat MO, King CH, Franco ML, Boryk R, Bisley JW, Dutson E, and Grundfest WS. A haptic feedback system for lower-limb prostheses. *IEEE Transactions on Neural Systems and Rehabilitation Engineering* 16: 270-277, 2008.

Farrell BJ, Bulgakova MA, Beloozerova IN, Sirota MG, and Prilutsky BI. Body stability and muscle and motor cortex activity during walking with wide stance. *J Neurophysiol* 112: 504-524, 2014.

Farrell BJ, Bulgakova MA, Sirota MG, Prilutsky BI, and Beloozerova IN. Accurate stepping on a narrow path: mechanics, EMG, and motor cortex activity in the cat. *J Neurophysiol* 114: 2682-2702, 2015.

Frigon A. The neural control of interlimb coordination during mammalian locomotion. *J Neurophysiol* 117: 2224-2241, 2017.

Galvez-Lopez E, Maes LD, and Abourachid A. The search for stability on narrow supports: an experimental study in cats and dogs. *Zoology (Jena)* 114: 224-232, 2011.

Garcia E, Arevalo JC, Munoz G, and Gonzalez-de-Santos P. On the biomimetic design of agile-robot legs. *Sensors* 11:11305-34, 2011.

Goldstein EB. *Sensation and perception.* Nelson Education, 30-32, 1989.

Goslow GE, Jr., Reinking RM, and Stuart DG. The cat step cycle: hind limb joint angles and muscle lengths during unrestrained locomotion. *J Morphol* 141: 1-41, 1973.

Gossard JP, Brownstone RM, Barajon I, and Hultborn H. Transmission in a locomotor-related group Ib pathway from hindlimb extensor muscles in the cat. *Exp Brain Res* 98: 213-228, 1994.

Gray J. *Animal locomotion*. London: William Clowes & Sons, 1968.

Graczyk EL, Schiefer MA, Saal HP, Delhaye BP, Bensmaia SJ, and Tyler DJ. The neural basis of perceived intensity in natural and artificial touch. *Science translational medicine* 8: 362ra142, 2016.

Gregor RJ, Smith DW, and Prilutsky BI. Mechanics of slope walking in the cat: quantification of muscle load, length change, and ankle extensor EMG patterns. *J Neurophysiol* 95: 1397-1409, 2006.

Grillner S. *Control of locomotion in bipeds, tetrapods, and fish.* Comprehensive Physiology, 2011.

Guertin P, Angel MJ, Perreault MC, and McCrea DA. Ankle extensor group I afferents excite extensors throughout the hindlimb during fictive locomotion in the cat. *J Physiol* 487 (Pt 1): 197-209, 1995.

Hak L, Houdijk H, Beek PJ, and van Dieën JH. Steps to take to enhance gait stability: the effect of stride frequency, stride length, and walking speed on local dynamic stability and margins of stability. *PLoS One* 8: e82842, 2013.

Halbertsma JM. The stride cycle of the cat: the modelling of locomotion by computerized analysis of automatic recordings. *Doctoral dissertation, TU Delft, Delft University of Technology*, 1983.

Hendershot BD, Bazrgari B, and Nussbaum MA. Persons with unilateral lower-limb amputation have altered and asymmetric trunk mechanical and neuromuscular behaviors estimated using multidirectional trunk perturbations, *J Biomech 46*: 1907-12, 2013.

Herr HM, Grabowski AM. Bionic ankle–foot prosthesis normalizes walking gait for persons with leg amputation. *Proceedings of the Royal Society of London B: Biological Sciences* 279: 457-464, 2012.

Hildebrand M. Symmetrical gaits of horses. *Science* 150: 701-708, 1965.

Hodson-Tole EF, Pantall AL, Maas H, Farrell BJ, Gregor RJ, and Prilutsky BI. Task dependent activity of motor unit populations in feline ankle extensor muscles. *J Exp Biol* 215: 3711-3722, 2012.

Hof AL, van Bockel RM, Schoppen T, and Postema K. Control of lateral balance in walking. Experimental findings in normal subjects and above-knee amputees. *Gait Posture* 25: 250-258, 2007.

Höhne A, Stark C, Brüggemann GP, and Arampatzis A. Effects of reduced plantar cutaneous afferent feedback on locomotor adjustments in dynamic stability during perturbed walking. *J. biomechanics*, 44: 2194-2200, 2011.

Hoogkamer W, Bruijn SM, and Duysens J. Stride length asymmetry in split-belt locomotion. *Gait Posture* 39: 652-654, 2014.

Hoogkamer W, Massaad F, Jansen K, Bruijn SM, and Duysens J. Selective bilateral activation of leg muscles after cutaneous nerve stimulation during backward walking. *J Neurophysiol* 108: 1933-1941, 2012.

Horak FB, and Macpherson JM. Postural Orientation and Equilibrium. In: *Handbook of Physiology: Section 12: Exercise: Regulation and Integration of Multiple Systems*, edited by Rowell LB, and Shepherd JT. New York: Oxford University Press: 255-292, 1996.

Hoy MG, and Zernicke RF. Modulation of limb dynamics in the swing phase of locomotion. *J Biomech* 18: 49-60, 1985.

Hultborn H. Spinal reflexes, mechanisms and concepts: from Eccles to Lundberg and beyond. *Progress in neurobiology* 78: 215-232, 2006.

Jaegers SM, Arendzen JH, and de Jongh HJ. Prosthetic gait of unilateral transfemoral amputees: a kinematic study. *Archives of physical medicine and rehabilitation* 76: 736-43, 1995.

Kaufman KR, Frittoli S, and Frigo CA. Gait asymmetry of transfemoral amputees using mechanical and microprocessor-controlled prosthetic knees. *Clinical Biomech 27*: 460-5, 2012.

Kriellaars DJ, Brownstone RM, Noga BR, and Jordan LM. Mechanical entrainment of fictive locomotion in the decerebrate cat. *J Neurophysiol* 71: 2074-2086, 1994.
Kuczynski V, Thibaudier Y, Hurteau MF, Dambreville C, Telonio A, and Frigon A. Lack of adaptation during prolonged split-belt locomotion in the intact and chronic spinal-transected adult cat. Abstract 241.14. In: *Annual Meeting of Society for Neuroscience*. Chicago, IL: Society for Neuroscience. Online., 2015.

Lam T, and Pearson KG. Sartorius muscle afferents influence the amplitude and timing of flexor activity in walking decerebrate cats. *Exp Brain Res* 147: 175-185, 2002.

Lewek MD, Feasel J, Wentz E, Brooks FP, and Whitton MC. Use of visual and proprioceptive feedback to improve gait speed and spatiotemporal symmetry following chronic stroke: a case series. *Physical therapy* 92: 748, 2012.

Lloyd CH, Stanhope SJ, Davis IS, and Royer TD. Strength asymmetry and osteoarthritis risk factors in unilateral trans-tibial, amputee gait. *Gait & posture 32*:296-300, 2010.

Loeb GE. The distal hindlimb musculature of the cat: interanimal variability of locomotor activity and cutaneous reflexes. *Exp Brain Res* 96: 125-140, 1993.

Lundberg A. Multisensory control of spinal reflex pathways. *Progress in brain research* 31: 11-28, 1979.

Lyle MA, Prilutsky BI, Gregor RJ, Abelew TA, and Nichols TR. Self-reinnervated muscles lose autogenic length feedback, but intermuscular feedback can recover functional connectivity. *J Neurophysiol* 116: 1055-1067, 2016.

Maas H, Prilutsky BI, Nichols TR, and Gregor RJ. The effects of self-reinnervation of cat medial and lateral gastrocnemius muscles on hindlimb kinematics in slope walking. *Exp Brain Res* 181: 377-393, 2007.

Maki BE. Gait changes in older adults: predictors of falls or indicators of fear. *Journal of the American Geriatrics Society* 45: 313-320, 1997.

Malone LA, Bastian AJ, and Torres-Oviedo G. How does the motor system correct for errors in time and space during locomotor adaptation?. *Journal of neurophysiology.* 108: 672-683, 2012.

Malone LA, and Bastian AJ. Spatial and temporal asymmetries in gait predict split-belt adaptation behavior in stroke. *Neurorehabilitation and neural repair* 28: 230-240, 2014.

Markin SN, Klishko AN, Shevtsova NA, Lemay MA, Prilutsky BI, and Rybak IA. Afferent control of locomotor CPG: insights from a simple neuromechanical model. *Ann N Y Acad Sci* 1198: 21-34, 2010.

Markin SN, Klishko AN, Shevtsova NA, Lemay MA, Prilutsky BI, and Rybak IA. A neuromechanical model of spinal control of locomotion. In: *Neuromechanical Modeling of Posture and Locomotion*, edited by Prilutsky BI, and Edwards DH, Jr. New York, NY: Springer 21-65, 2016.

McCrea DA. Spinal circuitry of sensorimotor control of locomotion. *J physiol* 533: 41-50, 2001.

McVea DA, Donelan JM, Tachibana A, and Pearson KG. A role for hip position in initiating the swing-to-stance transition in walking cats. *J Neurophysiol* 94: 3497-3508, 2005.

McCrea DA and Rybak IA. Modeling the mammalian locomotor CPG: insights from mistakes and perturbations. *Prog Brain Res* 165: 235-253, 2007.

McCrea DA and Rybak IA. Organization of mammalian locomotor rhythm and pattern generation. *Brain Res Rev* 57: 134-146, 2008.

McCrea DA, Shefchyk SJ, Stephens MJ, and Pearson KG. Disynaptic group I excitation of synergist ankle extensor motoneurones during fictive locomotion in the cat. *J Physiol* 487 (Pt 2): 527-539, 1995.

Mehta R, Kajtaz E, Gregor RJ, and Prilutsky BI. Effects of stretch-reflex removal by self-reinnervation of one-joint vastii and two-joint rectus femoris on hindlimb muscle activity and mechanics during walking in the cat. In: *Society for Neuroscience Meeting Program # 734-06*. Washington, DC: 2014.

Mehta R, and Prilutsky BI. Task-dependent inhibition of slow-twitch soleus and excitation of fast-twitch gastrocnemius do not require high movement speed and velocity-dependent sensory feedback. *Front Physiol* 5: 410, 2014.

Miller S, Van Der Burg J, and Van Der Meche F. Coordination of movements of the hindlimbs and forelimbs in different forms of locomotion in normal and decerebrate cats. *Brain Res* 91: 217-237, 1975.

Misiaszek JE. Control of frontal plane motion of the hindlimbs in the unrestrained walking cat. *J Neurophysiol* 96: 1816-1828, 2006.

Morton SM and Bastian AJ. Cerebellar contributions to locomotor adaptations during splitbelt treadmill walking. *J neuroscience* 26: 9107-9116, 2006.

Nardone A, Corna S, Turcato AM, and Schieppati M. Afferent control of walking: are there distinct deficits associated to loss of fibres of different diameter? *Clinical neurophysiology* 125: 327-345, 2014.

Nowak DA, Hermsdorfer J, Glasauer S, Philipp J, Meyer L, and Mai N. The effects of digital anaesthesia on predictive grip force adjustments during vertical movements of a grasped object. *The European journal of neuroscience* 14: 756-762, 2001.

Ollivier-Lanvin K, Krupka AJ, AuYong N, Miller K, Prilutsky BI, and Lemay MA. Electrical stimulation of the sural cutaneous afferent nerve controls the amplitude and onset of the swing phase of locomotion in the spinal cat. *J Neurophysiol* 105: 2297-2308, 2011.

Ortiz Catalan M, Brånemark R, and Håkansson B. BioPatRec: A modular research platform for the control of artificial limbs based on pattern recognition algorithms. *Source code for biology and medicine* 8: 11, 2013.

Ortiz Catalan M, Håkansson B, and Brånemark R. An osseointegrated human-machine gateway for long-term sensory feedback and motor control of artificial limbs. *Science translational medicine* 6: 257re6-257re6, 2014.

Park H, Oh K, Prilutsky BI, and DeWeerth SP. A real-time closed-loop control system for modulating gait characteristics via electrical stimulation of peripheral nerves. *Proceedings of 2016 IEEE biomedical circuits and systems conference (BIOCAS),* 2016.

Pantall A, Gregor RJ, and Prilutsky BI. Stance and swing phase detection during level and slope walking in the cat: Effects of slope, injury, subject and kinematic detection method. *J Biomech* 45: 1529-1533, 2012.

Pantall A, Hodson-Tole EF, Gregor RJ, and Prilutsky BI. Increased intensity and reduced frequency of EMG signals from feline self-reinnervated ankle extensors during walking do not normalize excessive lengthening. *J Neurophysiol* 115: 2406-2420, 2016.

Pearson KG. Common principles of motor control in vertebrates and invertebrates. *Annual review of neuroscience* 16: 265-297, 1993.

Pearson KG. Generating the walking gait: role of sensory feedback. *Progress in brain research,* 143: 123-129, 2004.

Pearson KG. Role of sensory feedback in the control of stance duration in walking cats. *Brain Res Rev* 57: 222-227, 2008.

Pearson KG and Collins DF. Reversal of the influence of group Ib afferents from plantaris on activity in medial gastrocnemius muscle during locomotor activity. *J Neurophysiol* 70: 1009-1017, 1993.

Prilutsky BI, Herzog W, and Allinger TL. Mechanical power and work of cat soleus, gastrocnemius and plantaris muscles during locomotion: possible functional significance of muscle design and force patterns. *Journal of Experimental Biology* 199 (Pt 4): 801-814, 1996.

Prilutsky BI, Maas H, Bulgakova M, Hodson-Tole EF, and Gregor RJ. Short-term motor compensations to denervation of feline soleus and lateral gastrocnemius result in preservation of ankle mechanical output during locomotion. *Cells Tissues Organs* 193: 310-324, 2011.

Prilutsky BI, Sirota MG, Gregor RJ, and Beloozerova IN. Quantification of motor cortex activity and full-body biomechanics during unconstrained locomotion. *J Neurophysiol* 94: 2959-2969, 2005.

Realmuto J, Klute G, and Devasia S. Nonlinear passive cam-based springs for powered ankle prostheses. *J Medical Devices* 9:011007, 2011.

Reisman DS, McLean H, Keller J, Danks KA, and Bastian AJ. Repeated split-belt treadmill training improves poststroke step length asymmetry. *Neurorehabilitation and neural repair*, 27: 460-468, 2013.

Reisman DS, Wityk R, Silver K, and Bastian AJ. Locomotor adaptation on a split-belt treadmill can improve walking symmetry post-stroke. *Brain*, 130: 1861-1872, 2007.

Rossignol S, Dubuc R, and Gossard JP. Dynamic sensorimotor interactions in locomotion. *Physiol Rev* 86: 89-154, 2006.

Rybak IA, Dougherty KJ, and Shevtsova NA. Organization of the Mammalian Locomotor CPG: Review of Computational Model and Circuit Architectures Based on Genetically Identified Spinal Interneurons(1,2,3). *eNeuro* 2: 2015.

Rybak IA, Stecina K, Shevtsova NA, and McCrea DA. Modelling spinal circuitry involved in locomotor pattern generation: insights from the effects of afferent stimulation. *J Physiol* 577: 641-658, 2006.

Schaarschmidt M, Lipfert SW, Meier-Gratz C, Scholle HC, and Seyfarth A. Functional gait asymmetry of unilateral transfemoral amputees. *Human movement science* 31: 907-917, 2012.

Selgrade BP, Thajchayapong M, Lee GE, Toney ME, and Chang YH. Changes in mechanical work during neural adaptation to asymmetric locomotion. *J Exp Biology: jeb-149450*, 2017.

Selgrade BP, Toney ME, and Chang YH. Two biomechanical strategies for locomotor adaptation to split-belt treadmill walking in subjects with and without transtibial amputation. *J Biomech 53:*136-43. 2017.

Sherrington CS. Flexion-reflex of the limb, crossed extension-reflex, and reflex stepping and standing. *J Physiol* 40: 28-121, 1910.

Stecina K, Quevedo J, and McCrea DA. Parallel reflex pathways from flexor muscle afferents evoking resetting and flexion enhancement during fictive locomotion and scratch in the cat. *J Physiol* 569: 275-290, 2005.

Shulyzki, R, Karim A, and Roman G. CMOS current-copying neural stimulator with OTA-sharing. *Proceedings of 2010 IEEE international symposium on circuits and systems (ISCAS)*, 2010.

Takahashi KZ, Lewek MD, and Sawicki GS. A neuromechanics-based powered ankle exoskeleton to assist walking post-stroke: a feasibility study. *J neuroengineering and rehabilitation* 12: 1, 2015.

Tan DW, Schiefer MA, Keith MW, Anderson JR, Tyler J, and Tyler DJ. A neural interface provides long-term stable natural touch perception. *Science translational medicine* 6: 257ra138, 2014.

Torres-Oviedo G, Vasudevan E, Malone L, and Bastian AJ. Locomotor adaptation. *Prog Brain Res* 191: 65-74, 2011.

Todorov E. Optimality principles in sensorimotor control. *Nature neuroscience.* 7: 907-915, 2004.

Tyler DJ. Neural interfaces for somatosensory feedback: bringing life to a prosthesis. *Current opinion in neurology* 28: 574-581, 2015.

Walmsley B, Hodgson JA, and Burke RE. Forces produced by medial gastrocnemius and soleus muscles during locomotion in freely moving cats. *J Neurophysiol* 41: 1203-1216, 1978.

Weber DJ, Friesen R, and Miller LE. Interfacing the somatosensory system to restore touch and proprioception: essential considerations. *J Mot Behav* 44: 403-418, 2012.

Wutzke CJ, Mercer VS, and Lewek MD. Influence of lower extremity sensory function on locomotor adaptation following stroke: a review. *Topics in stroke rehabilitation* 20: 233-240, 2013.

Zehr EP, Komiyama T, and Stein RB. Cutaneous reflexes during human gait: electromyographic and kinematic responses to electrical stimulation. *J neurophysiol* 77: 3311-3325, 1997.

Zehr EP, Stein RB, and Komiyama T. Function of sural nerve reflexes during human walking. *J Physiol* 507: 305-314, 1998.

VITA

Hangue Park

Hangue Park was born in Pohang, South Korea. He received both B.S. and M.S. degree from Seoul National University, Seoul, Korea, at 2006 and 2008, respectively. From 2001 to 2004, as an alternative to military service, he worked at Bluebird-soft where he designed circuit and system for industrial personal digital assistance (PDA). In his master's study from 2006 to 2008, he developed a wireless capsule endoscope system to substitute the colonoscopy that is unpleasant and often causes pressure. From 2008 to 2010, he worked at Samsung-Electronics where he designed SAW-less transceiver and phase locked loop for cell-phone applications. At 2010, he joined Georgia Institute of Technology. During the first few years, he developed intraoral tongue drive system (iTDS) to help disabled people to issue complex commands in more convenient way, using their voluntary tongue motion. His current research interests lie in artificial sensory feedback and closed-loop optimization of sensorimotor loop, to develop a neuroprosthesis. He believes that the neuroprosthesis research will promote understanding of the body-machine interface and rehabilitation outcomes of disabled people. He is also interested in developing smart bio-mimicking/bio-inspired circuits and systems for his research purpose. He received the best demonstration award in the 2012 IEEE Biomedical Circuits and Systems Conference, the 2nd place award and the best product showcase award in the 2012 Business Plan Competition at Georgia Tech, honorable mention in the 2014 Samsung Human-Tech Paper Award, and outstanding research award for Predoctoral Students in 2016 from the Association of Korean Neuroscientists.